

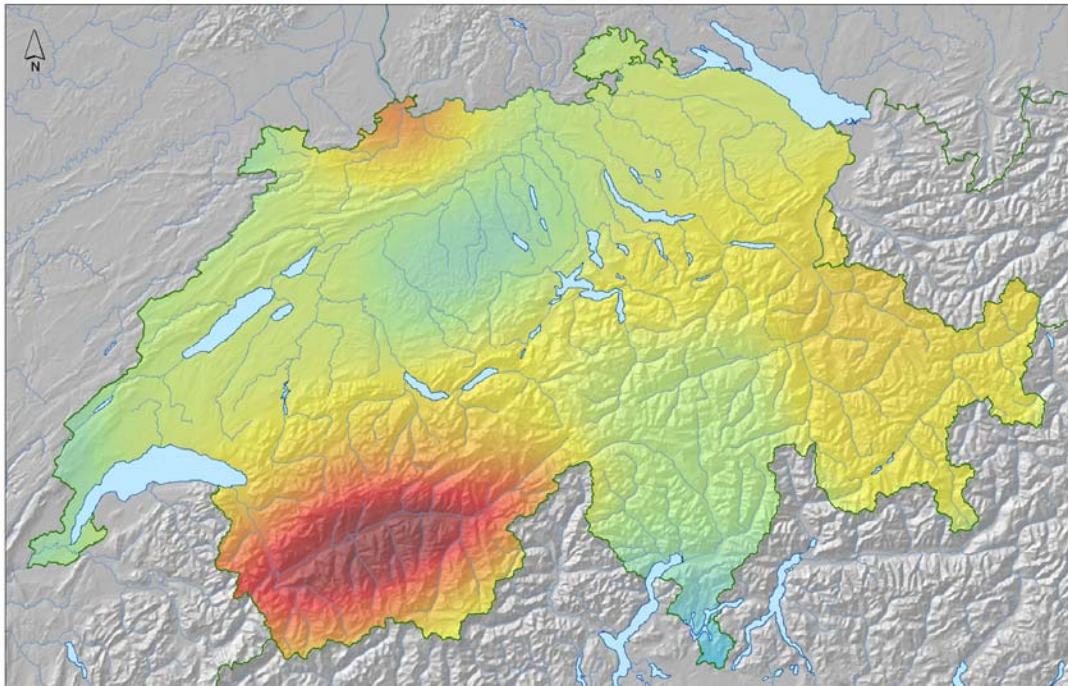


Swiss  
Seismological  
Service

**ETH**

Eidgenössische Technische Hochschule Zürich  
Swiss Federal Institute of Technology Zurich

# Seismic Hazard Assessment of Switzerland, 2004



**November 2004**  
**Swiss Seismological Service**

# **Seismic Hazard Assessment of Switzerland, 2004**

**Domenico Giardini, Stefan Wiemer,  
Donat Fäh and Nicolas Deichmann**

with major contributions from  
Souad Sellami, Sarah Jenny

and the hazard team at the Swiss Seismological Service:

M. Baer, F. Bay, A. Becker, F. Bernardi,  
J. Braunmiller, M. Ferry, M. Garcia-Jimenez,  
M. Gisler, S. Heimers, S. Husen, P. Kästli, U. Kastrup,  
F. Kind, U. Kradofer, M. Mai, S. Maraini, K. Monecke,  
M. Schnellmann, D. Schorlemmer, G. Schwarz-Zanetti  
S. Steimen, J. Wössner & A. Wyss.

**Version 1.1 – November 25, 2004**

Swiss Seismological Service, ETH Zurich,  
Schafmattstr. 30, 8093 Zurich, Switzerland.

E-mail: [info@sed.ethz.ch](mailto:info@sed.ethz.ch);

<http://www.seismo.ethz.ch>



# Table of Contents

<b>PREFACE AND ACKNOWLEDGEMENTS .....</b>	<b>5</b>
<b>1 ABSTRACT .....</b>	<b>7</b>
<b>2 HISTORY OF SEISMIC HAZARD ASSESSMENT .....</b>	<b>9</b>
<b>3 SEISMOTECTONIC FRAMEWORK OF THE STUDY REGION .....</b>	<b>13</b>
3.1 Seismotectonic Setting.....	13
Focal Mechanisms and Stress Orientation.....	15
3.2 Historical Observations .....	16
The 1356 Earthquake of Basel .....	18
The 1855 Earthquake of Visp .....	19
The 1946 Earthquake of Sierre .....	20
3.3 Instrumental Observations.....	21
3.4 Paleoseismic Investigations in Central and Northern Switzerland.....	25
<b>4 INPUT FOR PSHA IN SWITZERLAND .....</b>	<b>29</b>
4.1 Earthquake Catalog of Switzerland .....	29
4.2 Seismotectonic Zoning.....	31
Definition of Seismic Source Zones.....	31
Comparison with Previous Zonations .....	33
Depth Distribution of Events in Switzerland .....	34
4.3 Estimation of Recurrence Parameters.....	34
Data Completeness with Time .....	34
Explosion Contamination .....	36
Declustering the ECOS Catalog .....	38
Estimating Seismicity Rates .....	40
4.4 Maximum Possible Earthquake.....	46
4.5 Predictive Ground-Motion Models.....	47
Aleatory Uncertainty of PGMM .....	52
<b>5 HAZARD COMPUTATION AND RESULTS .....</b>	<b>53</b>
5.1 Monte - Carlo Simulation Approach.....	53
5.2 Hazard Results .....	55
5.3 De-aggregation of Hazard Results.....	63
5.4 Sensitivity to Input Parameters .....	66
<b>6 CONCLUSIONS AND OUTLOOK .....</b>	<b>69</b>
Outlook 2005 to 2008: Preparing the Next Generation of PSHA .....	71
Outlook 2005 to 2008: Site-specific Hazard Assessment for Switzerland.....	72
<b>7 REFERENCES .....</b>	<b>75</b>



## Preface and Acknowledgements

Earthquakes in Switzerland are a serious threat to society and human beings. While damaging earthquakes are fortunately rare in Switzerland when compared to seismically more active regions, damaging events have occurred in the past and will continue to do so in the future. Over the past 700 years, a total of 28 events of a moment magnitude  $M \geq 5.5$  are known to have occurred (Table 1), twelve of them caused severe damage (Intensity of VIII or higher). Moderate to high seismic risk in Switzerland results from the high population density and high degree of industrialization, as well as from the lack of preparedness due to the relatively long return periods of strong ground shaking. Critical infrastructure includes large dams, four nuclear power plants, major communication lines and numerous chemical plants.

The vulnerability of modern societies is increasing with time. Earthquakes strike generally without warning, and the best preparation a modern society can achieve is to upgrade the building stock infrastructure and critical facilities to a level where damage from earthquakes is minimized. The input for all measures of risk mitigations is the assessment of the hazard associated to the occurrence of earthquakes.

The Swiss Seismological Service (SED) at the ETH Zurich (ETHZ) is the federal agency in Switzerland responsible for monitoring earthquakes and assessing the seismic hazard of Switzerland. The SED operates the Swiss national broadband and strong-motion seismic networks and conducts the research necessary to assess the seismic hazard. The SED was associated in 1956 with the Institute of Geophysics at ETHZ.

This document, and the related web resources and publications, outline the activities of the Swiss Seismological Service related to earthquake hazard assessment in Switzerland in the years 1998–2004. The final result – the new probabilistic seismic hazard assessment for Switzerland and associated maps – is an important contribution of seismology to earthquake hazard mitigation.

This work was supported by ETHZ, the Swiss Nuclear Safety Board (HSK), the Swiss National Foundation (SNF), Swissnuclear and by re-insurance and insurance broker companies (SwissRe, MunichRe, Benfield Greig).

The SED is indebted to all who contributed in small or large part to the assessment of the seismic hazard of Switzerland.

Prof. Domenico Giardini

Director, Swiss Seismological Service.



# 1 Abstract

We present the results of a new generation of probabilistic seismic hazard assessment for Switzerland. This study replaces the previous intensity based generation of hazard maps of 1978. It is the first to systematically consider aleatoric and epistemic uncertainties and compute spectral hazard. Based on a revised moment-magnitude earthquake catalog for Switzerland and the surrounding regions, covering the period 1300–2003, sets of recurrence parameters ( $a$ - and  $b$ -value,  $M_{max}$ ) are estimated. Information on active faulting in Switzerland is too sparse to be used as source zones. We develop instead two models of areal sources. The first oriented more towards capturing historical and instrumental seismicity, the second guided largely by tectonic principles and expressing the alternative view that seismicity is less stationary and thus future activity may occur in previously quiet regions. We derive two distinct models of catalog completeness, in order to express the considerable uncertainty in rates stemming from the uncertainty in completeness.

To estimate three alternative  $a$ - and  $b$ -value sets and their relative weighting, we introduce a novel approach based on the modified Akaike Information Criterion, which allows us to decide when the data in a zone deserves to be fitted with a zone-specific  $b$ -value. From these input parameters, we simulate synthetic earthquake catalogs of 1 million year duration down to magnitude 4.0, which also reflect the difference in depth distribution between the Alpine Foreland and the Alps. Using a new predictive spectral ground-motion attenuation and scaling model for Switzerland, we estimate expected ground-motions in units of the 5% damped acceleration response spectrum at frequencies of 0.5–10 Hz for all of Switzerland, referenced to rock sites with an estimated shear wave velocity of 1500 m/s<sup>2</sup> in the upper 30m. We present hazard curves and uniform hazard spectra for selected cities in Switzerland as well as hazard maps for return periods of 100, 475, 2500 and 10'000 years. Full results are available on the Internet ([www.seismo.ethz.ch](http://www.seismo.ethz.ch)). The highest hazard is found in the Wallis, in the Basel region, in Graubünden and along the alpine front, with maximum ground accelerations at 5 Hz frequency reaching 150 cm/s<sup>2</sup> for a return period of 475 years, and 720 cm/s<sup>2</sup> for 10'000 years.



## 2 History of Seismic Hazard Assessment in Switzerland

Probabilistic Seismic Hazard Assessment (PSHA) is widely considered seismology's most valuable contribution to earthquake hazard assessment (Reiter, 1990; Musson, 1999; Frankel, 1996; Giardini, 1999). Estimating the chance of strong ground-motion at a given level for various locations is the most critical input for seismic zoning and building code design, and is commonly done for all countries worldwide. It is also common that PSHA is periodically reviewed in order to incorporate novel data and improved scientific understanding (Frankel, 1995; Frankel et al., 1997b). The assessment of seismic hazard is the first step in the evaluation of seismic risk, obtained by combining the seismic hazard with vulnerability and value factors (type, value and age of buildings, as well as infrastructure, population density, and land use). Seismic hazard is assessed by combining the history of past earthquakes with the knowledge of the present seismotectonic setting and the local properties of the waves generated by earthquakes.

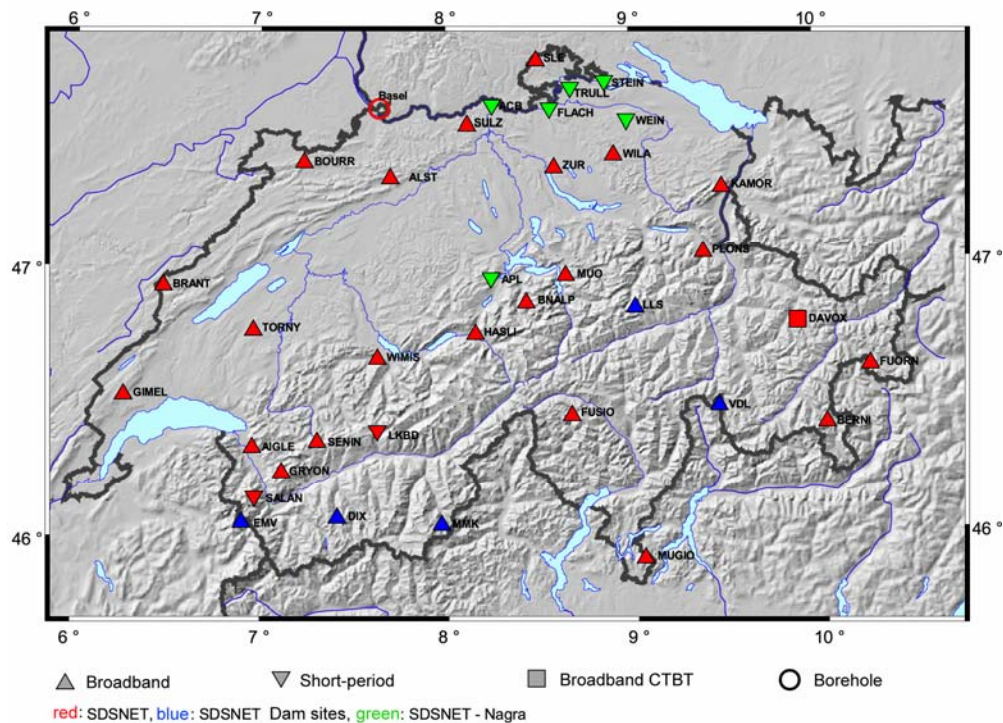


**Figure 1:** The digital network of broadband seismometers in Switzerland.

The Swiss Seismological Service (SED) at the ETHZ is the federal agency in Switzerland responsible for monitoring earthquakes and assessing the seismic hazard of Switzerland. The SED operates the Swiss national broadband and strong-motion seismic networks and conducts the research necessary to assess the seismic hazard. A snapshot of the current network coverage of Switzerland with 28 broadband digital

sensors and 8 short period stations is shown in Figure 1. This network, completed in 2003, is now capable of detecting events down to magnitudes of about 1.5 in all areas of Switzerland. Station DAVOX is part of the international network for monitoring the Comprehensive Test Ban Treaty (CTBT). Data from seismic stations in neighboring countries are integrated for events close to the borders. In addition, a network of 93 strong-motion sensors exists in Switzerland, concentrated near cities and installed at some of the larger dams. The data collected by these networks are the basis for the nation seismic hazard assessment.

A number of studies related to hazard assessment in Switzerland have been performed in the past:

In 1978, Säggerer et al. (1978) published the first PSHA for Switzerland. The hazard was based on the historical catalog available at the time, which contained epicentral Intensities,  $I_0$ , as quantification of size. To compute hazard, an intensity based attenuation function was used. Hazard was computed based on the Cornell (1968) approach, with a zoning model of about 20 zones, which to a large degree mirrored the spatial distribution of seismicity. This study produced the input for the Swiss building code (SIA code 160) as well as for critical facilities, such as nuclear power plants and large dams.

In 1995 a comprehensive study by Rüttener (1995), based on a historical parametric method, estimated the hazard and associated uncertainties at twelve sites within Switzerland. The computed parameter was again macroseismic intensity.

In 1998, Grünthal et al. (1998) slightly updated the hazard map, and provided a harmonized assessment between Germany, Austria and Switzerland (D-A-CH). The D-A-CH map was used as input for the Global Seismic Hazard Assessment Program (GSHAP; Giardini et al., 1999).

In 2002, the SESAME project (Seismotectonics and Seismic Hazard Assessment in the Mediterranean Region; IGCP Projekt 382) published a first unified seismic hazard model for the European-Mediterranean region (Jimenez et. al, 2003; Figure 2). For SESAME computations, the Ambraseys et al. (1996) relationships in terms of peak ground acceleration (PGA) and spectral acceleration (SA) were considered to be appropriate for the regional hazard assessment, since they were obtained on the basis of a European-wide strong motion data set with magnitudes ranging between 4.0 and 7.9 and four categories of soil condition (rock, stiff, soft, and very soft soil).

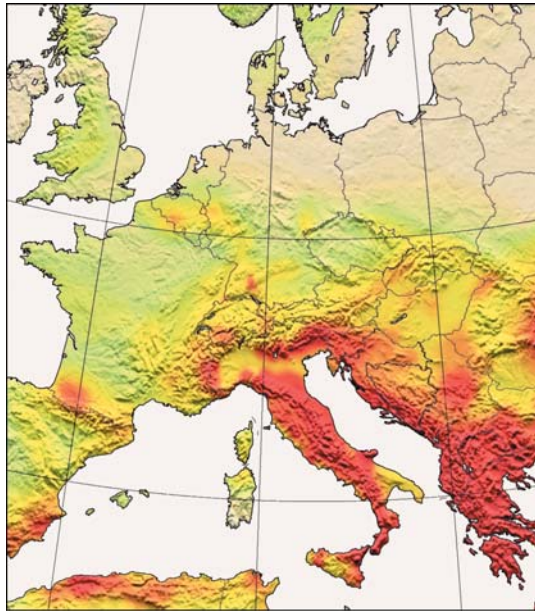


**Figure 2:** Map of the maximum ground-motion expected on average for a return period of 475 years. This map was created based on a homogenized set of source zones (Jiménez et al., 2003).

Starting in 1998, the SED initiated a number of complementary studies in view of a new generation PSHA for Switzerland. Several doctoral theses were specifically targeted towards improving individual elements of a forthcoming PSHA. A region-specific attenuation model for Switzerland was developed by Bay (2003, 2004). The seismotectonic framework of Switzerland was studied using focal mechanisms for stress tensor inversion (Kastrup, 2002; Kastrup, et al., 2004). The seismicity database was vastly improved through a series of studies devoted to paleoseismologic, historical, and instrumental seismicity (Becker et al., 2002; Meghraoui et al., 2001; Schwarz-Zanetti et al., 2003; Gisler et al., 2003; Schnellmann et al., 2003). A major result of these studies, a new moment based earthquake catalog for Switzerland, was published in 2003 (Fäh et al., 2003; Braunmiller et al., 2004). All of these studies represent the essential groundwork for the new PSHA and are discussed in more detail in the course of this report. All hazard relevant publications, software and databases are available for download on the web page of the SED ([www.seismo.ethz.ch](http://www.seismo.ethz.ch)).

In 2002, first results of the new generation PSHA were made available (Sellami et al., 2003). They were used as input for the seismic zoning of Switzerland used in the new Swiss building code (SIA code 261, 2003). The 2002 PSHA represented a preferred consensus model and did not include a full logic-tree approach. In this report, we describe the final SED PSHA model of 2004, available also on the SED web page, which contains a full uncertainty estimate based on alternative scenarios. In the final chapter, we present an outlook towards the next generation of PSHA for Switzerland.



### 3 Seismotectonic Framework of the Study Region

#### 3.1 Seismotectonic Setting

Switzerland contains several distinct geological and seismotectonic regimes related to the collision of the African and the European plates. In terms of crustal strain rate and seismicity rate, Switzerland is located in the transition zones between areas of high seismic activity (Greece, Italy) and areas of low seismic activity (Northern Europe).

The country can be subdivided into three main tectonic units (Figure 3): (1) The Alpine belt in the south, (2) the Jura in the north, and (3) the Molasse basin, in between (e.g., Trümpy, 1985; Hsü, 1995; Pavoni *et al.* 1997). Small to moderate but persistent seismic activity occurs beneath the Alpine belt and north of the Alps, including the Molasse basin, the Rhine Graben, and the Jura (e.g., Deichmann *et al.*, 2000; Baer *et al.*, 2003).

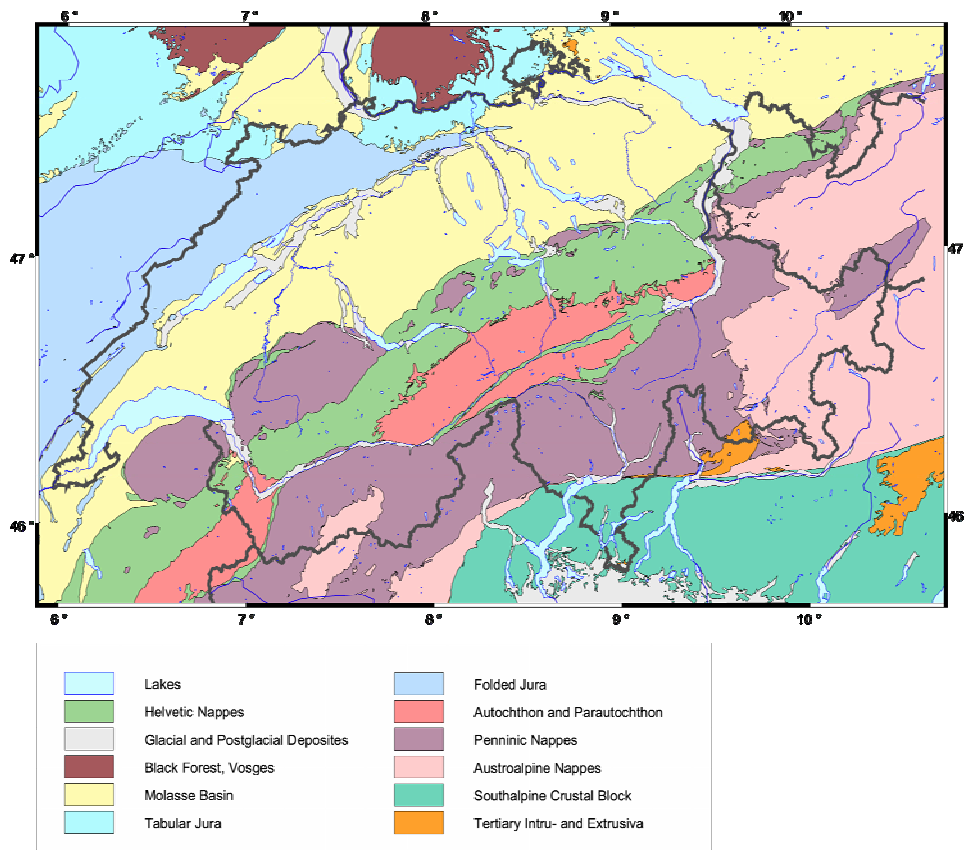


**Figure 3:** Seismotectonic map of Switzerland and surrounding region. Shown are the major tectonic/geological units, differentiated by color.

Below we describe some of the major tectonic features of the study region which influence the seismic activity and will be used to design the zoning models for the hazard.

*Helvetic Front:* This is the major tectonic separation between the Alpine Foreland and the Alps proper. Its definition is based on: (1) the depth distribution of the hypocenters (Deichmann, 1992; Deichmann et al., 2000), (2) geological information, and (3) density of the seismic events. This boundary, the Helvetic Front, is readily seen on any geological map (e.g., Trümpy, 1985). It is characterized by different lithologies with different rheological/mechanical properties to the south and north. The tectonic contact zone of the Helvetic Front dips towards the south at an angle of 30 to 45°. The seismic activity along the Helvetic Front is apparently contained within the Alps proper rather than in the foreland (Figure 6). Given that the seismogenic crust is constrained to be at most 20 km thick underneath the Alps proper, in contrast to the more than 30 km seismogenic thickness to the north (Deichmann et al., 2000; Husen et al., 2003), a broad thermal anomaly (Jaboyedoff & Pastorelli, 2003) might govern the depth distribution of seismicity. Alternatively, the seismic activity in the lower crust beneath the northern Alpine foreland and thus the lower resistance to brittle failure might also be a consequence of increased fluid pressure (Deichmann, 1992).

*Insubric Line:* The Insubric (also called peri-Adriatic) lineament is a long-known fundamental tectonic boundary in the Alps, separating the Southern Alps from the crystalline Alps to the north. It is a sharp and nearly vertical contact. A wealth of data provides several lines of evidence for different crustal characteristics on both sides of this fault. The Southern Alps were built on the Adria (Italy) microplate, whereas the crystalline Alps derive from continental fragments that either belonged to the southern margin of Europe, or were isolated within the Tethys Ocean before collision between Adria and Europe (e.g., Schmid and Kissling 2000). Geophysical information including reflection seismology (Kissling, 1993; Schmid et al., 1997; Ye et al., 1995), seismic behavior (less active towards the south), gravimetry, and Moho depth (Waldhauser et al., 1998) confirm the geological differences.

*Jura:* The Jura region is separated from other source zones on the basis of rock composition and the existence of a shallow-dipping contact zone between the deformed sedimentary cover and the apparently less deformed basement (pre-Triassic rocks) (e.g., Burkhard, 1990; Sommaruga, 1999; Truffert et al., 1990).

*Southern Rhinegraben:* The major structural element cutting the European lithosphere, it is characterized by sparse, sometimes destructive seismicity. This activity has been more pronounced in the southern part, where the graben intercepts the Jura folds. The 1356 Basel event is the largest known historical earthquake in central-northern Europe.

*Swaebian Alb:* The Swaebian Alb is a documented zone of episodic activity with consistent strike-slip focal mechanism oriented in a north-south direction.

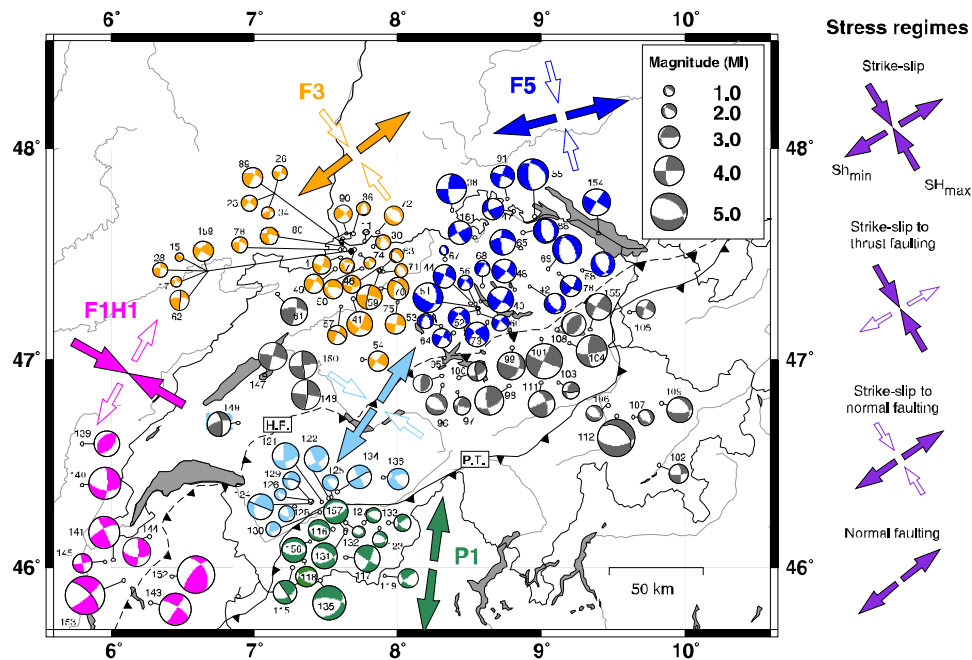


**Figure 4:** Focal mechanisms (beach-balls) and principal stress axes (arrows) derived from an inversion of the focal mechanisms. Arrows indicate prevalent stress regime (Kastrup, 2002). See the text for details.

### ***Focal Mechanisms and Stress Orientation***

A systematic analysis of 138 focal mechanisms in Switzerland and its surroundings showed that the style of faulting and the orientation of the stress field varies significantly both along strike and across the Alps (e.g., Kastrup, 2002; Kastrup et al., 2004). Whereas strike-slip mechanisms with a normal faulting component dominate in the Northern Alpine Foreland and some shallow thrust mechanisms are observed along the Northern Alpine Front, the Penninic domains of the Wallis and Graubünden are characterized by normal faulting with extensional axes at a high angle to the strike of the Alps (Figure 4). In the Northern Foreland the stress tensor reflects the large-scale convergence of Africa and continental Europe, with a maximum horizontal stress axis that rotates from east to west so as to remain roughly perpendicular to the Alpine arc. Thus the least compressive stress in the northern foreland is roughly parallel to the Alpine front. Across the Alps, the variation in azimuth of the least compressive stress is defined by a progressive counterclockwise rotation of about 45 degrees from the Foreland in the north across the Helvetic domain to the Penninic nappes in the southern Wallis. This apparent rotation of the stress field can be explained by the superposition of a local uniaxial deviatoric tension on the large-scale regional stress. The tensile nature and orientation of this local stress component is consistent with the spreading stress expected from lateral density changes due to the crustal root beneath the Alps (Kastrup et al., 2004). These results represent an important input for the definition of seismic source zones used

for hazard computations.

### 3.2 Historical Observations

The bulk of our knowledge of past seismicity relies on the historical record of earthquake damage. From these historical macroseismic observations we derive approximate locations and magnitudes of past events. On average, 10-15 earthquakes are felt each year within Switzerland, damaging events are expected every 5-10 years. Over the past 800 years, a total of 28 events of a moment magnitude  $M_w \geq 5.5$  are known to have occurred (Table 1). A map of all events known to have caused damage to buildings (macroseismic Intensities  $\geq VI$ ) is shown in Figure 5. Twelve of them reach an intensity of VIII or higher, causing severe damage. Destructive earthquakes of intensity IX or larger have occurred in the past, but their return periods exceed 1'000 years (Fäh et al., 2003; Meghraoui et al., 2001). The highest seismic activity is observed in the region of Basel and in the Wallis. Other regions of enhanced activity are central Switzerland, Graubünden, and the Rhine Valley of St. Gallen. As examples, we include here a brief description of three of the strongest historically known earthquakes in Switzerland (Figure 6-9).

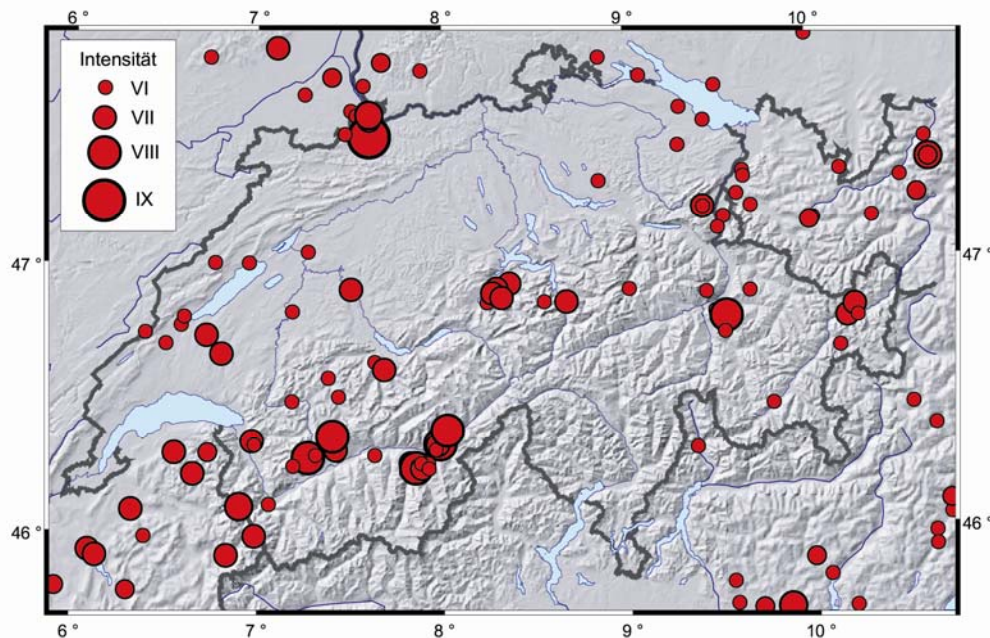


**Figure 5:** Map of Switzerland. Circles mark epicenters with epicentral intensity  $I_x \geq VI$  since the year 1'000, based on macroseismic observations (ECOS, 2002).

**Table 1:** List of all known historical earthquakes of magnitude  $M_w \geq 5.5$ .

Year	Month	Day	Hour	Latitude [deg]	Longitude [deg]	Magnitude [ $M_w$ ]	Inten- sity	Location
1295	9	4		46.79	9.54	6.5	VIII	Churwalden GR
1356	10	18	17	47.55	7.60	6.2	VIII	Basel
1356	10	18	21	47.47	7.60	6.9	IX	Basel
1363	6	24		47.80	7.10	5.5	VII	Thann/Haut-Rhin F
1372	6	1		47.83	7.15	5.5	VII	Mühlhausen F
1524	4			46.27	7.27	6.4	VIII	Ardon VS
1577	9	22	1	47.31	7.19	5.5	VI	Bassecourt
1584	3	11	11	46.33	6.976	6.4	VIII	Aigle VD
1601	9	18	1	46.92	8.36	6.2	VIII	Unterwalden
1650	9	21	3	47.55	7.53	5.6	VII	Basel
1682	5	12	2	47.98	6.52	6	VIII	Hautes-Vosges
1685	3	8	19	46.28	7.63	6.1	VII	Oberwallis
1729	1	13	21	46.63	7.63	5.6	VI	Frutigen BE
1736	6	12		47.48	7.62	5.5	VI	Aesch/Basel
1755	12	9	13	46.32	7.98	6.1	VIII	Brig/Naters VS
1770	3	20	15	46.48	7.18	5.7	VI	Chateau-d'Oex VD
1774	9	10	15	46.85	8.67	5.9	VIII	Altdorf UR
1787	8	27		47.16	9.81	5.5	V	Bludenz/Vorarlberg A
1837	1	24	1	46.32	7.97	5.7	VII	Birgisch VS
1846	8	17	6	46.77	6.58	5.5	VI	Yverdon-les-Bains VD
1855	7	25	11	46.23	7.85	6.4	VIII	Visp/Törbel VS
1855	7	26	9	46.23	7.88	5.6	VIII	Visp/Stalden VS
1879	12	30	12	46.21	6.65	5.5	VII	Chablais
1905	4	29	1	46.09	6.9	5.7	VI-VII	Massif du Mont Blanc
1924	4	15	12	46.30	7.96	5.5	VII	Brig VS
1946	1	25	17	46.35	7.40	6.1	VIII	Ayent VS
1946	5	30	3	46.30	7.42	6	VII	Ayent VS
1964	3	14	2	46.87	8.32	5.7	VII	Sarnen/Alpnach OW

### ***The 1356 Earthquake of Basel***

The earthquake that occurred on October 18, 1356 in the region of Basel is the strongest historically documented earthquake in central Europe. Macro seismic intensities reached IX in the city of Basel and the inferred magnitude is between 6.5 and 7. In addition to the damage caused by the earthquake itself, large parts of the city were destroyed by subsequent fires. Damage to buildings (intensity VI) was reported out to epicentral distances of several 100 km. Numerous castles in northern Switzerland, southern Germany and the Alsace seem to have been damaged by this earthquake. A reconstruction of the distribution of the damage in the city, based on the expenditures of the city of Basel, shows a strong correlation with the local soil conditions (Fäh et al., 2001). A repeat of this event has been estimated to cause damages on the order of several tens of billions of Swiss Francs to buildings alone, as well as hundreds to thousands of fatalities.

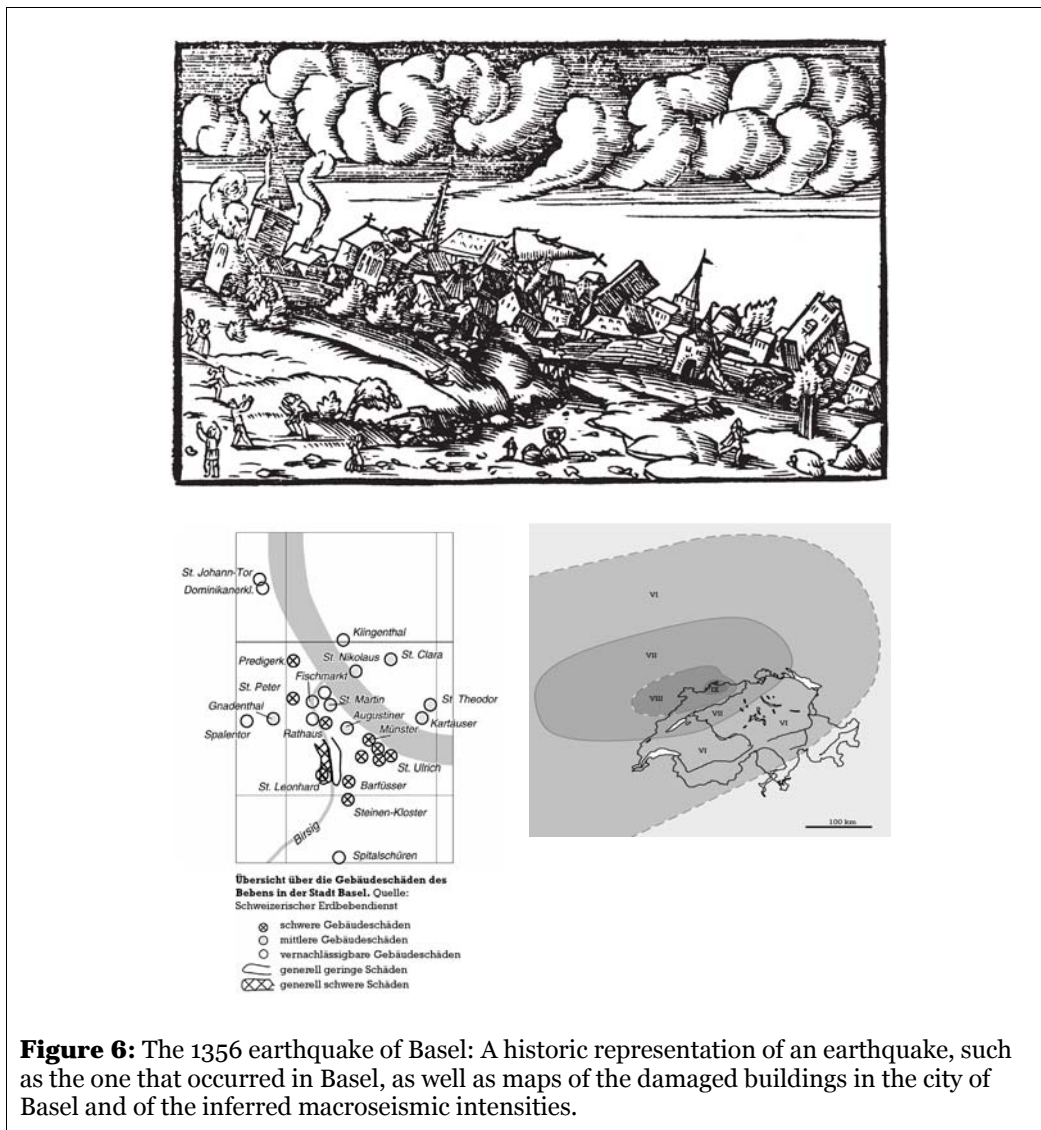


**Figure 6:** The 1356 earthquake of Basel: A historic representation of an earthquake, such as the one that occurred in Basel, as well as maps of the damaged buildings in the city of Basel and of the inferred macro seismic intensities.

### ***The 1855 Earthquake of Visp***

One of the strongest historically known earthquakes in Switzerland occurred on July 25<sup>th</sup>, 1855, in the Wallis. The epicenter was located in the region between Stalden/Törbel and Sankt Niklaus. The epicentral intensity reached VIII, with an estimated magnitude of 6.4. Between Visp and Sankt Niklaus hardly a single building remained undamaged: In some cases entire walls collapsed and the church in Visp lost the top of its bell tower. Numerous aftershocks, some reaching intensities up to VIII, occurred in the aftermath, inducing persistent fear and anxiety in the population for several months following the initial disaster.

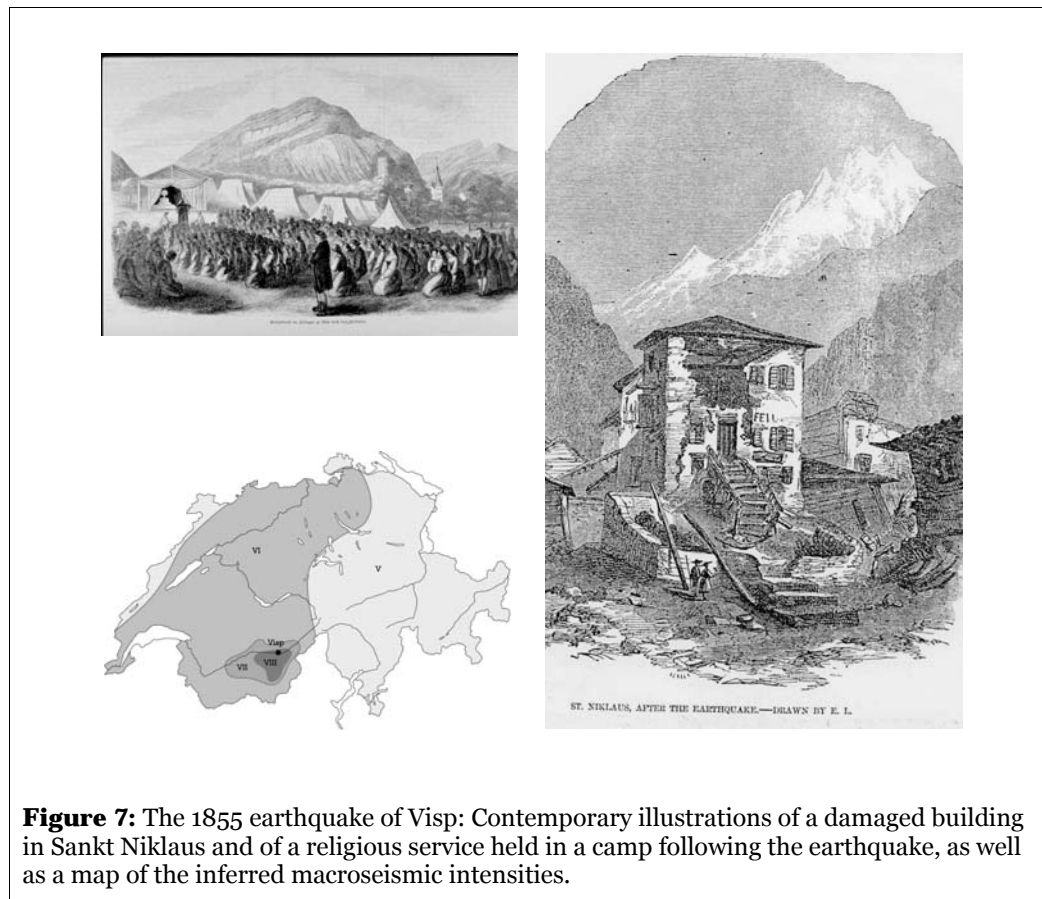


**Figure 7:** The 1855 earthquake of Visp: Contemporary illustrations of a damaged building in Sankt Niklaus and of a religious service held in a camp following the earthquake, as well as a map of the inferred macroseismic intensities.

### ***The 1946 Earthquake of Sierre***

The Wallis was also the site of the strongest earthquake of the 20th century in Switzerland. It occurred on January 25<sup>th</sup>, 1946, in the region of Sierre, with maximum intensities of VIII and a magnitude of 6.1. According to records of the Department of Public Works, 3485 buildings in the canton Wallis suffered some degree of damage. In the town of Sierre alone, 412 chimneys were destroyed, and in Chippis the ceiling of the church collapsed. The earthquake also caused four fatalities and numerous injuries. Hundreds of aftershocks followed over subsequent months. The strongest of these, on May 30<sup>th</sup>, 1946, reached an intensity of VII and triggered a landslide of 4 to 5 million cubic meters on the slopes of the Rawylhorn.



**Figure 8:** The 1946 earthquake of Sierre: Photographs of the collapsed ceiling in the church of Chippis and of the landslide off the Rawylhorn, triggered by an aftershock of the earthquake, as well as a map of the inferred macroseismic intensities.

### 3.3 Instrumental Observations

Since the early 20<sup>th</sup> century, seismographs have been installed worldwide to record the waves released by earthquakes and to achieve a precise determination of hypocentral locations and magnitudes. Improvements in seismometry enhanced the detection of smaller events (today in Switzerland we routinely record events with magnitudes below 1.0), resulting in a more comprehensive understanding of the seismicity. Instrumental observations complement the macroseismic observations for larger events, and are the basis for a homogeneous record of the seismicity in Switzerland since 1975.

With the exception of central Switzerland, which has shown little activity since the earthquake sequence of Sarnen in 1964, and of the recent lack of activity in the Oberwallis, the instrumentally recorded seismicity of the last 29 years (Figure 9) is concentrated in the same regions as the seismicity derived from the historical record (Figure 5).

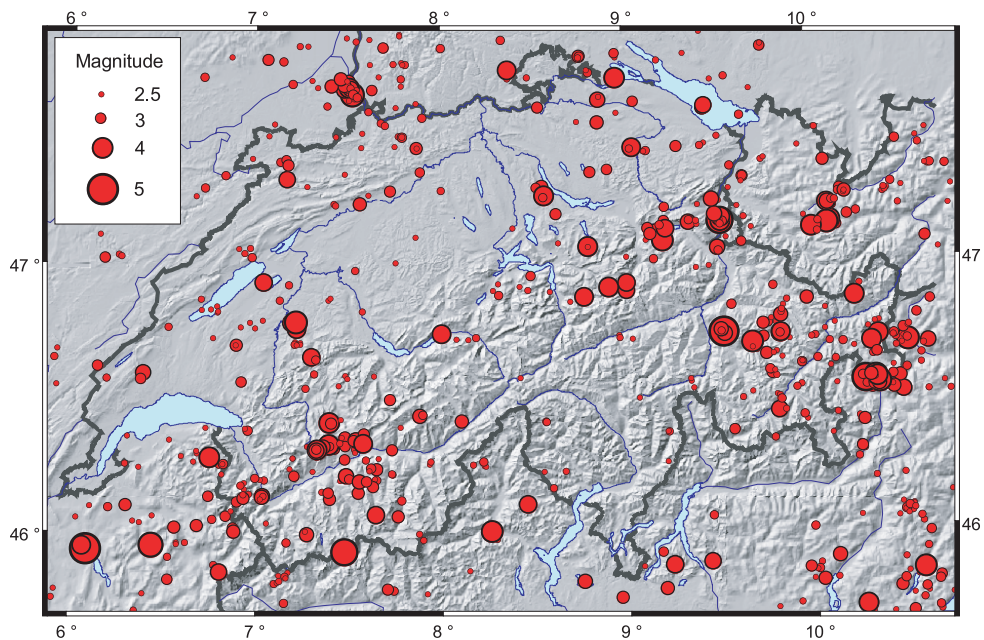


**Figure 9:** Epicenter map, showing the instrumentally recorded events with  $M_L \geq 2.5$  in the period 1975-2003.

An important parameter for the assessment of seismic hazard which can be derived using instrumental recording is the hypocentral depth of earthquakes. However, the routinely determined depth of earthquakes in Switzerland is poorly constrained for many events. Therefore, we rely on results from dedicated studies such as Deichmann et al. (2000) and Husen et al. (2003). The results of Deichmann et al. (2000), shown in Figure 10, are based on high quality locations of selected well recorded events. Husen et al. (2003) also derived a 3-dimensional velocity model and used a non-

linear location algorithm (Husen, 2003; Lomax et al., 2001) to further constrain depth and its uncertainty. Both studies consistently show a major difference in depth distribution between the Alps proper and the Northern Foreland (Jura, Molasse): Deeper earthquakes (mean depth = 13 km, maximum depth > 30 km) occur only in the north beneath the Molasse Basin, whereas in the south under the Alps, where the crust is up to 55 km thick, earthquakes are restricted to the upper 10-15 km (mean depth = 7 km; e.g., Deichmann et al., 2000) (Figure 10). This major difference across the Alpine Front is one of the principle design criteria used for our source zonation.

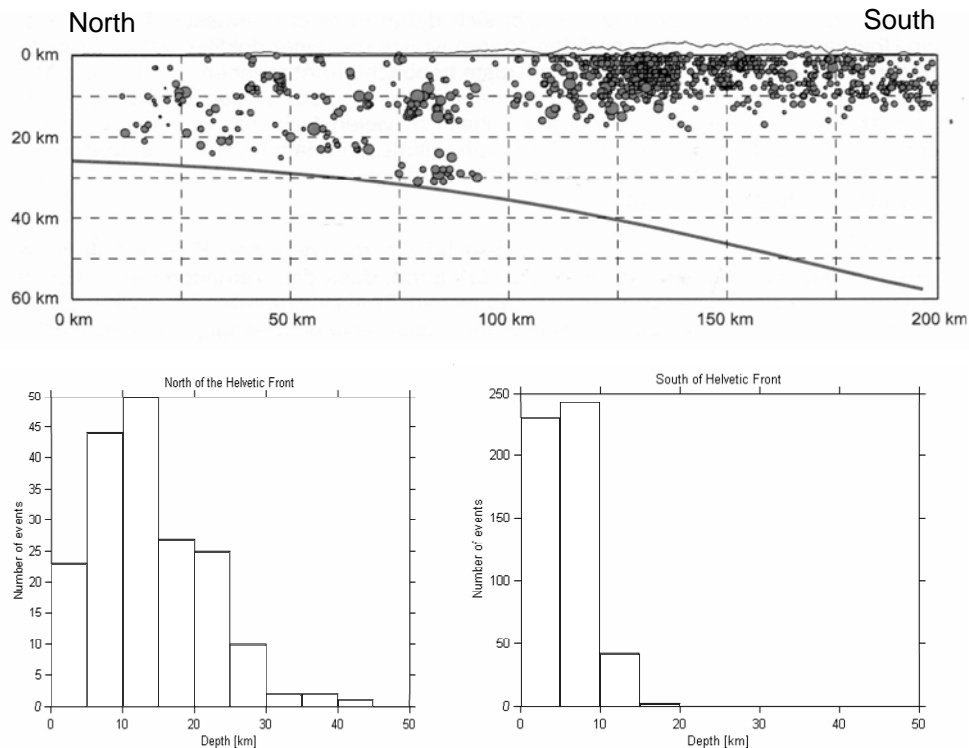


**Figure 10:** (Top) Cross-sectional view (north-south) through the study region. Hypocenters of well determined earthquakes in the period 1975–2000 are marked in as circles (for the selection criteria, see Deichmann et al. (2000)). Note the clear difference in the depth distribution between the Alpine areas and the Foreland. (Bottom) Depth histogram of events in the Foreland (left) and Alps (right), taken from Husen et al. (2003).

Knowledge of active faults and of deformation rates on such faults is virtually nonexistent in Switzerland. Whereas numerous faults are identified on geological maps at all scales, these do not seem to correlate with observed seismicity. In the literature, there is no convincing evidence for Quaternary movements that has offset topography and post-glacial features (e.g., Eckardt et al., 1983). However, within the generally rather diffuse epicenter distribution, two epicenter lineaments have emerged in recent years, which seem to be related to active faults at depth within the crust. The first is an almost rectilinear 20-30 km long north-south striking epicenter alignment east of the city of Fribourg (Figure 11).

Based on the good agreement with the focal mechanisms, with the subsurface structures identified in reflection seismic experiments and in geomagnetic studies, as well as with morphological features of the region, it could be demonstrated that the earthquake lineament of Fribourg corresponds to an active fault-zone capable of hosting a possible magnitude 6 event (Kastrup, 2002). The second lineament is a narrow earthquake zone that is located along the northern border of the Rhone Valley in the Wallis and that possibly extends in a southwestern direction all the way into the Haute-Savoie. The northern Wallis segment of this epicenter alignment is probably a long-lasting consequence of the 1946 earthquake sequence of Sierre. However, in recent years, an increase of activity southwest of this region suggests the possible existence of an active fault-zone whose dimensions could accommodate an earthquake considerably larger than what is known to have occurred previously. Ongoing investigations, such as the precise relative locations of events in individual sequences within the larger earthquake zone (Figure 12), will contribute towards clarifying this issue.

Due to the low deformation rates, detailed geodetic measurements for individual faults do not exist in Switzerland to date. However, geodetic deformation rates help to define broad regional differences in seismic potential. In Switzerland and in neighboring areas, geologically estimated deformation rates are homogeneous and overall very low, consistent with recent GPS measurements. The average total convergence rate between Africa and Europe for the past 49 Myrs was about 0.9 cm/yr (Regenauer-Lieb and Petit, 1997), which is in good agreement with the rate of 0.94 cm/yr for the past 3 Myrs, as given by NUVEL-1 (DeMets et al., 1990). These numbers are reasonably consistent with long-term geological strain rates. Vertical movements are too small to distinguish isostatic signals due to post-glacial rebound from tectonic signals.

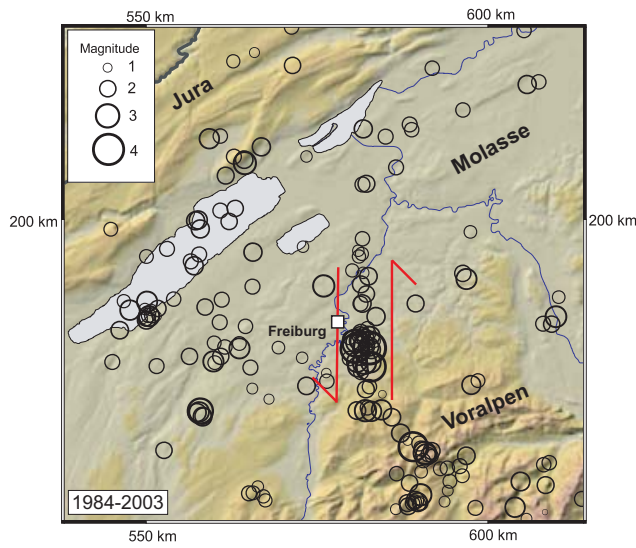


**Figure 11:** Epicenter map of northwestern Switzerland for the years 1984-2003 with the earthquake lineament of Fribourg and the slip directions along the inferred faultzone at depth.

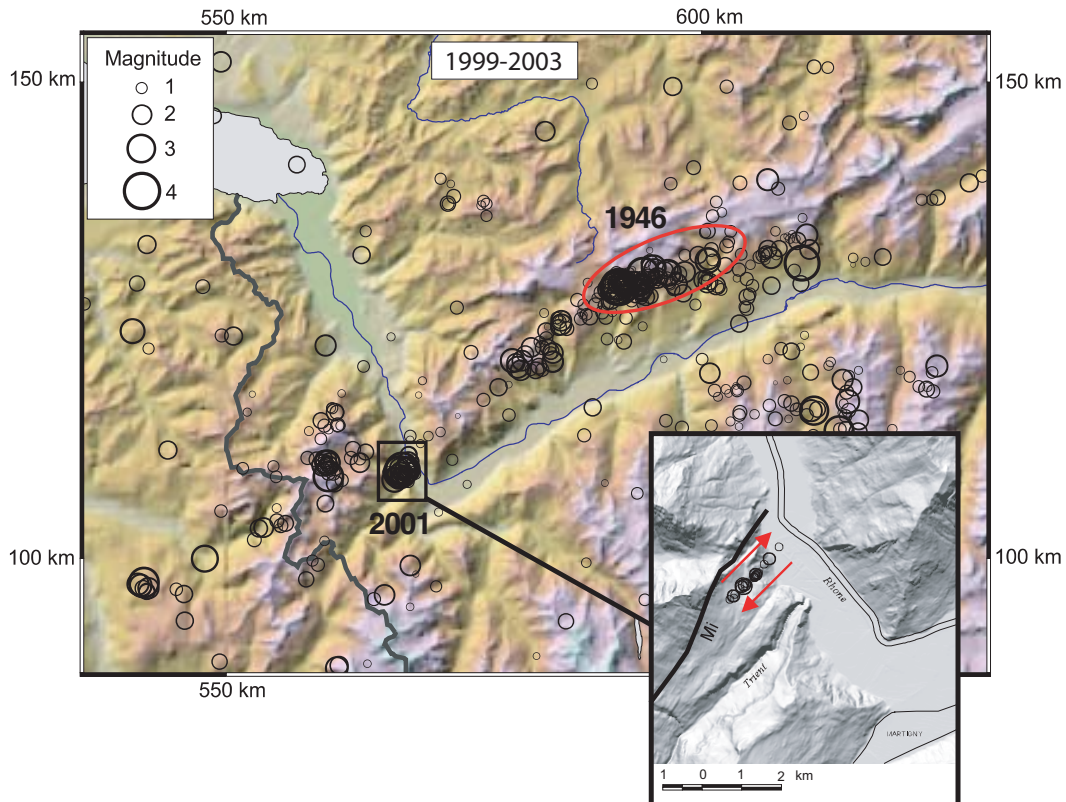


**Figure 12:** Epicenter map of the Wallis for the time period 1999-2001, showing the striking alignment along the northern flank of the Rhone Valley and its extension to the SW into the Haute-Savoie. The red ellipse identifies the epicentral region of the 1946 earthquakes of Sierre. The enlargement in the inset shows the results of the high-precision relative locations of the earthquake sequence of Martigny in 2001 as well as the slip directions inferred for the corresponding fault at depth (Deichmann et al. 2002).

### ***3.4 Paleoseismic Investigations in Central and Northern Switzerland***

Earthquakes are the response of the Earth's crust to tectonic deformation and geodynamics processes. As such, understanding of earthquake occurrence requires the knowledge over long time scales. Our knowledge of earthquakes relies largely on the memory of historical earthquakes. Paleoseismology is the science aiming at identifying active faults and prehistorical earthquakes.

In recent years, palaeoseismic investigations have been successful in many areas of the world in complementing the historic earthquake record with prehistoric events. These investigations are focused on surface faulting (e.g., Camelbeeck and Meghraoui, 1998) and on a variety of geological archives that contain earthquake-related damage and deformation features such as soft-sediment deformation in lakes (e.g., Sims, 1973, 1975; Rodriguez-Pascua et al., 2000), sand injections in flood plain deposits (Obermeier, 1996), slope instabilities (e.g., Keefer, 1984) or cave collapses (e.g., Postpischl et al., 1991). The potential for identifying a complete record of major prehistoric events is restricted to areas where the geological record is complete and earthquake-induced deformation structures are preserved in a wide range of environments. Paleoseismological research is particularly important in regions such as Switzerland where recurrence intervals for strong earthquakes are long and exceed the time span covered by the instrumental and historic earthquake catalogs.

Until 1997, paleoseismological investigations were not conducted in Switzerland, and the common understanding in the geological community was that traces of prehistorical earthquakes could not be found. Deformation structures were often recognized in lake sediments. Although earthquakes have been known as a possible source of such deformation structures, a systematic reconstruction of the sedimentation history in a number of contiguous lakes with the goal of reconstructing the historical and prehistorical occurrence of triggers in lake sediments had not been attempted so far in the Alps. Also, while geologically active faults abound in the Alpine and peri-Alpine domains, the connection between seismic activities and the seismogenic faults had yet to be identified in Switzerland.

In 1997, the Swiss Seismological Service, in cooperation with the Institute of Geology at ETH Zurich and the Swiss Federal Institute for Environmental Science and Technology (EAWAG), launched a number of investigations with the aim of identifying approaches suitable for application in northern and central Switzerland and to reconstruct the Late Pleistocene and Holocene record of strong earthquakes (Becker and Davenport, 2003; Becker et al., 2002; Schnellmann et al., 2002, 2004). These investigations, under the collective project title *PALEOSEIS - Reconstructing the paleoseismic record in Northern and Central Switzerland* focussed on multi-archive, interdisciplinary investigations of strong prehistorical earthquakes.

Among the many highlights of these investigations are: The first comprehensive reconstruction of the complete sedimentation history of a number of lakes (Lungerersee, Baldeggersee, Seelisbergsee, Vierwaldstättersee) with the purpose of

identifying deformation structures; the development of calibration functions to map the seismic shaking with distance and magnitude on the basis of deformation structures recognized in lake sediments; the identification of the causative fault of the 1356,  $I_o=IX$  Basel earthquake—the largest historical event in central-northern Europe; a multi-disciplinary approach combining an array of geological, geomorphological and geophysical techniques to the characterization of the surface expression of major seismogenic faults; the first comprehensive reconstruction of the complete sedimentation history of a large lake with the purpose of locating and characterizing all subaqueous slumping events; the development of innovative tools to map, date and characterize the fine structure of lacustrine sediments associated to subaqueous sliding; the characterization of the fine structure and deposition characteristics of subaqueous slumps; the definition of rigorous criteria to classify triggering mechanisms for subaqueous slumpings; the study of earthquake-triggered rockfalls and landslides; the investigation of secondary and tertiary hazards by modelling tsunami waves generated by the slumping triggered by earthquakes; the first joint investigation of historical and prehistorical earthquakes, integrating different paleoseismological techniques and results to identify and date prehistorical seismic events.

These results change our understanding of the earthquake record in northern and central Switzerland and of how earthquakes affect the geological record. Most relevant for our study are the investigations related to the Rheinach fault near Basel, now believed to have been also the source of the 1356 Basel event (Meghraoui et al., 2001). Paleoseismologic studies (Meghraoui et al., 2001; Becker et al., 2002) suggest that similar size events have indeed taken place on the Reinach fault (Figure 13). There is evidence for at least three earthquakes, which occurred on that branch of the fault within the last 8'500 years with vertical displacements ranging from 0.5 m to 0.8 m.

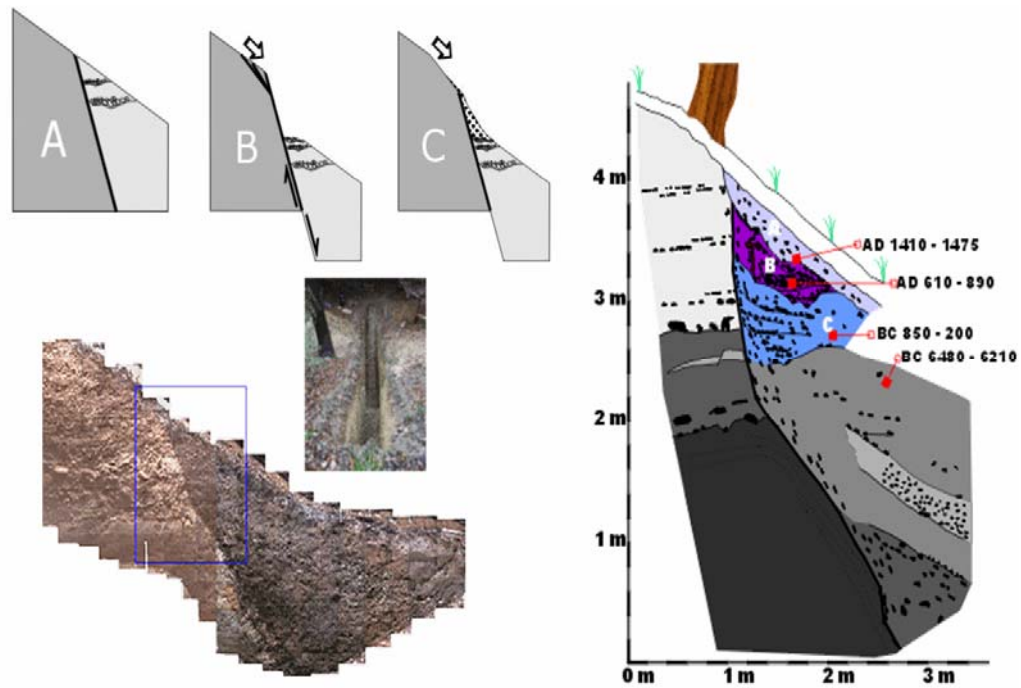


**Figure 13:** Results from the trenching across the Rheinach fault south of Basel. The schemes A-C illustrate the creation of the sediment layers seen in the image in the bottom left. The right frame illustrates a geologic reconstruction of the layers along with the Carbon-14 dates of the different layers.



## 4 Input for PSHA in Switzerland

Input parameters that are needed for performing a PSHA following the Cornell approach (Cornell, 1968; Reiter, 1990) are:

- A seismotectonic source model, which defines fault or areal zones of equal seismic potential. The definition of source zones relies to a large degree on expert judgment, which is based on the assessment of the seismotectonic framework, on past seismicity, and on considerations regarding the temporal and spatial stationarity of earthquake activity.
- An earthquake catalog, which is used to derive recurrence rates and to estimate the maximum possible earthquake for each source zone.
- A predictive ground-motion model (PGMM), which describes the attenuation of amplitudes (acceleration, velocities) as a function of distance as well as the scaling of ground-motion as a function of magnitude. Individual models are constructed for different frequencies and local site conditions.

Below we describe how these input parameters were derived for Switzerland.

### 4.1 *Earthquake Catalog of Switzerland*

The historical earthquake catalog and macroseismic database for Switzerland have been revised during the period 1998-2003 (Fäh et al., 2003). The resulting Earthquake Catalog of Switzerland (ECOS), covering also the border regions, integrates information from different sources:

- The Macroseismic Earthquake Catalog of Switzerland (MECOS 02) with events since 250.
- The annual reports of the Swiss Earthquake Commission since 1879.
- The epicenter locations of the Swiss Instrumental Network since 1975.
- Additional information from twelve earthquake catalogs of neighboring countries and international agencies.

The earthquake catalog includes events up to December 2003. It can be downloaded from our website ([www.seismo.ethz.ch](http://www.seismo.ethz.ch)), along with a detailed report describing its compilation.

Three levels of investigation were conducted, depending on the size and location of an event: Historical, macroseismic and seismological. For earthquakes of the last 1'000 years with intensity VI or higher, all available historical information were collected and translated into macroseismic fields. Those were then evaluated to determine source parameters (epicenter, hypocentral depth class, epicentral intensity, maximum intensity, macroseismic magnitude) and to assess their uncertainties. Earthquakes within Switzerland with epicentral intensity less than VI were reviewed for the period beginning in 1878, or in some cases, when special

information was found in historical sources, even for earlier times. In total, more than 600 events have been reevaluated in these historical investigations. Of these events, 177 earthquakes were strong enough to cause damage and were thus assigned intensities of at least VI in the new catalog. About 260 events in previous catalogs have been identified as fake events or as multiple listings for the same event, due to different calendar styles, misprints, or misinterpreted compilations.

Moment magnitude,  $M_w$ , was chosen as the common measure of earthquake size for both the historically known and the instrumentally recorded events. This involved first a reassessment of instrumental magnitudes, in order to standardize the various types of magnitude scales and the different measurement procedures of various institutions to a common basis (Braunmiller et al., 2004). Then, a set of calibration events with values of intensity as well as magnitude was established. This calibration set was used to assign a magnitude value to the historical earthquakes. In case of larger events, the magnitude assessment is based on an analysis of the entire macroseismic field, according to the method of Bakun (Bakun and Wentworth, 1999; Wesson et al., 2003). For smaller events, magnitudes are computed from epicentral intensities using an empirical relationship (Fäh et al., 2003). While the uncertainty of instrumentally determined magnitudes is estimated to be on the order of 0.3, the error of magnitude estimates based on the conversion from intensities can be as large as 1.0.

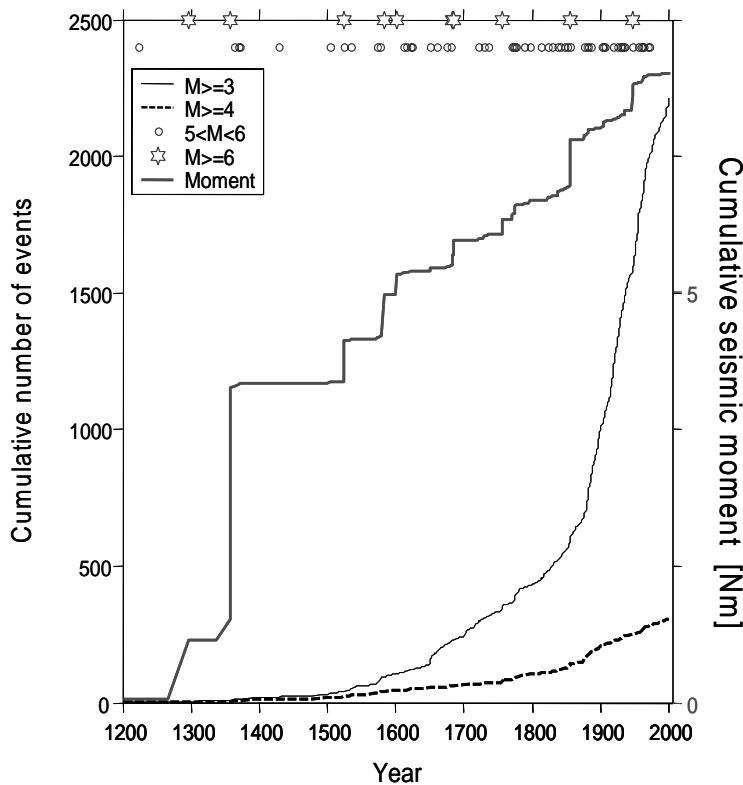


**Figure 14:** Cumulative number of events and cumulative moment as a function of time. Plotted are all events in the ECOS database. Circles mark events with  $M_w \geq 5$ , stars events with  $M_w \geq 6$ . Moment in units of  $10^{26}$  Nm is computed using the formula of Kanamori and Anderson (1975).

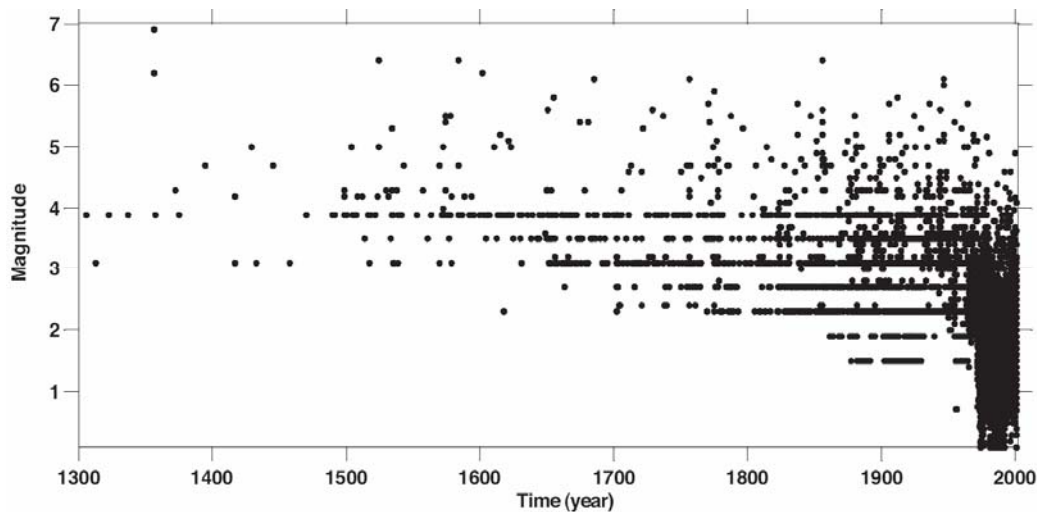


**Figure 15:** Time-magnitude distribution of the events in the ECOS (2002) database.

After removal of all events identified as explosions and of all events judged to be uncertain, ECOS comprises a total of about 20'000 earthquakes. Cumulative number of events and cumulative moment release over time are shown in Figure 14. Figure 15 shows a time-magnitude plot of the entire ECOS database since 1300. Note that magnitude 2-4 events are binned in 0.3 magnitude intervals before 1970, as a result of the conversion from epicentral intensity to magnitude. Completeness increases with time, but varies for different regions.

## 4.2 Seismotectonic Zoning

### *Definition of Seismic Source Zones*

The assessment of seismic hazard requires the interpretation of past seismicity and tectonic knowledge to forecast likely locations of future shaking. Several methods have been proposed, but there is no ideal and proven way to derive a set of seismic source zones; zoning remains inherently a matter of expert judgment. It is therefore important to capture and propagate the uncertainty of any zoning model.

Seismotectonic zoning is intrinsically linked to the question of stationarity in both space and time. Will the seismicity of the future follow the pattern of the past? Will areas which were active in the last centuries remain active also in the next 50–100 years? Or have areas of past seismicity now exhausted their potential and will remain quiet while other areas will become more active? These issues are especially critical in areas of spatially dispersed seismicity such as Switzerland, because the lack of knowledge of active faulting requires the use of areal sources as the primary zoning tool. Areal sources can be either used to closely trace the historical seismicity (historical approach), or they can be used to also reflect seismotectonic knowledge. In

the latter case, the activity in an area could spread with the same probability to a neighboring area of identical seismotectonic character. As an alternative, smoothed seismicity models have been used in some hazard studies (Frankel, 1995; Ruettener et al., 1996) to distribute historical seismicity over a larger region. These models generally use a constant smoothing kernel across the entire region, thus avoiding potential bias. Their disadvantage is that they ignore existing boundaries and do not allow for the integration of external knowledge, and that the choice of a smoothing parameter is likewise subjective.

For our hazard computations, we developed two models of areal sources. Model 1 (SEIS) is mostly driven by historical seismicity; model 2 (TECTO), using generally larger zones, attempts to capture the major tectonic features of the region. For the peripheral regions around Switzerland, we relied largely on the existing source models that were developed previously for the international hazard mapping projects GSHAP and SESAME (Grünthal et al., 1999; Giardini et al. 1999; Jiménez et al., 2003). The geometry of the two source zone models is plotted in Figure 16. Source zone geometries are available for download from our web site ([www.seismo.ethz.ch](http://www.seismo.ethz.ch)).

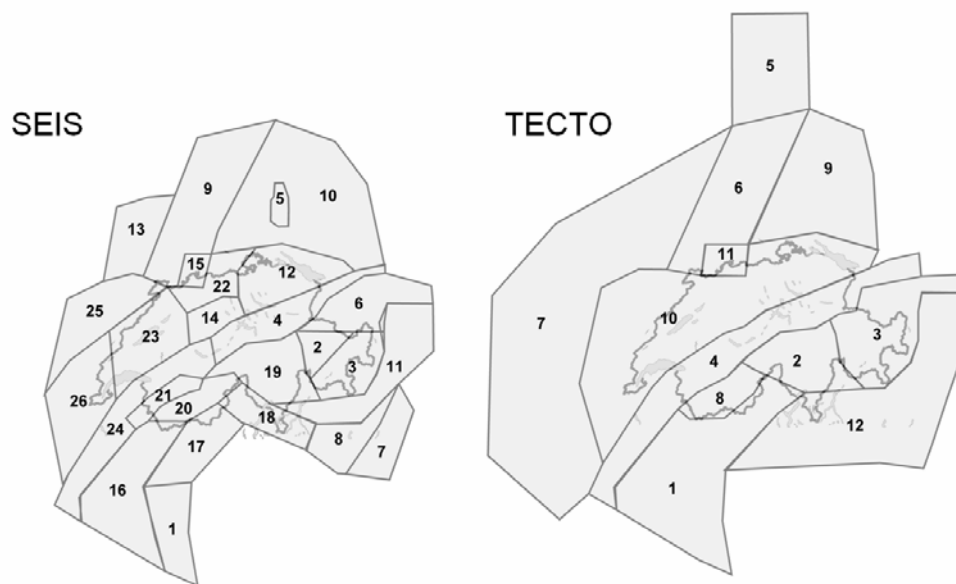


**Figure 16:** Maps of Switzerland. (Left): source zones of model 1, SEIS, which is largely based on the historical seismicity. (Right): source zones of model 2, TECTO, which assumes that the seismicity follows broad tectonic regions. The numbers refer to the names of source zones, as listed in Appendix 2 in Table A3.

Below we describe how the major tectonic features of the study region have been introduced into the design of the zoning models shown in Figure 16.

*Helvetic Front:* The major tectonic separation between the Alpine Foreland and the Alps proper is introduced as a single, arched zone in model TECTO, and subdivided in an eastern and western arc in model SEIS.

*Insubric Line:* The Insubric lineament is introduced only in model SEIS, whereas in

TECTO its contribution to seismic activity is considered negligible.

*Jura*: The Jura region is separated from other source zones in SEIS, while it is combined with the larger Molasse region in TECTO.

*Southern Rhinegraben*: To incorporate the Rhinegraben activity, we define in both models a wide north-south trending zone that includes the Rhinegraben and its shoulders. In principle, the Rhinegraben could be further subdivided into a northern and a southern part along the Variscan suture zone (Lalaye-Lubine Fault from the Vosges to Baden-Baden in the Black-Forest, the Erstein Sill below the sedimentary infill of the Rhinegraben; Villemin et al., 1986; Sissingh, 1998; Burg et al., 1994); however, because this region is far from our study area, we did not do so. In both models, however, we define a specific Basel source zone, which contains the Basel activity of the historical and paleoseismic record. We feel that this subdivision is justified, because this segment, while tectonically similar to the remainder of the Rhinegraben, has persistently produced more activity in the past and is likely to continue to do so in the future.

*Swaebian Alb*: The Swaebian Alb is characterized as a specific source zone in the SEIS model only.

We decided not to use faults as linear or areal source zones. Although numerous active faults have been mapped by geologists, only a few show seismicity related to it. We can associate the Fribourg Fault (Figure 11; Kastrup, 2002) and the Vuache Fault, which produced a 5.3  $M_L$  earthquake on 15 July 1996 (Thouvenot et al., 1998), as well as the broad epicenter alignment in the northern Wallis, associated with the 1946 Sierre event (Figure 12) with the instrumental seismicity. The Rheinach Fault (Meghraoui et al., 2001; Becker and Davenport, 2003; Becker et al., 2002) seems to be related to the 1356 Basel earthquake as well as to several earlier events. Additionally to be mentioned are the north-south striking Rhinegraben boundary faults. The information on active faults in Switzerland is restricted to these four or five cases and the known seismic activity along these faults is in our opinion insufficient to characterize them as source zones. Doing so would possibly introduce a bias in the hazard assessment, because the information density on known faults is so sparse and therefore few selected areas would receive a 'special' treatment. Instead, we used the location and orientation of these faults to delimit the shape of wider source zones.

### ***Comparison with Previous Zonations***

The zone models adopted as a basis for the present hazard computations differ fundamentally from the previous model (Sägesser and Mayer-Rosa, 1978), which was also used in the D-A-CH map (Grünthal et al., 1998) and the following GSHAP and SESAME projects (Grünthal et al., 1999; Giardini et al., 1999; Jiménez et al., 2003). Whereas in the present models the entire study area is subdivided into contiguous source zones, in the earlier version individual source zones are defined as disconnected polygons within a regional background area. As a consequence, the

earlier zonations mirrors more closely the observed spatial distribution of seismicity and thus implicitly assumes a greater degree of stationarity than the new models, specifically than model TECTO. Some of the changes in zonation are also due to new information that emerged from the catalog revision and from recent microseismicity (e.g., Figure 11 and 12).

### ***Depth Distribution of Events in Switzerland***

The focal depth of earthquakes is an important input to PSHA, not only for defining source zones, but also for ground-motion predictions. In our hazard computations (Chapter 5), based on the high-precision relocations of Deichmann et al. (2000) and Husen et al. (2003) listed in Appendix 2 in Table A1, we assign two different depth distributions for events north and south of the Alpine Front. We did not, however, feel that the data allows us to further subdivide the regions based on focal depth.

## ***4.3 Estimation of Recurrence Parameters***

### ***Data Completeness with Time***

To model the seismicity in each zone, we need to estimate the recurrence parameters,  $a$  and  $b$ , in the Gutenberg-Richter relation  $\log_{10} N = a - bM$ , where  $N$  is the cumulative number of events, the  $a$ -value the productivity of a volume, and the  $b$ -value the relative size distribution (Ishimoto and Iida, 1939; Gutenberg and Richter, 1944) (Figure 17). This estimation is critically dependent on the correct identification of the magnitude of completeness,  $M_c$ , below which only a fraction of all events in a magnitude bin are detected by the network (Kijko and Graham, 1999; Rydelek and Sacks, 2003; Wiemer and Wyss, 2000, 2003). Completeness as a function of space and time in the ECOS catalog varies, first of all, country-by-country, because the different countries use different methods to compile the catalogs. Completeness estimates for historical datasets are largely a matter of expert judgment, based on an evaluation of various plots of the seismicity. The simplest plot of magnitude as a function of time gives a first overview of catalog completeness. Visual inspection of frequency-magnitude plots and repeated calculations of recurrence parameters for different values of  $M_c$  provide additional insight. A useful tool for visualizing the temporal dependence of completeness consists of plotting the frequency of occurrence of events for different magnitude bins as a function of time. An example of such a “Stepp-plot” (Stepp, 1972) is shown in Appendix 1. This iterative process leads to a definition of completeness periods through time for each country. Results are then checked against historical estimates of completeness, as given in the ECOS catalog.

For Switzerland, an independently derived estimate of completeness based on a historian’s estimate of data source availability can also be consulted (Fäh et al., 2003). In Figure 18, we show how Switzerland is subdivided into different regions based on the availability of historical sources. In Appendix 2 (Table A2) we list the

estimated completeness threshold for these regions. For the instrumental data, completeness is also computed using an algorithm developed for completeness mapping (Wiemer and Wyss, 2000).

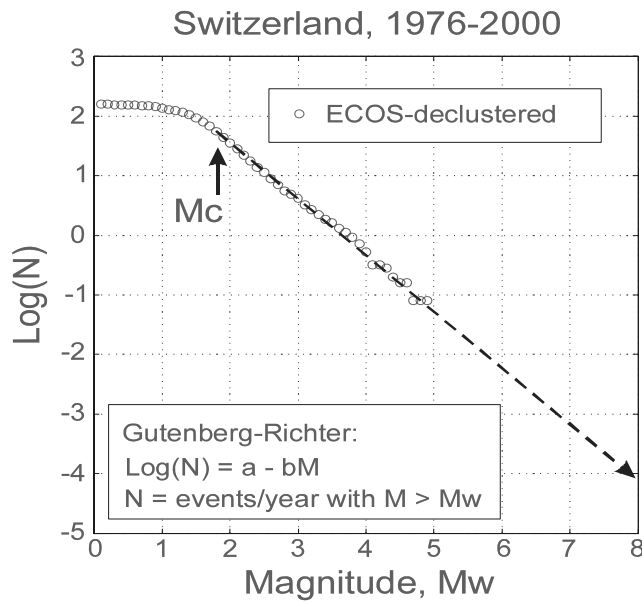


**Figure 17:** Cumulative frequency-magnitude distribution of earthquakes in Switzerland and surrounding regions (circles) The data is limited to the period 1976–2000. The estimated magnitude of completeness is  $M_c = 1.8$ . The overall  $b$ -value of this set is 0.94.

Because sources cross national borders, and because even within individual countries differences in  $M_c$  for different time periods are apparent, we interactively review the normalized cumulative frequency-magnitude distribution of events for each source zones. In some cases, we adjust the completeness threshold. We list in Appendix 2 in Tables A3 and A4 the final determined  $M_c$  threshold for each source zone of models TECTO and SEIS.

Completeness estimation, especially for historical data, is subject to large uncertainties. To express these uncertainties and to allow for the fact that historical data for low magnitudes is less reliable, we define an additional alternative model 2 with a higher  $M_c$  cutoff. This alternative model 2 results in relatively higher weights to the recent earthquakes in the instrumental dataset. We thus have two completeness models for each source region, as listed in Appendix 1 and Appendix 2 (Tables A3 and A4).

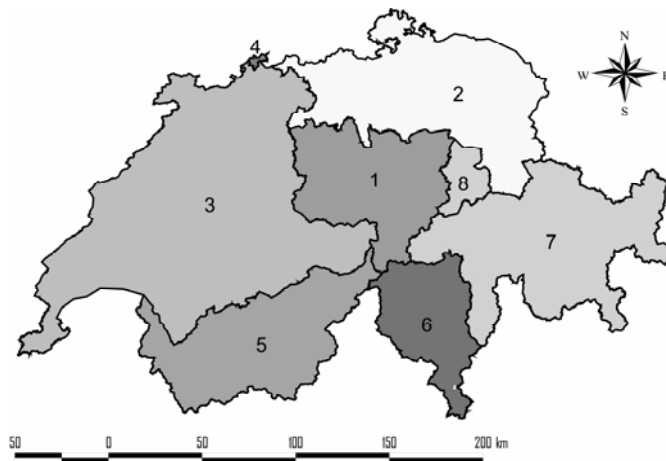


**Figure 18:** Map of Switzerland, indicated are regions of different completeness of the earthquake catalog, as specified in the Appendix 2, Table A2.

### ***Explosion Contamination***

The ECOS catalog contains a number of unidentified explosion events. Despite the best efforts of network operators to identify these events, it is common in all regional earthquake catalogs to have such unidentified events, because the separation of explosion events from tectonic ones is a difficult task (Fäh and Koch, 2002; Koch and Fäh, 2002; Wiemer and Baer, 2000; Wuster, 1993). These events are mainly limited to the most recent 30 year period of data. Their magnitudes are believed to be mostly smaller than  $M_w=2.5$ ; however, these small events potentially effect the  $a$ - and  $b$ -value computation in some regions, especially because the size distribution of explosions is generally much steeper (higher  $b$ -values) than of tectonic earthquakes (Wiemer and Baer, 2000). To estimate the amount of unidentified explosions, we plot a histogram of the time of the day of all events not marked as explosion in the ECOS database (Figure 19). This plot reveals a typical pattern for a quarry blast rich region (Wiemer and Baer, 2000): Detection is best in the nighttime hours (Rydelek and Sacks, 1989), in other words  $M_c$  is lower. The peak during daytime hours around 12 UTC, however, is not explained by improved completeness, but caused by artifacts. From Figure 19 we estimate that the ECOS data contains roughly 500 explosions.

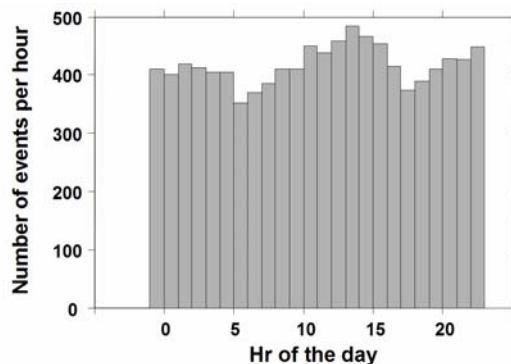


**Figure 19:** Histogram of the hourly activity of the ECOS catalog from 1970–2001. Hours are given in UTC.

To further investigate these explosions, we map the ratio of nighttime-to-daytime

number of earthquakes,  $R$  (Wiemer and Baer, 2000). The map in Figure 20 was computed using sampling volumes of 60 events. Ratios of  $R > 2$ , plotted in blue to purple colors, show a statistically significant (as compared to a uniform probability density function) increased seismicity during daytime hours, and are indicative for the presence of quarry blasts (Wiemer and Baer, 2000). On the other hand, statistically significant low ratios (red colors in Figure 19) could also be indicative of man-made activity (e.g., nighttime underground mining activity). However, their interpretation is less reliable, because they show the same trend as the aforementioned daily variations in  $M_c$  due to daytime noise. An example of the hourly distribution of events in an anomalous region is shown in the inset in Figure 20. To remove the explosion contamination, we follow the iterative approach outlined in Wiemer and Baer (2000). First of all, the most significant anomaly in the entire data set is identified. Its spatial extent is determined based on a maximization of the significance of the ratio  $R$ . For this anomaly, all events in daytime hours are removed. This process is repeated until no  $R$  anomaly remains significant at the 1% level.

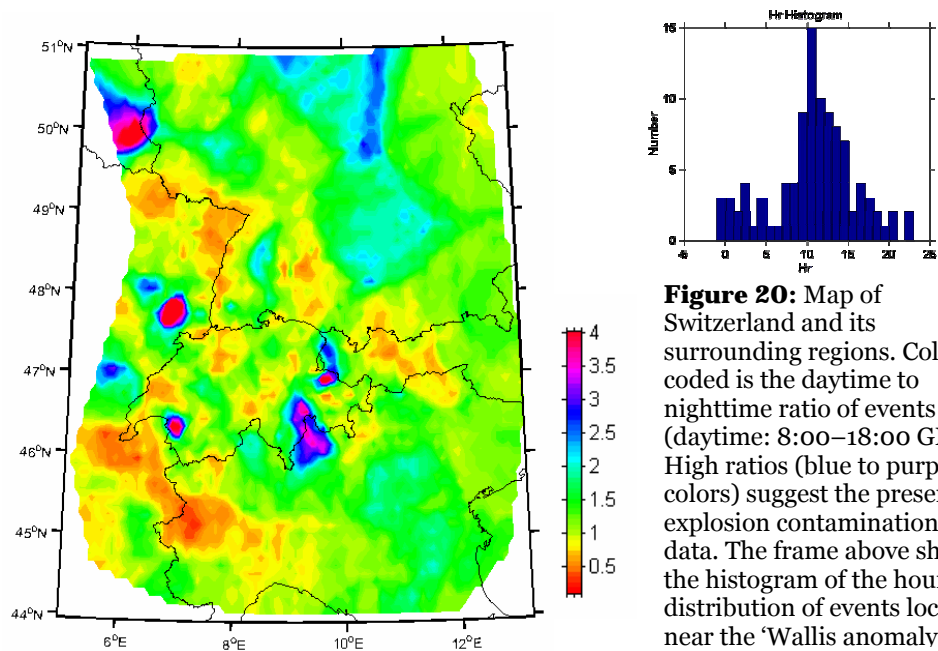


**Figure 20:** Map of Switzerland and its surrounding regions. Color-coded is the daytime to nighttime ratio of events (daytime: 8:00–18:00 GMT). High ratios (blue to purple colors) suggest the presence of explosion contamination in the data. The frame above shows the histogram of the hourly distribution of events located near the ‘Wallis anomaly’.

The final ‘dequarried’ catalog contains fewer earthquakes during daytime hours, because inevitably some daytime tectonic earthquakes are also removed. However, because the removed real event set is independent of magnitude scaling, and presumably follow the true natural size distribution, the effect is only a minor reduction in activity rate for these volumes (Figure 20). It is also limited to the instrumental data. This unavoidable rate reduction is considerably less biasing than the original bias in rate and  $b$ -value caused by the explosions. In an additional step, we also removed manually events near a mining area in France (6.8° W/49.4° N). This region shows an anomalously low daytime to nighttime ratio, and a peculiar

time distribution and magnitude size distribution of events. The numerous events in this region after 1980 correspond almost entirely to mining related activity (J.P. Burg, personal communication, 2002). Our final set of possible quarry explosions that we removed from the data set contains 1037 events in the period 1975–2001.

### ***Declustering the ECOS Catalog***

Declustering attempts to separate the time-independent part of seismicity (background) from the time-dependent or clustered parts (aftershocks, foreshocks, and swarm type activity). For most hazard related studies, it is required that the seismicity behaves in a time-independent fashion (Reiter, 1990; Giardini, 1999; Frankel, 1995). Working with the time-independent dataset (from now on called 'declustered') avoids biasing the average-rate assessments with data from, for example, prominent aftershock sequences that may not be representative of the average behavior of a crustal volume.

As a first test, we investigate whether or not the temporal distribution of events within the ECOS catalog is poissonian (Knopoff, 1964; Gardner and Knopoff, 1974; Reasenber, 1985) which would argue that declustering may not be necessary. Wyss and Toya (2000) addressed the question of stationary behavior most recently: They found that seismicity below 60 km, recorded mainly in subduction zones, is in most analyzed volumes poissonian. Wyss and Toya argue that seismicity can be separated into two parts: A poissonian background and a time dependent, clustered part that is influenced by interaction between events through stress and fluids (e.g., aftershocks). This time-dependent part is, however, much more prominent in shallow crustal environments, where typically more than 40% of all earthquakes are believed to be clustered.

We apply a  $\chi^2$ -test (Taubenheimer, 1969) to a variety of ECOS subsets (in space, magnitude and time) testing for the Null hypothesis: Earthquakes in the ECOS dataset are independent and follow a Poissonian distribution. For all subsets, we find that the Null hypothesis can be rejected at a significance level of 99.9%. Therefore, declustering the dataset is needed.

There is no unique way to separate time-dependent earthquakes from background ones. Their physical properties are the same, and no established statistical criterion exists, mainly because in the scientific community, no definition of what exactly an aftershocks or foreshock is exists. The two categories of events most readily defined are aftershock sequences and foreshocks. Aftershocks are a response of the surrounding crust to the stress change (and/or fluid pressure, etc.) introduced by a mainshock. This activity decays exponentially and is generally well modeled through the modified Omori law (Kisslinger and Jones, 1991; Omori, 1894; Utsu et al., 1995). Foreshocks can either be interpreted as the response of a physical process that ultimately leads to a mainshock, or as mainshocks themselves, with an 'aftershock' which happens to be larger than its preceding 'foreshock' (Agnew, 1991; Hough and Jones, 1997; Jones, 1984; Maeda, 1996; Reasenber, 1999; Reasenber and Jones,

1989). In a statistical sense, aftershocks and foreshock sequences can be treated in much the same way (Reasenbergs and Jones, 1990). There are generally many more aftershocks than foreshocks, but the treatment of individual foreshocks, such as the ~M6.2 foreshock that preceded the 1356 ~M6.9 Basel mainshock by a few hours, may be important for hazard related studies.

Other frequently considered types of time-dependent seismicity are earthquake swarms and doublets. Neither is defined precisely in seismology. In general terms a swarm, different from typical aftershock-foreshock sequences, contains several earthquakes with about the same maximum magnitude (rule of thumb: within 0.3 magnitude units, otherwise, the largest one may be called the mainshock). A swarm can last from minutes to years. Doublets are particular swarms with only two events of similar magnitude.

We explored the two main declustering algorithms used in seismicity studies. The first approach was introduced by Gardner and Knopoff (Gardner and Knopoff, 1974) and has been used in numerous hazard related studies (e.g., Frankel, 1995). It simply defines a space and time window after each event. All subsequent events within this window are declared aftershocks and omitted from the declustered catalog—unless their magnitude exceeds the mainshock's. In this case, a new larger space-time window will be searched and its area omitted. The parameters of the space time window are assumed universal for the entire study region and study period, and are only dependent on magnitude. We explored first of all the original parameters given in Gardner and Knopoff (1974). In addition, we apply window parameters optimized for central Europe by Grünthal (Figure 21), and alternatives given by Uhrhammer (1986) and Youngs et al. (1987). The diversity of the window parameters illustrates again the non-uniqueness of declustering.

The second approach we evaluated is by Reasenbergs (Reasenbergs, 1985), who defines interaction windows in space-time in a somewhat more sophisticated way that attempts to introduce physical properties behind triggering. The spatial and temporal extent of a cluster is not fixed, as it is in the windowing method, but depends on the development of an individual sequence. Several free parameters in Reasenbergs's algorithm determine the degree of clustering that is applied. He optimized these parameters for northern California based on instrumental data. A few attempts have also been made to optimize the parameters for other regions, such as Utah and Japan (Arabasz and Hill, 1996; Wyss et al., 1996).

When comparing the results of the two algorithms in terms of total number of identified dependent events (38.8% versus 47.7%) and in terms of their contribution to the total moment released (0.94 % versus 1.99%), Reasenbergs's and Grünthal's declustering approach vary considerably. However, sensitivity tests show that the difference in terms of resulting hazard is minor. We selected Grünthal's approach as our preferred method, because its parameters are optimized for central Europe and results seem to fit selected recent sequences in Switzerland (Deichmann, personal communication, 2002).

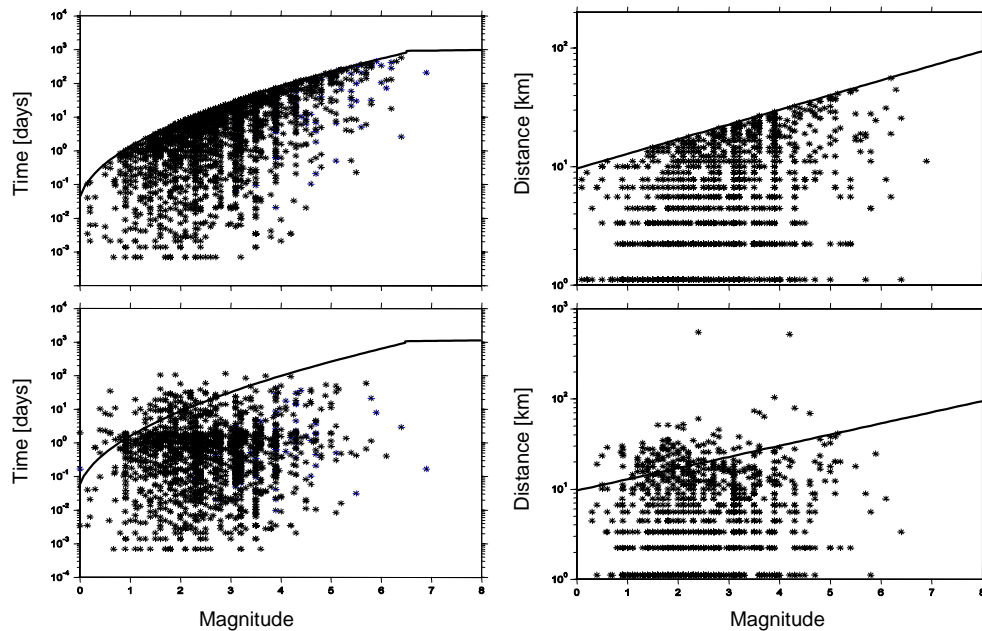


**Figure 21:** Temporal (left column) and spatial (right column) extend of identified dependent events. The top row shows the results based on Grünthal's central Europe parameters, the bottom row the results based on Reasenbergs windowing parameters. The solid lines in the bottom row are the same as in the top and intended for comparison only, since Reasenbergs algorithm does not use fixed windowing parameters.

### ***Estimating Seismicity Rates***

Various approaches have been used to estimate recurrence parameters in the past. The debated questions in this respect, despite the aforementioned issues of completeness, are related to the most appropriate way to determine  $a$ - and  $b$ -values (least squares, weighted least squares, maximum likelihood; see (Bender, 1983)) and to the question to the allowed degree of spatial variability of  $b$ -values. We reviewed the existing literature and found no approach that we found fully satisfying. In light of the recently well established spatial variability in  $b$ -values (Gerstenberger, 2003; Schorlemmer et al., 2004a; Schorlemmer et al., 2004b; Wiemer and Wyss, 1997, 2002), we feel that using an overall constant  $b$ -value, as done in many parts of the USA (Frankel et al., 1997a), is not appropriate. However, we are also very uncomfortable with the sometimes large variability of  $b$ -values seen in regional zonations (Giardini et al., 1999; Jiménez et al., 2003), which we believe are often simply statistical variations due to the small sample sizes investigated (Wiemer and Wyss, 2002). The question of when a regional  $b$ -value versus local ones should be used has in our opinion not been answered systematically before, and here we present a new approach that integrates model selection theory for decision making.

The basic principles of our recurrence rate estimation are:

- *Objectivity and reproducibility.* The rates should be computed in an automatic fashion and reflect significant statistical measures;
- *Principle of simplicity.* We will use a simple model with few parameters unless the data requires a different approach.

To achieve these goals, we develop a multi-step scheme to assess the earthquake-size distribution and activity rate. We use the truncated exponential distribution, which is the earthquake-recurrence relationship most commonly used in PSHA (Cornell, 1968). It is derived from the Gutenberg and Richter (1944) recurrence model by truncating the rate density of earthquakes at a maximum magnitude,  $M_{max}$ . Other recurrence relationships were considered, but ultimately rejected because: 1) there is little evidence for the validity of different recurrence laws in the literature; 2) faults based characteristic models badly fit the source zoning applied in our study. To estimate recurrence parameters with data sets of variable completeness with time, we use Wiecherts approach. In our opinion, using a maximum-likelihood estimator (Aki, 1965; Bender, 1983; Shi and Bolt, 1982; Utsu, 1999) to determine the recurrence parameters is most appropriate, because all available data are weighted appropriately. A least squares, or linear fit, while pleasing to the eye, clearly gives too much weight to the few large events (Bender, 1983; Wiemer and Wyss, 2002).

In a first step, we assess the overall  $b$ -value of the region,  $b_0$ . In regional hazard studies, an overall  $b$ -value is often used in order to stabilize the result by avoiding undue fluctuations of  $b$  particularly in zones of low seismicity (Frankel, 1995; Frankel et al., 1997b). We use  $M_c$  established in the previous section and documented in Appendix 2 in Tables A3 and A4. From the frequency-magnitude distribution of all events within Switzerland or within 100 km of the Swiss border (Figure 22), we can observe that the historical data, particularly for the period 1881–1975, shows a higher activity rate than the instrumental data. We carefully investigated the possibility that a systematic shift in magnitude occurred between instrumental and intensity based data (Braunmiller et al., 2004; Fäh et al., 2003a); however, we could not find such evidence. In addition, we note that the shift in activity between the two periods is only present in some regions, most noticeably in the Wallis. This suggests that this shift is at least partially caused by a true, natural change in activity rate, which is well established for some regions, such as the Wallis, based on macroseismic observations.

Independent of its cause, the change in activity rate causes a complication when estimating recurrence rates: If one ignores the fact that the two periods have different activity rates, or  $a$ -values, then a systematic bias towards a lower  $b$ -value is introduced. This forces us to consider a model that allows not just one  $a$ -value, but two: One for the instrumental, one for the historical data. This model has three free parameters:  $a_1$ ,  $a_2$ , and  $b$  (dashed line in Figure 22). We take its  $b$ -value of 0.90 as our regional  $b_0$  estimation. It is consistent with the slopes observed in both the historical and instrumental data for this region.

### Assessing Recurrence in each Zone

The next step is to assess the recurrence parameters in each zone. Keeping with our objective to only change the overall  $b$ -value when the data requires (or allows) so, and also keeping in mind the possibility that the activity rates between the instrumental and historical data may differ, we design three different models of recurrence. This allows us to capture the uncertainty in recurrence rate estimation. These models are:

- I. Constant  $b = b_0$ , variable  $a$ -value determined on the entire observation period (taking into account the duration of each completeness period). This model has one free parameter (the  $a$ -value).
- II. Variable  $b$ - and  $a$ -value. Here we determine both the best fitting  $a$ - and  $b$ -value (in a maximum-likelihood sense), hence the model has two free parameters.
- III. Constant  $b = b_0$  and two variable  $a$ -values ( $a_1$  and  $a_2$ ): One for the instrumental period (1975–2000), one for the historical period 1300–1975. The average  $a$ -value is then computed as the weighted (for the period length) average of the two  $a$ -values (two free parameters).

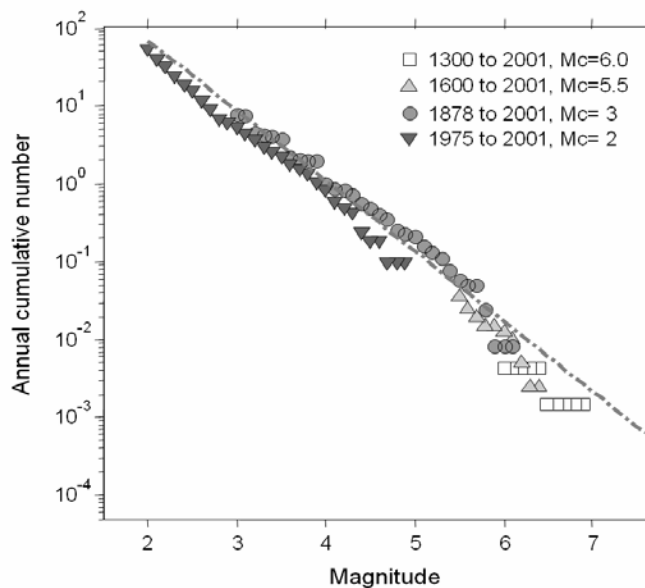


**Figure 22:** Annual cumulative number of events within Switzerland and neighboring regions. The frequency-magnitude distribution is broken down into four completeness periods, as given in the legend. The dashed gray line represents the best fitting model to the data, with a  $b$ -value of 0.90. This value is used as the regional  $b$ -value,  $b_0$ .

We then measure the relative goodness of fit of each model to the data in each zone, and establish relative weights. The fit of each model to the observed data is computed as a likelihood score; however, because the models have different degrees of freedom (i.e., free parameters), these likelihood scores cannot be compared directly. If two models have the same likelihood score, the one with fewer free parameters should be the preferred model, because a simpler model tends to be more robust. The maximum-likelihood estimate (Ogata, 1983) for each model is computed by a constrained nonlinear grid search over the free parameter space, maximizing the log

likelihood function. To find the best fitting model we use the corrected Akaike Information Criterion,  $AIC_c$  (Kenneth et al., 2002):

$$AIC_c = -2 \max(\ln L) + 2(P) + \frac{2P(P+1)}{N-P-1}$$

with  $\log L(a, b)$  being the log-likelihood function,  $P$  the number of free parameters and  $N$  the sample size. In contrast to the original Akaike Information Criterion (Akaike, 1974; Imoto, 1991; Ogata, 1999), the corrected  $AIC_c$  penalizes for the amount of samples, which becomes critical for small sample sizes. The  $AIC_c$  is useful in selecting the best model in the set; however, if all the models are poor,  $AIC_c$  still selects the one estimated to be best, but even that model may be poor in an absolute sense (Kenneth et al., 2002). The model with the lowest  $AIC_c$  is the preferred model. This assures that a model with more free parameters (which implies reduced predictability) is only adopted when the data require doing so. For most zones in our whole-Switzerland model, the first model is preferred ( $b = 0.9 = \text{const.}$ ) and variable  $a$ -value). In the Basel zone and in few other zones, a lower  $b$ -value is preferred. The  $AIC_c$  can also be used to obtain weighted alternative models in order to express the epistemic uncertainties in a logical tree approach. The best model is determined by examining their relative distance to the “truth”. The first step is to calculate the difference between model  $i$  and the model with the overall lowest  $AIC_c$ :  $\Delta_i = AIC_c(i) - \min(AIC_c)$ . The relative weight can then be described as:

$$w_i = \frac{\exp(-0.5 * \Delta_i)}{\sum_{r=1}^R \exp(-0.5 * \Delta_r)}$$

where  $w_i$  are known as *Akaike weights* for model  $i$  and the denominator is simply the sum of the relative likelihoods for all candidate models.

In the Basel area, we are able to use paleoseismological data as a constraint on the recurrence estimates. Integrating these events into the historical and instrumental record, we are able to construct a frequency-magnitude distribution spanning the period 5800 BC–2002 AD (Figure 22). It suggests that the activity can be modeled well using a power-law distribution of earthquakes size. In Figure 23, we show the fit of the three models and their relative weights for eight zones, taken from the SEIS and TECTO models, and for either completeness models 1 or 2. Note that in some cases all three models give almost identical results, while in others the three models differ significantly. All estimated  $a$ - and  $b$ -values are listed in the Appendix in Tables A3 and A4.

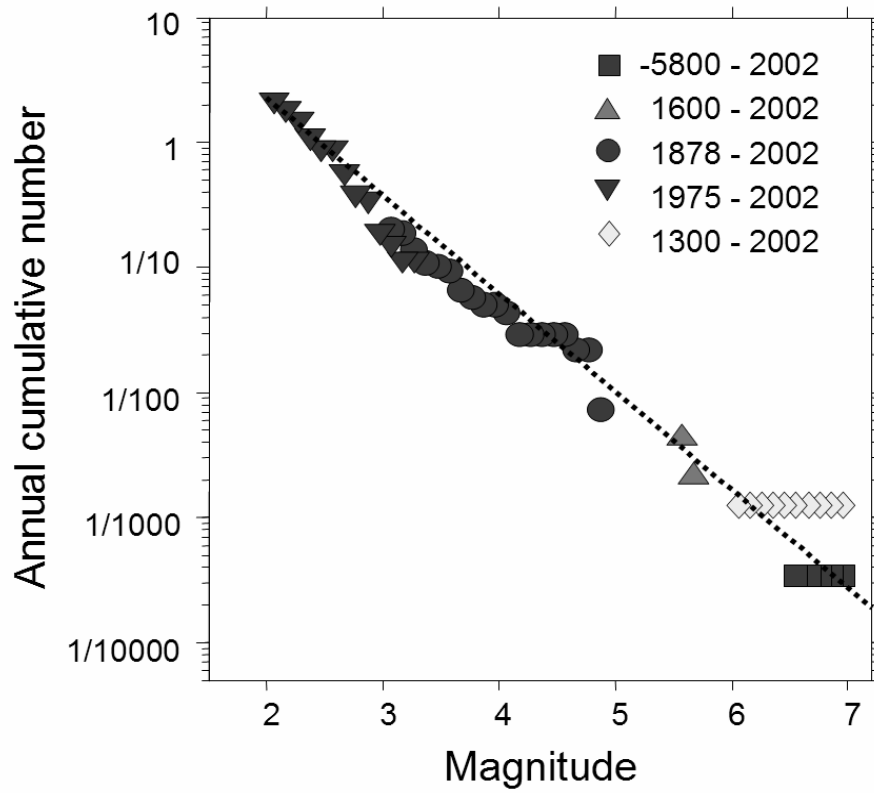


**Figure 23:** Cumulative number of events versus magnitude for the Basel region. Different colored symbols indicate different completeness periods.

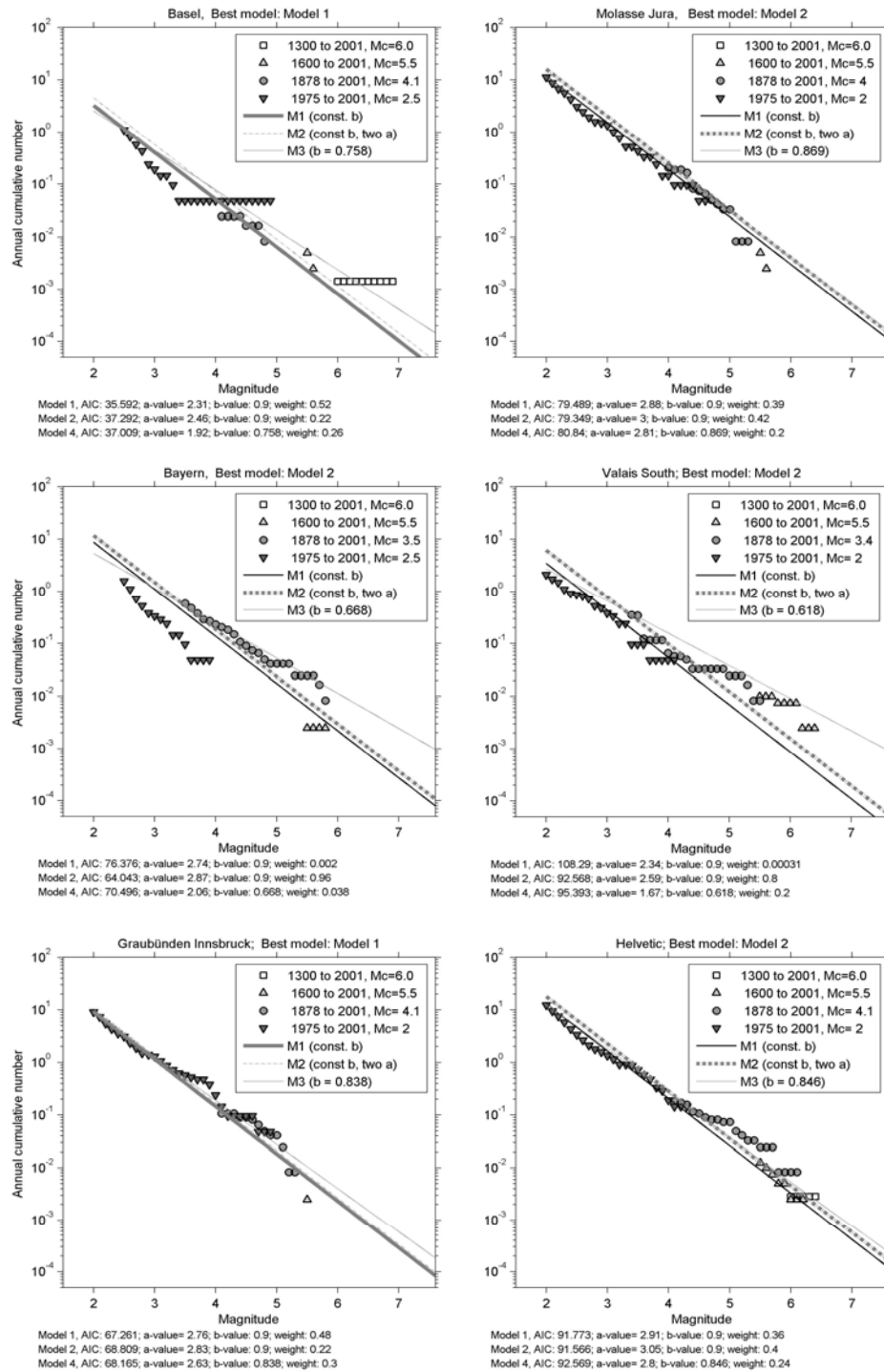


**Figure 24:** Examples of the rate estimation for eight zones from the SEIS and TECTO models. The recurrence parameters, AIC<sub>c</sub> scores, and estimated weights are given in the bottom of each frame.

#### **4.4 Maximum Possible Earthquake**

The maximum possible earthquake,  $M_{max}$ , is recognized as a critical parameter with considerable influence on the final hazard at least for long return period. It is the recurrence parameter the most difficult to assess in the study area, because the physical understanding of  $M_{max}$  is poor and because the database to derive this parameter is statistically very limited. We considered several techniques for estimating or bounding  $M_{max}$  used in past hazard studies: 1) The EPRI approach (Johnston et al., 1994) based on a global database of stable continental regions; 2) regional strain-based constraints (Regenauer-Lieb and Petit, 1997; DeMets et al., 1990); 3) global statistical models (Kagan 1999; Kagan and Jackson, 2000); 4) seismotectonic constraints (maximum available feature) (Coppersmith, 1994; Wells and Coppersmith; 1994); 5) Kijko's numerical approach to assess  $M_{max}$  based on observed seismicity (Kijko and Graham, 1998; Kijko et al., 2001); 6) 'One step beyond' method (e.g., Slejko et al., 1998). In our assessment, none of these provides a convincing and well constrained answer to the  $M_{max}$  problem. We, therefore, decided to first of all derive main guiding principles for our  $M_{max}$  determination:

- $M_{max}$  should be relatively large, because we see no evidence from worldwide studies or seismotectonic constraints that rule out M6 class events in any region of Switzerland. This kind of events may have recurrence rates exceeding 10'000 years in most zones and might not be traceable in the historical or geological record.
- Our  $M_{max}$  assessment should somewhat reflect the uncertainty that exists in this parameter.
- $M_{max}$  should not vary between zones; the choice of  $M_{max}$  is in our opinion a generic one. This reflects the believe that no fundamental differences between tectonic regions exist that would justify a different behavior when it comes to  $M_{max}$ .

To incorporate the principles, and to keep a simplistic model, we use only two different  $M_{max}$  in our model as logic tree branches:  $M_{max} = 7.2$  and  $M_{max} = 7.5$ . This model has the advantage of being simple, yet allowing to capture the influence of  $M_{max}$  for sensitivity analysis. As it will turn out, the hazard sensitivity to  $M_{max}$  is only minor.

## 4.5 Predictive Ground-Motion Models

Ground-motion relations, which estimate peak ground-motions as a function of earthquake magnitude and distance, are critical to seismic hazard assessment. A predictive ground-motion model (PGMM) describes the attenuation of amplitude with distance due to geometrical spreading and intrinsic attenuation as well as the scaling of amplitude with magnitude. Commonly referred to as ‘attenuation laws’, PGMM is generally the parameter with the largest influence on the final hazard results. It also is generally the largest contributor to uncertainties in hazard.

Ground-motion relations require a calibration for the region of interest, because of commonly observed strong differences between diverse seismotectonic regimes, crustal structures, earthquake scaling, and site conditions. A number of ground-motion relationships have been proposed for central Europe in the last two decades. Most studies adopt a functional form introduced by Joyner and Boore (1981), with a constant geometrical spreading for all distances (e.g., Sabetta and Pugliese, 1987 (Italy); Ambraseys et al., 1996 (Europe); Smit, 1996 (Switzerland)). Smit’s work, targeted to estimating ground-motion in Switzerland, is restricted to Fourier Spectral and Peak Ground Accelerations. Because horizontal component data were insufficient, Smit (1996) applied a generic factor ( $H/V = 1.5$ ) to derive the attenuation of horizontal ground-motion from vertical ground-motion. A different approach, recently applied by Malagnini *et al.* (2000 a,b) in Italy and Germany as well as by Malagnini and Herrmann (2000) in Italy, uses a stochastic simulation method (McGuire and Hanks, 1980; Hanks and McGuire, 1981; Boore, 1983, Yazd, 1993; Raoof et al., 1999) to predict ground-motions.

Recently, a dedicated study of attenuation and scaling for Switzerland was published by Bay (2002) and Bay et al. (2003, 2004). Following the approach by Malagnini et al. (2000a, b) and Malagnini and Herrmann (2000), Bay et al. modeled spectral ground-motion (1 to 15 Hz) as a function of distance for events spanning the magnitude range  $3.0 < M_w \leq 7.0$  in Switzerland. The parameters required to simulate ground-motion with a stochastic approach were inverted from 2958 horizontal- and vertical-component waveforms of small to moderate size events ( $2.0 \leq M_L \leq 5.2$ ) in the distance range 10–300 km, recorded on hard rock sites with an estimated shear-wave velocity of about 1500 m/s in the upper 30 m. The parameters determined in the attenuation model are response-spectral displacements, pseudo-spectral velocities and pseudo-spectral accelerations (Boore, 2001, 2003).

Developing ground-motion relationships in areas of moderate seismicity such as Switzerland is complicated by scarce data for larger events. In such areas, it is therefore particularly important to quantitatively assess uncertainties in ground-motion scaling. Uncertainties in ground-motion and resulting uncertainties in seismic hazard tend to be larger in areas of low to moderate seismicity than in regions of higher activity. Uncertainties are commonly separated into aleatory and epistemic components (e.g., Toro et al., 1997). Aleatory uncertainties (natural randomness)

reflects the intrinsic variability of ground-motion and cannot be reduced with more or better observations. By contrast, epistemic uncertainties result from inaccurate or incomplete information and can be reduced or eliminated given better models or additional observations. In Bay et al. (2003, 2004), epistemic uncertainty is caused mainly by the lack of large events in the observational data set.

From Bay et al. (2003, 2004), we compile a set of three predictive ground-motion models that in our assessment adequately describe the uncertainty in ground-motions in Switzerland. We distinguish between the two parts of a ground-motion model. 1) The true attenuation part, which we consider well described by the model given by Bay et al. (2003, 2004), because intrinsic attenuation and geometrical scaling are assumed to be scale invariant. A normalized plot of the frequency-dependent attenuation as a function of distance is shown in Figure 25. 2) The scaling with magnitude, on the other hand, may be poorly constrained based on the small to moderate events in Switzerland. Here we use scaling relationships derived for other regions where large events have occurred.

Earthquake scaling is a currently much debated topic in seismology. It is critical when extrapolating towards larger magnitude events (McGarr, 1999; Mayeda and Walter, 1996; Ide and Beroza, 2001; Ide et al., 2003). The critical scaling parameter often referred to is ‘stress drop’,  $\Delta\sigma$ , or ‘apparent stress drop’ (Brune, 1970; Choy and Boatwright (1995), which is only somewhat related to the actual physical drop in stress during an earthquake (Mayeda and Walter, 1996; Ide and Beroza, 2001). Even in areas with excellent monitoring and with data sets containing several large events, such as California or Japan, it remains currently hotly debated if stress drop is constant or scales with magnitude. Bay et al. (1993) proposed a set of scaling models that are able to explain the small stress drop ( $\Delta\sigma \approx 3$  bars) observed for very small events in Switzerland, but is consistent with observed damages from larger events and with worldwide scaling relationships. We use the three scaling models as input for the hazard computations in order to express epistemic uncertainty:

1. Increasing stress drop to a maximum of  $\Delta\sigma \approx 30$  bars. In this model, which best fits the Swiss data at small magnitudes, stress drop scales proportionally to moment as  $M_o^{0.25}$ . The upper bound for this increase is set to a stress drop of  $\Delta\sigma \approx 30$  bars, as it is found from a compilation of worldwide studies (Ide and Beroza, 2001).
2. Same as model 1, but increasing to a maximum value of  $\Delta\sigma \approx 50$  bars. This model assumes that the largest events may have a higher than average stress drop.
3. Constant stress drop of  $\Delta\sigma \approx 30$  bars for all magnitudes. This model does not fit small magnitude seismicity in Switzerland well; however, it is a viable alternative for the hazard relevant event with  $M \geq 5.0$ , where no Swiss data is available.

The three alternative models are shown in Figure 26. In each frame, we plot attenuation as a function of distance for a given magnitude. We also considered using alternative European attenuation functions, such as the often used Ambraseys et al. (1996); however, we felt that it would not be appropriate, because:

- The site class of Ambraseys is quite different, his reference rock has a shear-wave velocity in the upper 30 m that is about half of the one estimated for our sites. While a conversion to a reference site is possible, it adds additional uncertainty.
- The magnitude scales considered are different. While Ambraseys  $M_S$  measurements can be converted to  $M_w$ , which again adds additional uncertainty, this is difficult for magnitudes below 5.0, where  $M_S$  is not well defined. Such small events contribute significantly to the hazard in countries of moderate seismicity. We feel that using a PGM model that is derived based on the same magnitudes used for recurrence estimation is most appropriate, because we are at internally consistent.

- The events considered and the tectonic environment are quite different. The majority of Ambraseys earthquakes stem from the Mediterranean area. Attenuation is different in Switzerland (Figure 25), Ambraseys PGMM does not well fit the Swiss data in terms of attenuation or scaling of small events.

In Figure 26, we plot for comparison the three considered PGMMs and Ambraseys et al. (1996). For most distances, Ambraseys PGMM shows significantly higher ground-motions; however, for distances of less than about 10 km, the Swiss models exhibit higher ground-motions.

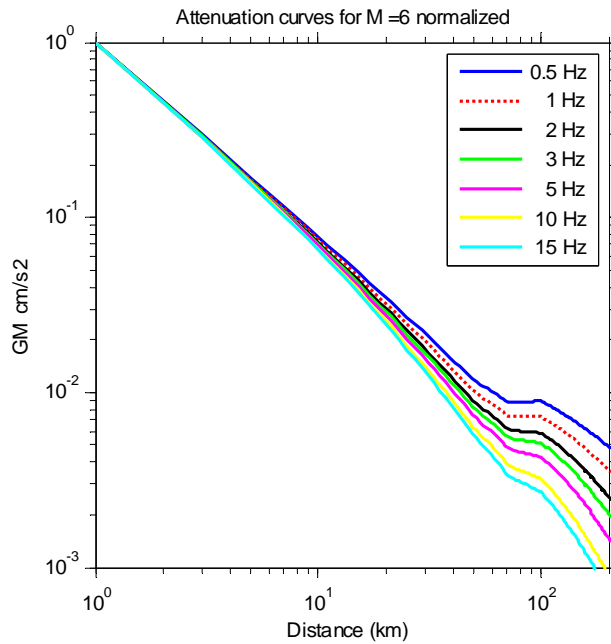


**Figure 25:** Attenuation of ground-motion as a function of distance, based on Bay et al. (2003, 2004). Amplitudes are normalized to 1, the assumed magnitude is 6. Different frequencies are plotted as different colors.

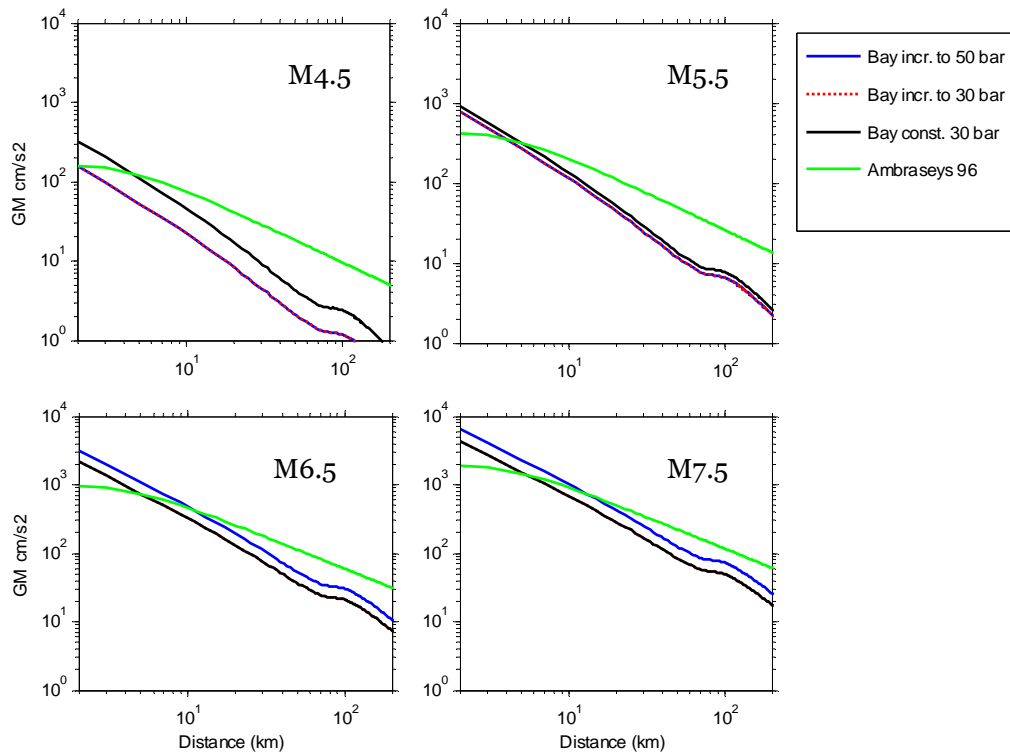


**Figure 26:** Predictive ground-motion relations at 5 Hz. Shown is the ground-motion in [cm/s²] as a function of distance for four ground-motion relationships. Each frame shows one assumed magnitude.

### ***Aleatory Uncertainty of PGMM***

The aleatory uncertainty of the PGMM of Bay et al. (2004) includes parametric and modeling uncertainties. The parametric uncertainty,  $\sigma_{lg}$  accounts for event-to-event variations due to source, path and site properties. The modeling uncertainty,  $\sigma_{lg,model}$ , is determined from the misfit between modeled ground-motion data and recorded data; it includes residuals due to physical processes not included in the model (EPRI, 1993; Toro et al., 1997). Bay et al. (2004) computed an average  $\log_{10} \sigma_{lg} = 0.35$ . Note, however, that this value includes scatter from source, path, and site effects. We feel that we are not able to divide  $\sigma_{lg}$  into intra- and inter-event contributions, or reduce the site contamination, because the available database is too sparse. When computing site specific hazard, however, one has to be careful to consider that  $\sigma_{lg}$  already contains a sizeable (but unknown) site uncertainty component. We also somewhat arbitrarily truncate the uncertainty distribution of the PGMM at  $2 \sigma_{lg}$ . The true shape of the uncertainty distribution is unknown, but it is unlikely to be a Gaussian out to several standard deviations, because the resulting ground-motions are unphysically high (Bommer et al., 2004). This truncation has little impact on the median or mean hazard results; however, it becomes relevant for very low probability scenarios and for the uncertainty estimates.

A final decision regarding the PGMM involves the shape of the model for very small distances. The PGMM cannot continue to increase proportionally to  $1/r$ , because the associated ground-motion would approach infinity. No data are available for Switzerland to constrain this roll over distance,  $r_{min}$ , and very little data exists with hypocentral distances below 2 km worldwide. Recent results from borehole strong motion sensors in Japan, however, suggest that the recorded values of ground-motions very close to the source are still increasing. Therefore, we feel that it is not appropriate to clip ground-motions already at distances of approximately 10 km, as it is done, for example, in Ambraseys et al. (1996) (Figure 26). Because  $r_{min}$  is uncertain, we considered treating it as such through a logic tree branch, which allows us to also study the sensitivity of the results to this parameter. In our final model, we only use  $r_{min} = 1$  km, since sensitivity analyse showed only a minor influence of  $r_{min}$  on hazard for the return periods we considered.

## 5 Hazard Computation and Results

### 5.1 Monte - Carlo Simulation Approach

Various computer codes to estimate seismic hazard based on a Cornell-type approach (Cornell, 1968) are available, some commercial, some open source (Bender and Perkins, 1987). For a number of reasons given below, we decided to develop our own Matlab-based Monte-Carlo implementation of the Cornell method to compute probabilistic seismic hazard for Switzerland and its uncertainty. Our method is in principle identical to that of Musson (2000). The reason for preferring the Monte-Carlo approach are in Musson's words:

*„The input required for a seismic hazard study using conventional Probabilistic Seismic Hazard Assessment (PSHA) methods can also be used for probabilistic analysis of hazard using Monte-Carlo simulation methods. This technique is very flexible, and seems to be under-represented in the literature. It is very easy to modify the form of the seismicity model used, for example, to introduce non-Poissonian behaviour, without extensive reprogramming. Uncertainty in input parameters can also be modelled very flexibly— for example, by the use of a standard deviation rather than by the discrete branches of a logic tree. In addition (and this advantage is perhaps not as trivial as it may sound) the simplicity of the method means that its principles can be grasped by the layman, which is useful when results have to be explained to people outside the seismological/engineering communities, such as planners and politicians.“*

Building a hazard input model is a complex and error-prone procedure. To us, the simplicity of the Monte-Carlo approach and its flexibility are of great importance—the Matlab code we developed contains only a few hundred lines of code. Its disadvantage—somewhat longer computing times—is of lesser importance given the speed of modern workstations. Our code was validated against outputs of Frisk88 (Georisk Eng.) for selected input models, which gave identical hazard curves for the same set of simple input models. An additional advantage of developing our own code is that we are able to distribute the code freely. The code and the input parameters are available for download from our web site [www.seismo.ethz.ch](http://www.seismo.ethz.ch).

The process of hazard computation for a given frequency, including the logical tree branching, follows these four steps:

1. Create a synthetic catalog of earthquakes, based on the  $a$ ,  $b$  and  $M_{\max}$  parameters in each source (Appendix 2, Table A3). The catalog spans 1 million years and contains events down to magnitude 4.0, typically 2 million events. The depths of events are explicitly given, following the distribution shown in Figure 10. Alternative  $a$ - and  $b$ -models and their weighting are considered within each catalog by creating subcatalogs of a duration that corresponds to the  $AIC_c$  weighting factor (e.g., weight 0.6 = 600'000 years). Thus, to each

- source corresponds three branches for the different weighting of the recurrence parameters and  $M_{max}$ .
2. Alternative source zonations, completeness and  $M_{max}$  models result in alternative catalogs, a total of 8 in our case ( $2 \times 2 \times 2 = 8$  branches). One example of such a catalog and its frequency-magnitude distribution is shown in Figure 27.
  3. Three alternative predictive ground-motion models at a given frequency  $f_i$  result in 3 branches. We also draw 100 times randomly an uncertainty of the attenuation function from a distribution with mean zero, standard deviation 0.35, truncated at two standard deviations.
  4. Each earthquake  $E_i$  from the catalog creates a ground-motion  $Y_i$  at the receiver site  $R_i$ . We rank these ground-motions in descending order starting with the highest observed ground-motion in any one-year period. From these, we can readily extract the annual probability of exceedance for any given probability level. For example, at  $10^{-3}$  probability, we look for the 1000th events in the order. Alternatively, we can find the annual probability of exceeding a given ground-motion by counting all instances of ground-motion reaching or exceeding the given threshold and dividing by the length of the catalog.

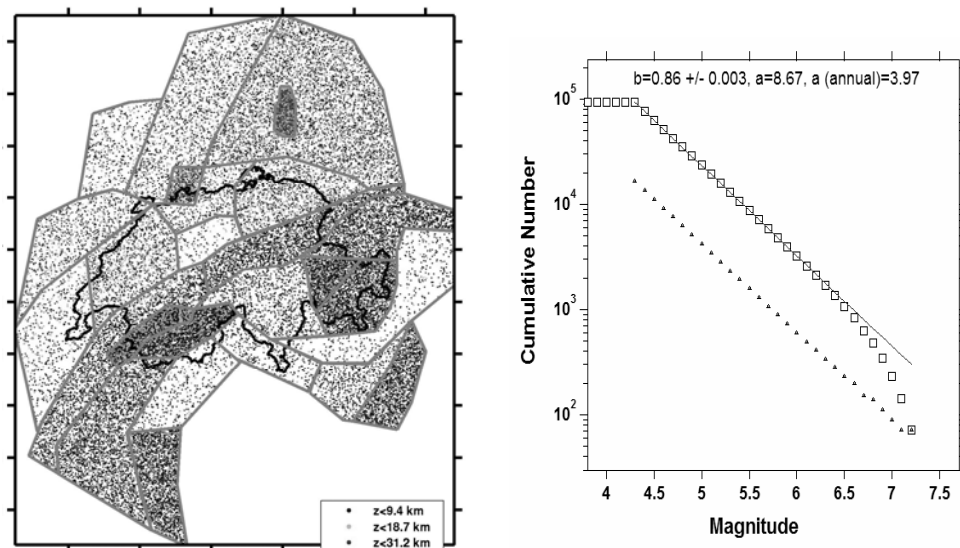


**Figure 27:** Example of a synthetic catalog. (Left) Map of epicenters and sources zones used in model SEIS. (Right) Cumulative frequency-magnitude distribution of events. In this case,  $M_{max}$  was assumed 7.2. Note that for plotting purposes, the catalog in this figure contains only 50'000 years, and the map only displays events with  $M \geq 5$ .

The total number of alternative branches considered is 72, and 72'000 measurements of probability or ground-motion at a given site are computed in total. From these, we compute the median hazard and any desired fractiles, for example the 14 and 84 percentiles that represent the one-sigma standard deviation. Our logic tree setup

including the weights of all branches is shown schematically in Figure 28. To compute hazard maps, this procedure is repeated for all nodes spaced evenly on a 5 x 5 km grid covering Switzerland. Implemented on a modern PC or workstation, a hazard curve for a given site is computed in about 10 minutes. The process is readily parallelized on any coarsely granular cluster of computers, resulting in a performance gain linear to the number of computers available.

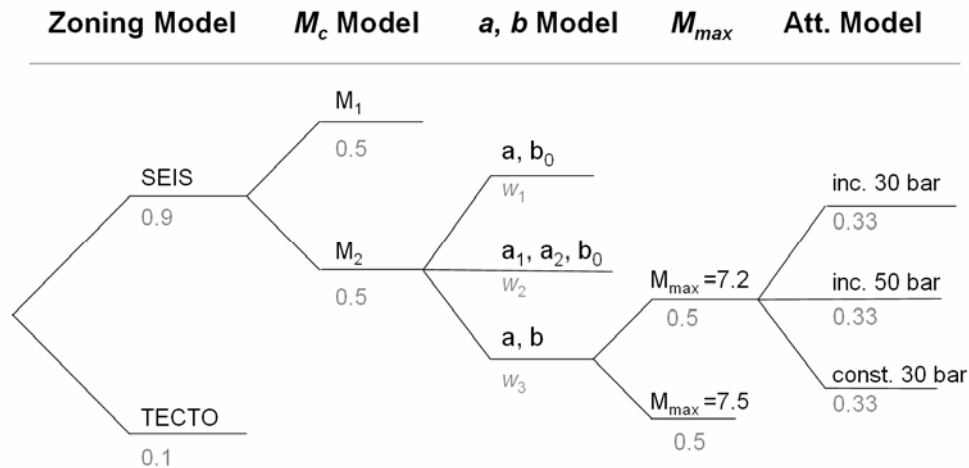


**Figure 28:** Logic-tree setup for the SED 2004 hazard model. Weights for each branch are given in gray beneath the branch. For the  $a$ - and  $b$ -value estimation, the weight ( $w$ ) is zone dependent, as explained in Chapter 4.

## 5.2 Hazard Results

In this Section, we present selected results from our analysis of seismic hazard in Switzerland. The complete set of results is presented on our web page [www.seismo.ethz.ch](http://www.seismo.ethz.ch), where it can be downloaded. We compute and show only ground accelerations in units of 5% damped acceleration response spectrum at a given frequency. Ground velocities or displacements could also be computed, using the PGMM of Bay et al (2004). We choose the frequency of 5 Hz as representative, because it corresponds to the portion of the spectrum where the local soil conditions are likely to enhance seismic motion and to the resonance frequency of 2-5 story buildings, which represents the largest contributor to the building stock of Switzerland.

First of all, we plot seismic hazard curves (annual probability of exceedance as a function of ground-motion) for four selected sites in Switzerland, the locations of Basel, Sion, Zurich and Geneva (Figures 29 and 30). Plotted are the median hazard curves and the 16 and 84 percentiles, representing the one standard deviation. About half of the uncertainty distribution is a result of the sigma of the attenuation

functions. As expected, results show the highest hazard at Sion in the Wallis, where historically (Figure 3) most of the damaging events have been located. The hazard curve for Basel is lower; however, it is well within one standard deviation of the Sion curve and, therefore, the difference is not statistically significant. Results for Geneva and Zurich are nearly identical and significantly lower than for Sion or Basel. We also present uniform hazard spectra (Figure 31) for eight sites in Switzerland for the frequency range 0.5 – 10 Hz. At all sites, the spectra show a gradual increase of expected ground acceleration with frequency up to 10 Hz.

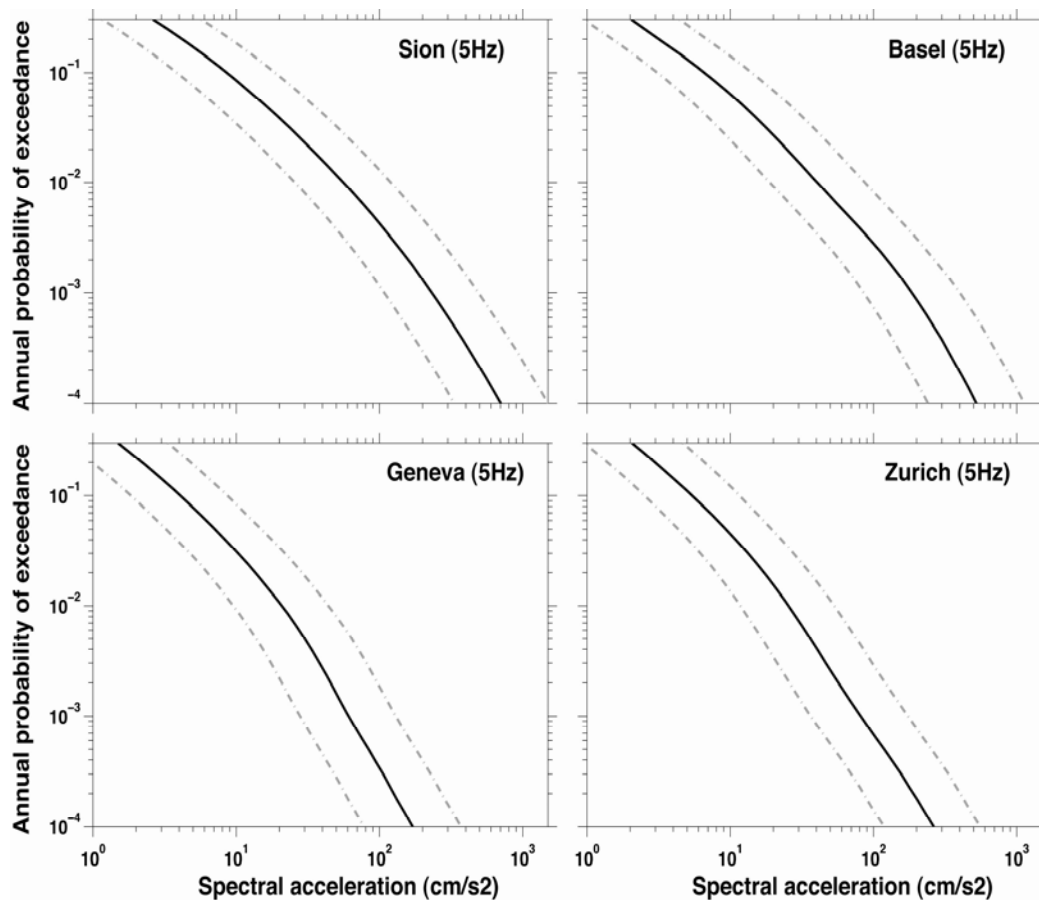


**Figure 29:** Hazard curves for four cities in Switzerland. Plotted is the annual probability of exceedance as a function of ground acceleration in units of 5% damped acceleration response spectrum at 5 Hz.

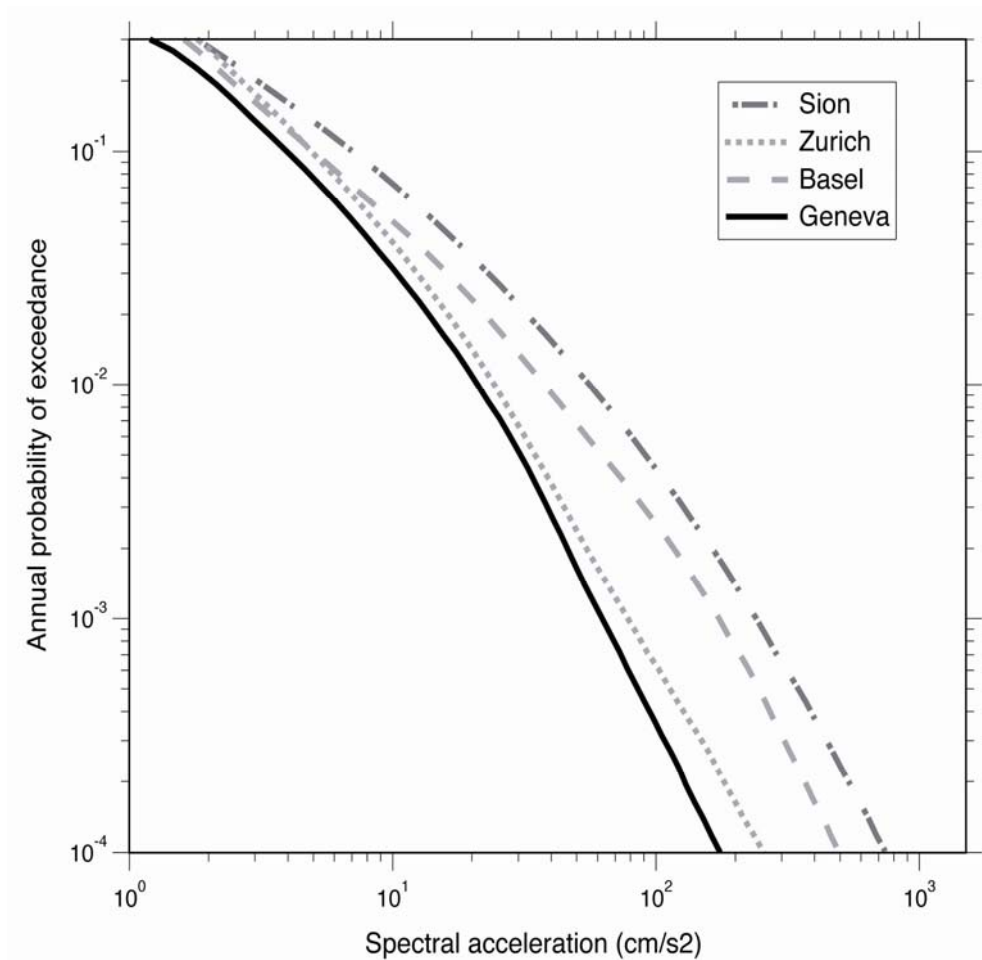


**Figure 30:** Comparison of hazard curves for four cities in Switzerland, taken from Figure 29.

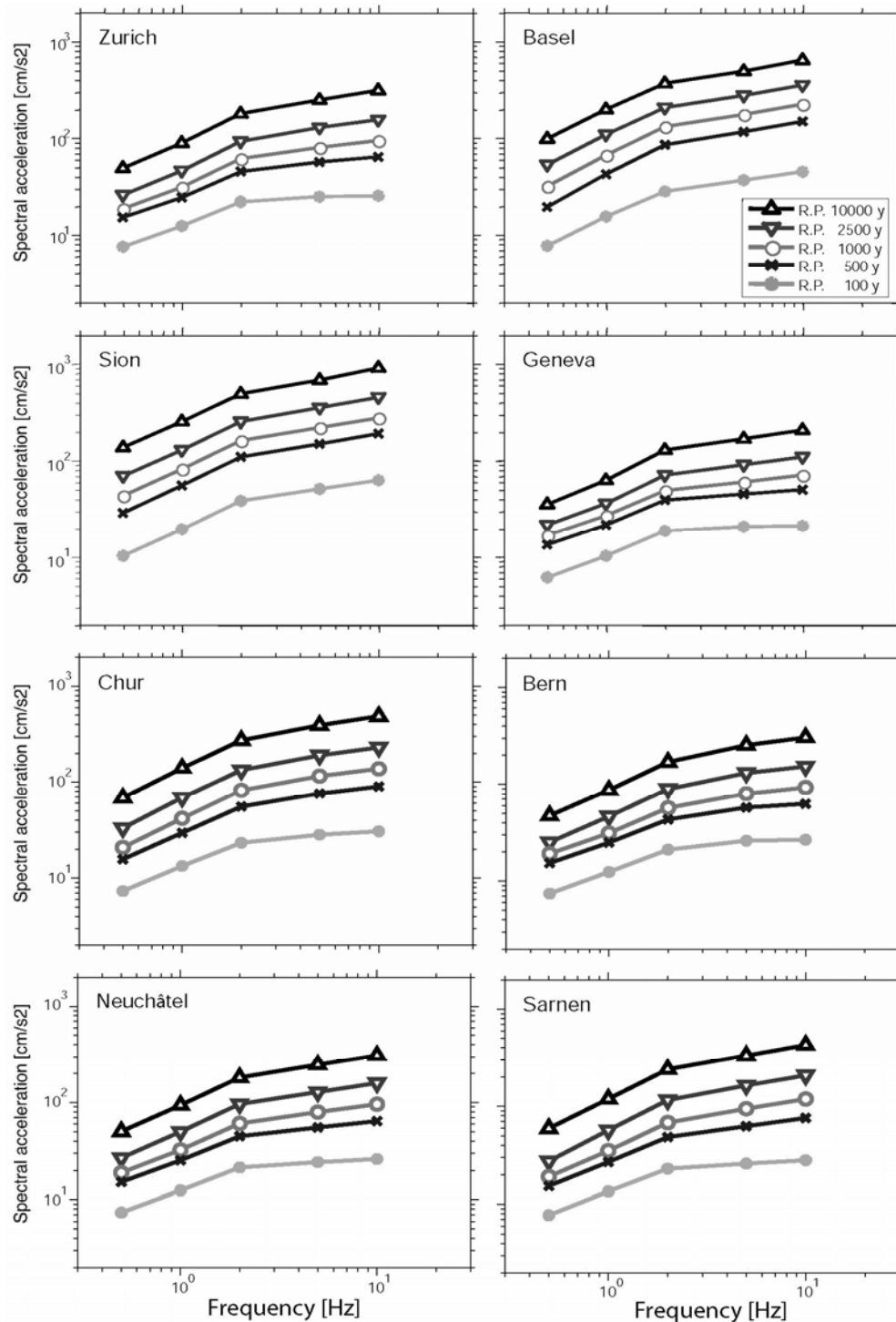


**Figure 31:** Uniform hazard spectra for eight cities in Switzerland. Plotted are the ground accelerations in units of 5% damped acceleration response spectrum as a function of frequency. The spectra are computed for return periods (R.P.) of 100, 500, 1000, 2500, and 10'000 years.

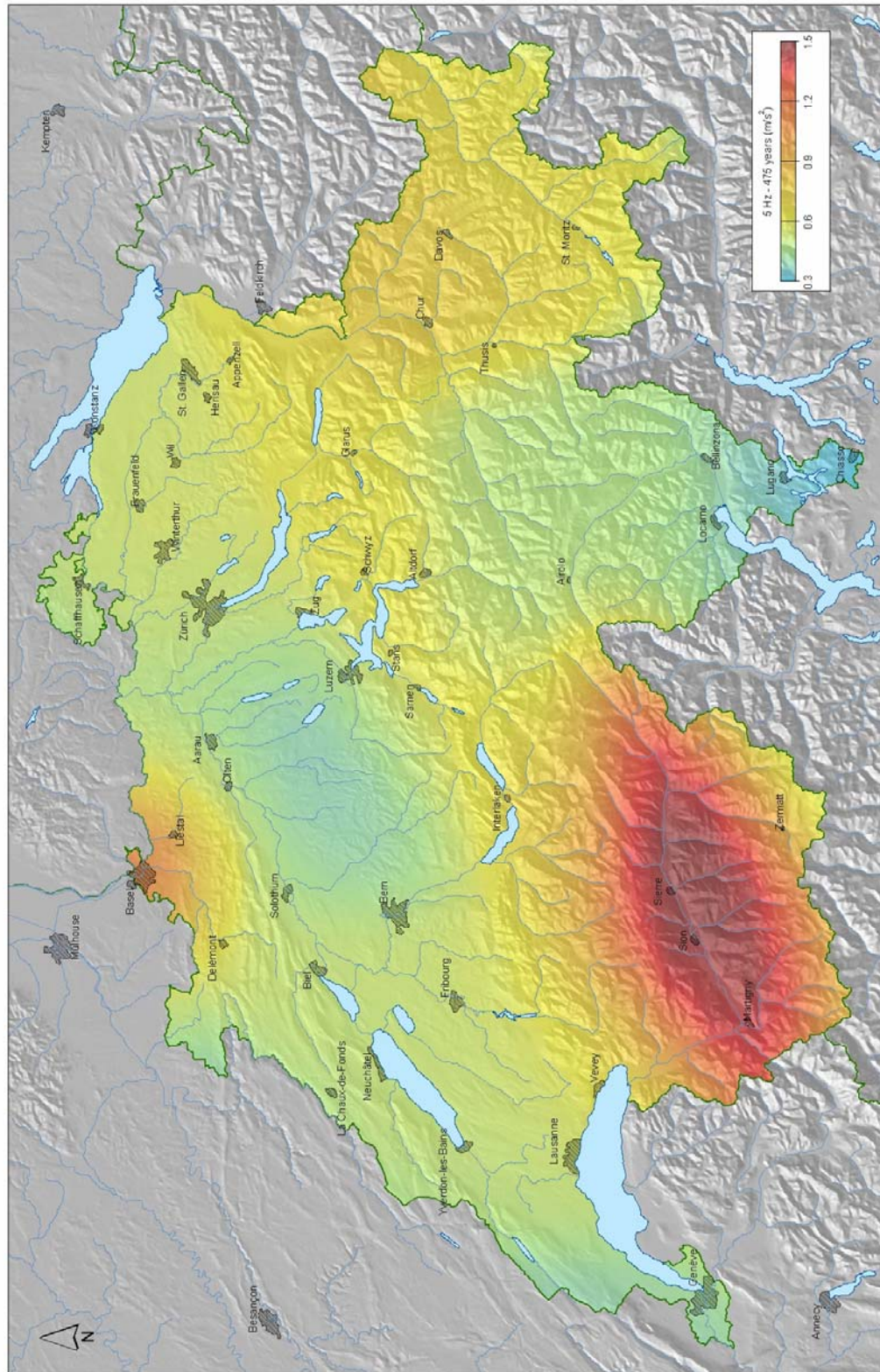
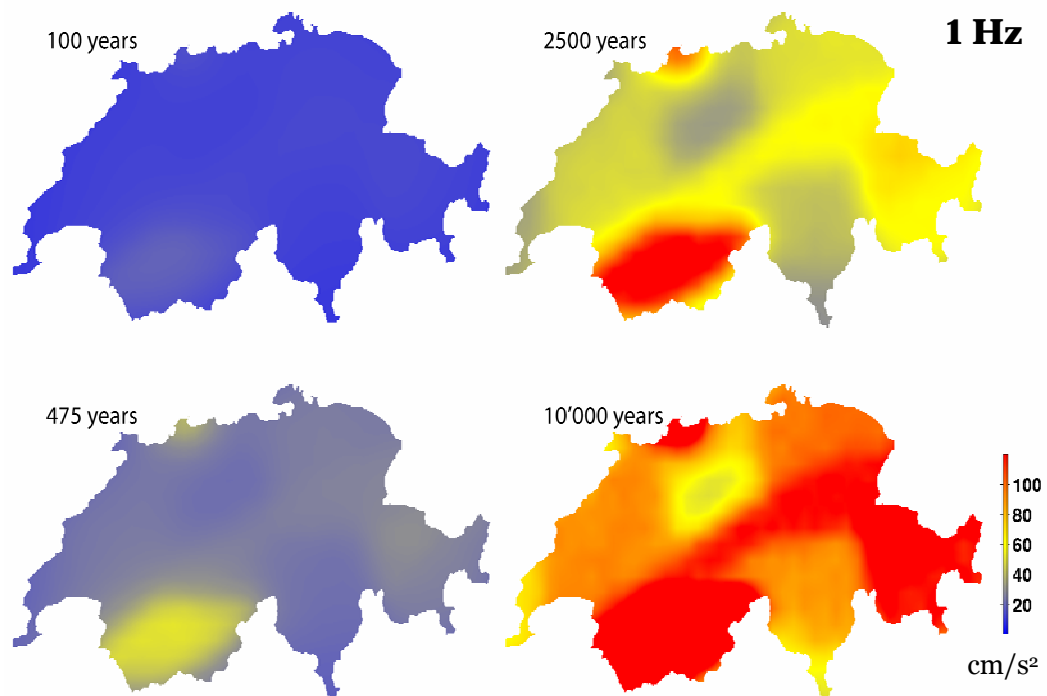
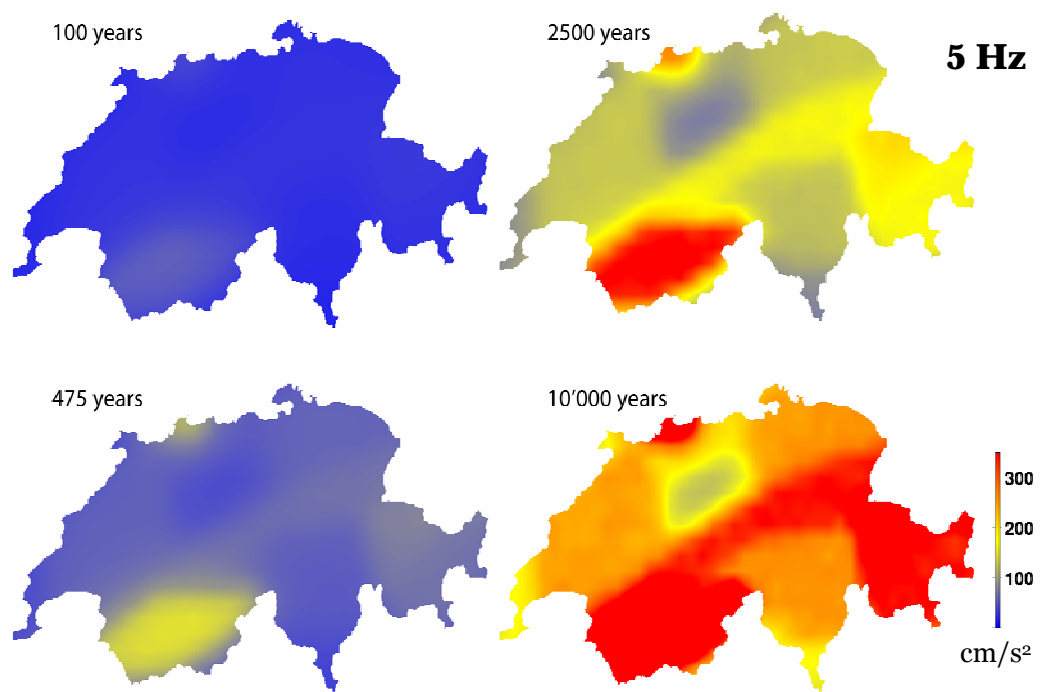


**Figure 32 (previous page):** Seismic hazard map of Switzerland, depicting the level of horizontal ground-motion in  $\text{cm/s}^2$  (in units of 5% damped acceleration response spectrum at 5 Hz frequency) expected to be reached or exceeded in a period of 475 years (10% exceedance chance in 50 years). The map is calibrated for a rock ground condition ( $V_s$  approximately 1500 m/s). Overall, the hazard level of Switzerland ranges between 5 and 15% of the acceleration of gravity (50-150  $\text{cm/s}^2$ ). This level of hazard qualifies as intermediate at global scale. This map is also available in poster size (contact: [info@sed.ethz.ch](mailto:info@sed.ethz.ch)).

**Figure 33 (next page):** Same as Figure 31, but for return periods of 100, 475, 2500, and 10'000 years. The top four frames are results for 5 Hz, the bottom 4 reflect results at 1 Hz. Note that the scale ( $\text{cm/s}^2$ ) for the longest return period is clipped, in order to use just one scale. The maximum value reaches 713  $\text{cm/s}^2$ .



Hazard maps (in units of 5% damped acceleration response spectrum (in  $\text{cm/s}^2$  at 5 Hz and 1 Hz frequency) are shown in Figures 31-33 for return periods of 100, 475, 2500 and 10'000 years. The maximum ground-motions observed at 5 Hz are 52, 151, 361 and 713  $\text{cm/s}^2$ , respectively, and located in the Wallis. Other areas of increased hazard are located in the Basel region, along the Helvetic Front and in Graubünden. The maps are calibrated for a rock ground condition (approximately a shear wave velocity of  $V_s=1500$  m/s in the upper 30 m). For softer soil conditions, site amplifications must be considered and can be on the order of a factor of 2-4 with respect to hard rock conditions (Fäh et al., 2003b). With longer return periods, hazard is more concentrated in the areas of highest hazard, the Wallis and Basel. In other words, the difference between the lowest hazard areas in Switzerland, the Ticino, and the highest hazard area, the Wallis, increases from about a factor of two for return periods of 100 years, to a factor of seven for return periods of 10'000 years. This is a result of the lower  $b$ -values in the high hazard areas in some models (Appendix 2, Tables A3 and A4), which become increasingly relevant for longer return periods. Hazard maps for a frequency of 1 Hz are shown in Figure 33. Their values of course, are much lower than the ones for higher frequencies. In addition, one notices that the hazard is slightly less concentrated, which is a result of the reduced slope of the attenuation function at lower frequencies (Figure 25).

Relative uncertainty in percent

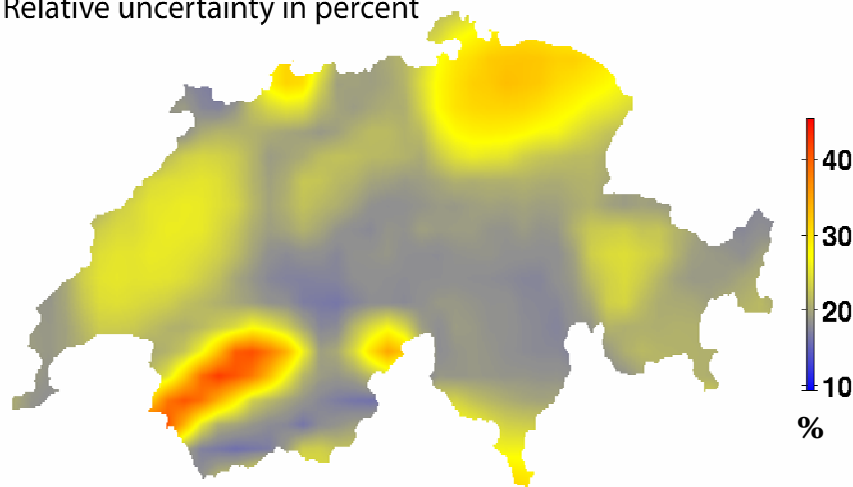


**Figure 34:** Map of the relative uncertainty (in percent) in the forecasted ground-motion. The maps are based on a 475 year return period and 5 Hz frequency. Aleatory uncertainties in attenuation are not included.

In Figure 34, we show the one-sigma uncertainty in percent, computed for a return period of 475 years and 5 Hz frequency (Figure 32). We show the uncertainty without taking into account the aleatory uncertainties in PGMM, because this contribution dominates the uncertainty distribution and would mask the spatial variation of

uncertainty due to the other parameters. Plotted is the value of the 84 percentile minus the 16 percentile. The average uncertainty is about 25%. We see that the largest uncertainty (about 40%) exists in the northern part of the Wallis. Here, differences in the zoning models TECTO and SEIS and differences in the rate models create larger than average uncertainties. Likewise in northeastern Switzerland, differences in zoning and  $b$ -value estimation result in above average uncertainties.

### ***5.3 De-aggregation of Hazard Results***

De-aggregation of hazard is required to understand what types of events contribute the most hazard for a given site. By specifying either a return period, or a design ground-motion, one determines from which magnitude and distance range the hazard to a site stems. The results of the de-aggregation depend on the site of interest. We choose three sites: Sion, Basel, and Zurich.

The general trend of all de-aggregation results is that for longer recurrence intervals the main hazard contribution comes from larger events and closer-by distances. The overall shape of the de-aggregation plots is determined by the attenuation law while the spread of the values is largely a result of the sigma of the attenuation law.

For Sion, we find that for a recurrence period of 100 years (ground-motion 53 cm/s<sup>2</sup>), most hazard is contributed from magnitude 4–5 events at distances of 5–15 km (black squares in Figure 35). However, larger distances and magnitudes also contribute (gray squares). For 475 years (ground-motion level of 151 cm/s<sup>2</sup>), magnitude 5.0–6.0 events dominate. At 2500 and 10'000 years (ground-motion levels of 368 and 708 cm/s<sup>2</sup>, respectively), we find that most hazard is still contributed from magnitude 5.0–6.5 events at distances of 5–10 km. However, at these large ground-motion levels, nominally small events of class M5 or smaller contribute significantly to the hazard; these events would be very close to the site, and thus cause unusually large ground-motions.

For Basel and Zurich the results are quite comparable. A larger contribution to the hazard comes from deeper events, which is a result of the greater hypocentral depths in the Foreland compared to the Alps (Figures 36 and 37). For return periods of 2500 and 10'000 years, for Basel we see a larger contribution from the higher magnitude range, similar to the Sion case. It is interesting to note that even for long return periods, the rare largest events ( $M \geq 7$ ) are not a significant contributor to design hazard.

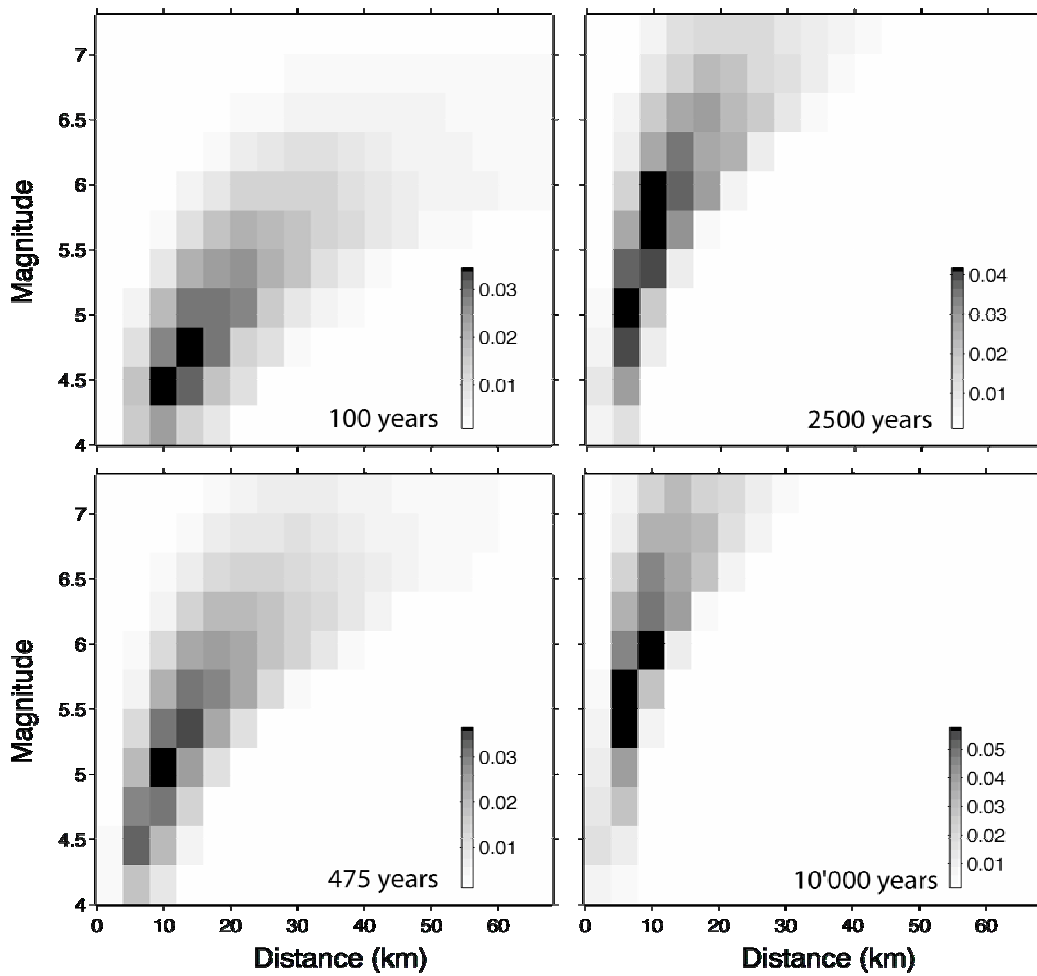


**Figure 35:** De-aggregation results for the site of Sion. The gray-scale shows the fractional contribution of each magnitude-distance bin. The different frames show four return periods: 100, 475, 2500, and 10'000 years.

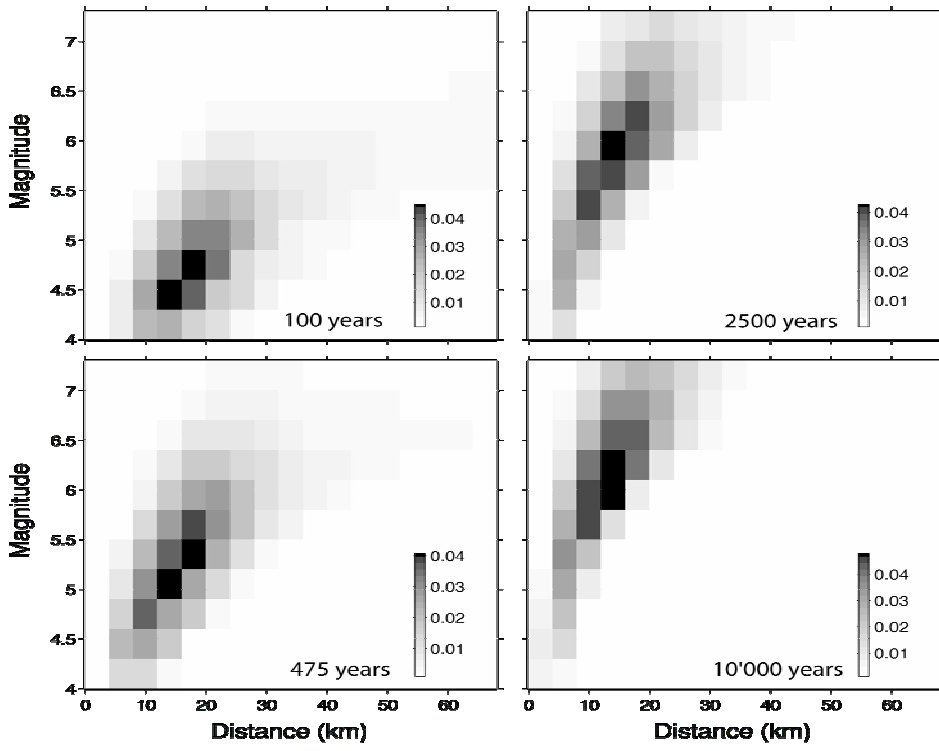


**Figure 36:** Same as Figure 35 but for the site of Basel.

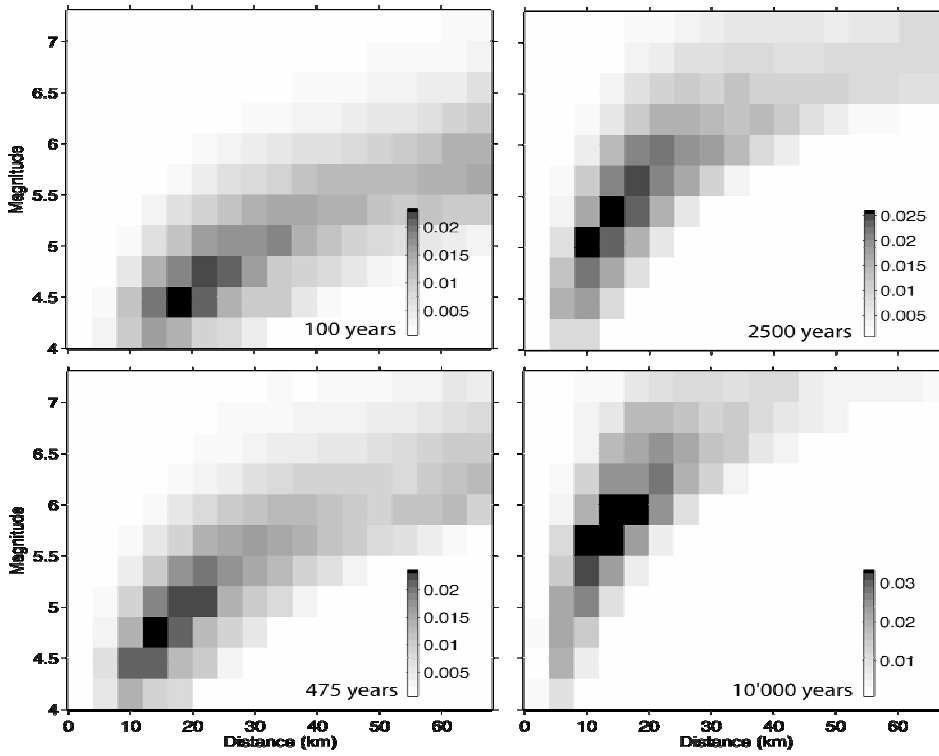


**Figure 37:** Same as Figure 35 but for the site of Zurich.

## 5.4 Sensitivity to Input Parameters

Sensitivity is studied in order to detect which parameters are the most critical for the hazard computation. This can also offer guidance for future research activities. A number of input decisions were made based on sensitivity feedback computed from a preliminary hazard model. This helped us to determine that:

- The type of declustering does not play a significant role in the hazard assessment; Reasenbergl declustering or the Gardener and Knopoff approach with different sets of input parameters do not significantly change the hazard output. Therefore, we decided to not include a logic tree alternative branch for different declustering algorithms.
- Similarly, removing explosion events does not play a significant role; hazard results do not change significantly if de-quarrying is applied or not. Therefore, no logic tree alternative branch is included for different dequarring.
- Soft borders in the hazard computation (gradually changing rates across zone boundaries) do not play a significant role, as long as the smoothing distance remains small. Therefore, again no logic tree alternative branch is included for different border types.

The choice of the zoning model has, as expected, a significant impact on the resulting hazard. When comparing the maps at 5 Hz for a return period of 475 years for the SEIS and TECTO models (Figure 39), we find that the latter reaches peak values about 25% lower than the first. The overall appearance of the TECTO model is smoother; a result of the larger source zones (Figure 39). Specifically, the hazard at Basel is reduced in absolute terms and relative to other regions, such as Graubünden. We feel that the TECTO model represents well alternative scenarios that assume that the seismicity of the next years changes from what has been observed as persistent clusters of activity in the past 1000 years (Figures 3 and 5). However, we assume that such a change is an unlikely scenario, which is why we only give a 10% weight in the logic tree to the TECTO model.

Likewise, the choice of the attenuation model has a significant impact on the hazard. We show in Figure 40 the 5 Hz maps for a return period of 475 years, computed for the three alternative attenuation laws used (Bay et al., 2004). For comparison, we also plot a map using Ambraseys et al. (1996), which is not used in our logic tree (see Chapter 4). The results show that differences between the first three models are on the order of 10%, with the model assuming an increase to 50 bar stress-drop giving the highest hazard, followed by the one that assumes a constant stress-drop of 30 bars. Note, however, that the difference between the models depends on the return period investigated. Overall, this epistemic difference between the models is well within the aleatory uncertainty of each model. If we use the Ambraseys et al. (1996) model, we end up with a hazard that is about 50% higher and also smoother as a results of the less steep attenuation (Figure 25).

The choice of the magnitude of completeness ( $M_c$ ) model has some influence on the

final hazard, again documented for the 5 Hz/475 yr map in Figure 41.  $M_c$  model 2 (see chapter 4.3) results show up to 10% higher values overall, and, specifically for the Wallis region, with a slightly different spatial distribution of hazard.

We also investigated the minimum truncation distance of the attenuation laws. As expected, truncation at larger distances than the assumed 1 km reduces the hazard somewhat. This decrease is stronger for the Alpine region than the Foreland/Basel region, because of the more concentrated depth-range of hypocenters. However, as seen in the de-aggregation plots (Figures 35-37), hypocentral distances below 5 km contribute in relatively minor way to the hazard, thus our choice of a truncation distance is not critical for hazard assessment.

Lastly, the choice of the maximum magnitude  $M_{max}$  has a minor (smaller than 10%) influence on the hazard, as demonstrated for the hazard curves for Sion (Figure 38). The curves for an assumed  $M_{max}$  of 7.2 or 7.5 differ little, and this difference increases little towards lower probabilities. Because of the large uncertainty of the  $M_{max}$  determination, this small sensitivity to  $M_{max}$  is favorable for our hazard assessment.

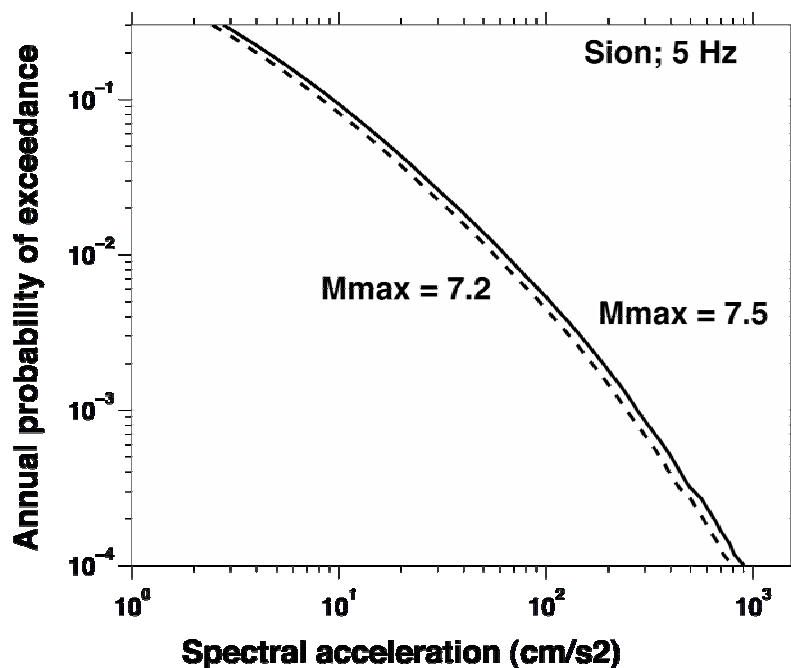


**Figure 38:** Comparison of the hazard curves at Sion (5Hz) for two assumed maximum magnitudes: 7.5 (solid line) and 7.2 (dashed line).

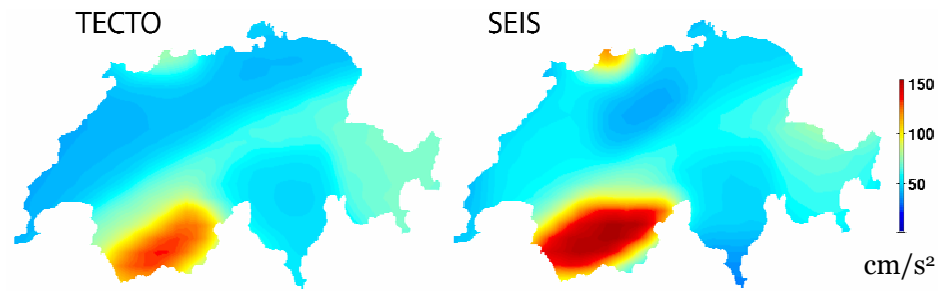


**Figure 39:** Hazard maps at 5 Hz/475 years return period (ground-motion in cm/s<sup>2</sup>) for the two different zoning approaches. (Left) Model TECTO. (Right) Model SEIS.

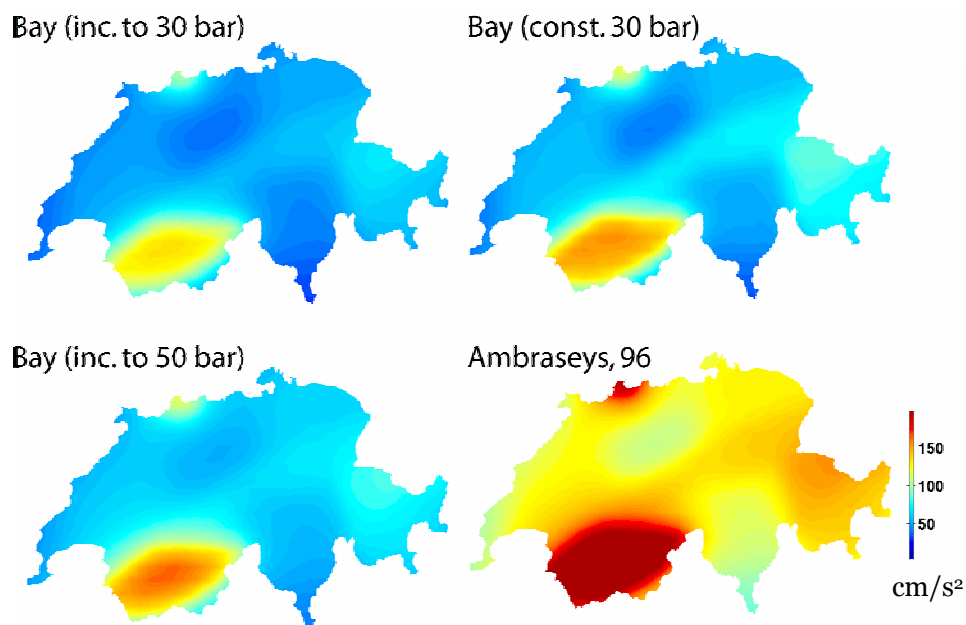


**Figure 40:** Hazard maps at 5 Hz/475 years return period (ground-motion in cm/s<sup>2</sup>), compared are four different attenuation functions. (Top left) Bay (2004) increasing to 30 bar. (Bottom left) Bay (2004) increasing to 50 bar. (Top Right) Bay (2004) constant 30 bar. (Bottom Right) Ambraseys et al (1996)(not used in the final hazard computation).

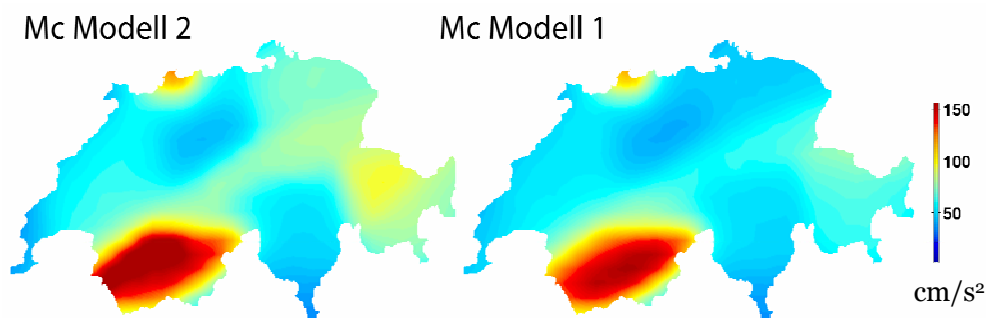


**Figure 41:** Hazard maps at 5Hz/475 years return period (ground-motion in cm/s<sup>2</sup>), compared are the different completeness models.



**Figure 42:** Zoning map of Switzerland as defined in the SIA 261 building code. Four zones of different seismic hazard are distinguished.

The fact that the uncertainty in the hazard model is large (Figure 29) is often difficult to communicate to non-experts. More than half of the uncertainty in the hazard model is due to the aleatory uncertainty in the predictive ground-motion model. This is a result common to recent hazard studies worldwide. It stems from the fact that observed ground-motions from earthquakes are quite variable, and this variability is not quantifiable and thus difficult to integrate into a predictive model. The large uncertainty in the predictive ground-motion relationship used here ( $\log_{10} \sigma_{lg} = 0.35$ , Bay et al., 2004), common to most seismic hazard studies, is a combination of the variability in source, path and to some degree also site effects. Reducing this uncertainty is a major challenge for seismology in the future.

Additional uncertainty stems from the fact that temporal and spatial non-stationarity of the earthquake catalog today is clearly seen but not easily understood. We do not know why regions such as the Wallis are periodically more active for some years to decades, and we have currently no means of forecasting the next periods of higher activity. The Wallis, for example, has been relatively quiet in the past 30 years when compared to other periods of history—but what does that imply for the next thirty years? Consequently, current PSHA for Switzerland must assume a time-independent Poissonian recurrence model, which results in larger uncertainties. Likewise, the physical processes that determine spatial and temporal changes in the earthquakesize distribution are poorly understood and hence cannot be integrated well into a predictive model other than by extrapolation of the past. While we have made some progress in understanding spatial variability in  $b$ -values (e.g., Schorlemmer et al., 2004a), there remains a significant research need.

Our hazard model, while largely following the well established route of PSHA established by Cornell (1968), includes several innovative aspects. First of all, we introduce a more objective way to assess the  $b$ -values in individual zones. Using the  $AIC_c$  (Chapter 4), we are able to decide, based on an established statistical criterion, if the data in a specific zone warrants to be fitted with a zone specific  $b$ -value, or if the overall  $b$ -value is superior. Using AIC weights we are able to express objectively a range of alternative scenarios for the different ( $a$ ,  $b$ )-models. This addresses a long-

## 6 Conclusions and Outlook

In this report, we present a new generation of probabilistic seismic hazard assessment for Switzerland. The new PSHA replaces the last generation by Sägesser and Mayer-Rosa (1978). The 2004 PSHA builds upon extensive research and database compilation over the last 10 years, as documented throughout this report. Progress was made in particular by using a Swiss specific attenuation law, which provides physical units of ground acceleration, velocity, or displacement. In addition, both the historical and instrumental earthquake database was vastly improved and converted to a uniform moment magnitude scale. We also developed a new zonation, which takes into account an improved understanding of the seismotectonic framework of the region. Finally, we implemented a new computation scheme based on a Monte-Carlo approach and a logic tree, to fully characterize the seismic hazard and its associated uncertainties.

The resulting hazard maps differ from previous assessments in a few aspects. It is not possible to compare absolute values, since the old generation of maps were created from an intensity-based attenuation law. While the main activity centers in the Wallis and Basel remain dominant in the hazard, the 2004 maps are smoother across the country. Smoother hazard is found specifically along the Alpine Front, in the Graubünden and in the Wallis. These changes reflect the realization of seismologists that the instrumental and historical record is too short to be simply extrapolated into the future. Events of magnitude 6-7 are now believed to be possible in all regions of Switzerland, but in areas of low seismicity, their return periods may be too long (> 10'000 years) to be known from the historical or even the paleoseismic record.

The new national building code of Switzerland (SIA code 261, 2003; Figure 42) already reflects the changes seen in the 2004 hazard model both in terms of the zoning of Switzerland as well as the design acceleration. While the full PSHA was not ready at the time that the SIA code was designed, a preliminary version was available, and the final PSHA presented in this report does not significantly change as compared to the preliminary one. In fact, the 2003 hazard edition is entirely included in the statistical characterization presented here. One of the most significant advances of the 2004 PSHA as compared to earlier ones is that we are able to provide for the first time a full uncertainty model. Using a combined Monte-Carlo and logic tree approach (Chapter 5.1), we derive median and mean hazards, as well as all desired fractiles. We commonly plot the one-sigma uncertainty (e.g., Figures 29 and 34). This uncertainty highlights again the fact that differences between the local hazards are in fact small, and often not statistically significant. For example, while the difference between the hazard in Basel and Sion is quite prominent in the hazard maps (e.g., Figure 31), it is hardly statistically significant when uncertainties are taken into account (Figure 29).

standing need in hazard assessment, and it stabilizes the resulting model by avoiding large fluctuations in  $b$ -values. We recommend using such procedures in future hazard assessments as a tool to improve the model generation. Secondly, we programmed and applied a Monte-Carlo approach for hazard assessment (Musson, 1999; Chapter 5.1), which, in our opinion, is superior to classical approaches based on the integration over source zones. This method is more flexible and more transparent; it simplifies the hazard assessment procedure and reduce the chance of errors. Our Matlab based code is available for download from our web site. Combined with the also available input data, all results shown in this report can be reproduced.

The publication of the '*Seismic Hazard Assessment of Switzerland, 2004*' is the culmination point of many years of investigations. However, the progress in our understanding of the earthquake process as well as the collection of new data and the development of innovative approaches are not stopping. We are working toward the future generations of seismic hazard, in two principle directions: (a) the improvement of regional seismic hazard and (b) the assessment of site-specific hazard. In the following, we detail the expected progress and activities in the forthcoming 2005–2008 period.

### ***Outlook 2005 to 2008: Preparing the Next Generation of PSHA for Switzerland***

Routinely updating earthquake hazard models is a priority for the SED and for the hazard users. The SED plans, as is done in many other seismically active countries, to revise the PSHA routinely, with a five year schedule. This ensures the smooth integration of state-of-the-art knowledge as well as a response to changing needs of the user community. Our goal is to improve continuously the hazard relevant scientific understanding and databases over the next four years. Specifically, we anticipate progress in the following areas:

- *Improved predictive ground-motion models.* As the largest contributor to uncertainty, this area offers the most promise for reducing hazard uncertainty. The new generation of broadband sensors will make it possible to refine the study by Bay et al. (2004) by expanding it to higher and lower frequencies and by developing regionalized attenuation models. The enhanced database will allow deriving separate intra- and inter-event uncertainties and possibly to distinguish between stress-drops for different faulting styles (Cocco and Rovelli, 1989). An improved knowledge of the local conditions at Swiss recordings stations will allow us to better constrain site effects. Lastly, an improved understanding of scaling of earthquake ground-motion is needed to move with confidence from the observable ground-motions of small events in Switzerland to the more infrequent moderate and large ones.
- *Improved treatment of uncertainties.* The combined Monte-Carlo and logic tree model we built (Figure 28) represents what we consider an adequate representation of uncertainties. However, it would be preferred to include

more branches and additional sources of uncertainty, such as the uncertainty in magnitudes and locations, additional ground-motion models, different depth distributions, faulting style specific attenuation laws or preferred rupture orientations. Incorporating a larger logic tree stabilizes the resulting hazard and might identify sources of uncertainty thus far overlooked.

- *Time-dependent seismicity models.* Improving our understanding of time-dependence in the earthquake generation on all scales would allow us to build less uncertain hazard models. Time-dependence can be introduced by accurate description of the clustering processes of earthquakes (foreshock-mainshock-aftershock sequences or earthquake swarms). It can also consider annual or even decadal changes of seismicity, which may be caused by stress shadows of large events, or episodic loading of faults or regions. Future earthquake models built for countries of high seismic activity will be more physically-based and time-dependent. In this context, validation and testing of models is critical, in order to be able to distinguish between the forecasting capabilities of different model classes.
- *Improving the macroseismic, historical and paleoseismic database.* Past large events still offer much valuable information about earthquake activity in Switzerland. We need to improve our understanding of the relationship between macroseismic data and ground-motion in Switzerland in order to be able to calibrate better the size of past earthquakes. In addition, many historical sources of past earthquakes in Switzerland remain untapped thus far, offering opportunities to improve and clean our database. Likewise, the study of paleoseismic events is our best chance to constrain the recurrence of the very largest events in Switzerland, and also to learn more about the maximum possible earthquakes.

### ***Outlook 2005 to 2008: Site-specific Hazard Assessment for Switzerland***

The current map and model of seismic hazard are computed for rock conditions; however, local site conditions can cause variations in hazard over distances of a few hundred meters that are greater than the variations across the whole country.

The attenuation model for the Alpine Foreland is valid for good quality bedrock with an estimated shear-wave velocity of about 1500 m/s in the upper 30 m. Most of the urbanized areas, however, are located along river valleys over young, soft surface deposits. Ground-motion is generally much larger on top of such deposits as compared to bedrock outcrops, because of effects of the local site on the signal amplitude and frequency content and on the duration of ground-motion. Therefore, local site effects must be accounted for when moving from the hazard assessments presented here to hazard assessments than can be used from engineers and planners to derive an adequate building design.

In building codes such as the Swiss SIA 261 code, local site effects are taken into

account by the definition of a number of soil classes. However, the lack of reliable soil descriptors introduces a high level of uncertainty that can be reduced with additional geophysical investigations. Microzonation is the preferred approach to estimate local ground amplification as a function of frequency. For an area of low seismicity such as Switzerland, different microzonation methods can be applied. The highest level of investigations to understand site effects are reliable 3D models of the geological and geophysical structure, and numerical modeling of ground-motion amplification. Observations of weak motions in areas with dense instrumental coverage allow cross-checking of numerical results.

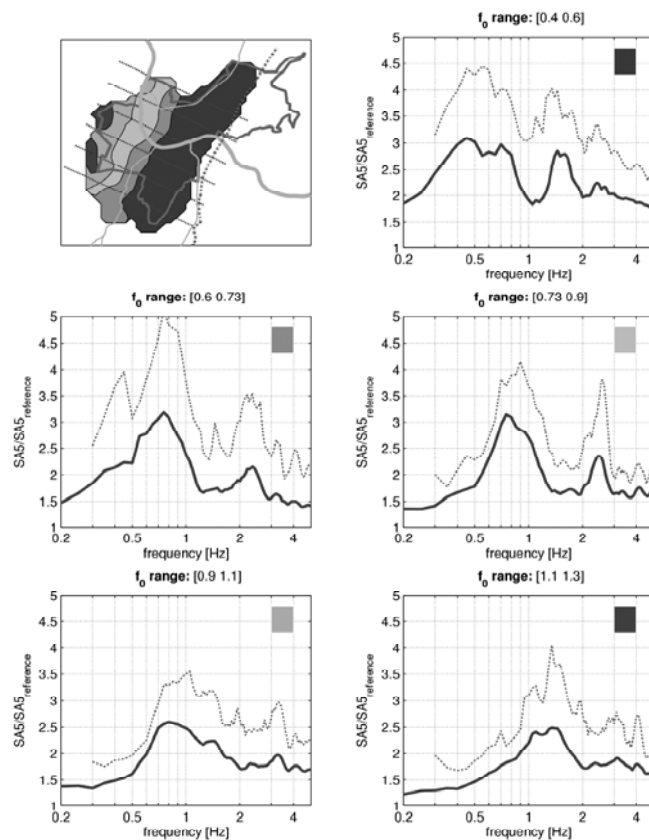


**Figure 43.** Quantitative microzonation of the city of Basel (Kind, 2002; Kind et al., 2003). The area of Basel is divided into different zones. For each zone the average (light gray curve) and maximum (dark gray curve) spectral amplification with respect to a hard-rock site has been estimated with numerical modeling, using a 3D geophysical model of the site.

In Switzerland, several microzonation studies have been carried out during the last years with the main purpose of developing and applying methods for mapping site effects (Mayer-Rosa and Jimenez, 2000). Three pilot-projects have been conducted, dealing with all aspects of seismic hazard assessment. A pilot project in the Canton Obwalden (Swiss project within the International Decade of Natural Disaster Reduction; Schindler et al., 1993) focused on the geological correlation of intensity anomalies with local soil conditions. This work was motivated by various empirical correlations between surface geology and seismic intensity increments and a pilot study for some areas in the Swiss Foreland (Fäh, 1985). The project "Earthquake hazard and microzonation in Switzerland" (NFP31 "Climate Changes and Natural Hazards", Mayer-Rosa et al., 1997) focused on three test sites, including the eastern Rhine valley, Basel and the Wallis, with the purpose of assessing regional seismic

hazard and seismic microzonation.

In the city of Basel as well as in the Wallis continuing applications could be initiated during the NFP31 project, which resulted for example in a qualitative microzonation map of the city of Basel (Fäh et al., 1997; Noack et al., 1997, 1999). The SISVAL-IDNDR project (Frischknecht, 2000; Wagner et al., 2000) performed a microzonation study in the Wallis, in parallel to a study by the Canton Wallis (Résonance, 2000).

Between 1998 and 2002, the ETH project "Earthquake scenarios for Switzerland" (Fäh et al., 2000) focused on all aspects of seismic hazard and risk assessment. One of the main tasks was to improve microzonation methods and apply them to the area of Basel (Figure 43). Significant progress was made by developing new methods to estimate S-wave velocities of the soils (Fäh et al., 2001, 2003; Steimen et al., 2003; Kind et al., 2004; Roten et al., 2004). The problem of computing the three-dimensional amplification effects in the Basel area was solved by Oprsal et al. (2004). Results and methods from the previous studies are now applied in the Interreg project "Microzonation in the southern Rhinegraben area". In the Wallis region, the Interreg project "SISMOVALP—Seismic hazard and alpine valley response analysis" will develop representative alpine valley shapes and compute earthquake scenarios. In both Interreg projects generic spectra will be proposed and compared with the level of protection currently pursued at a national or European (EC8) scale. As databases of local site conditions and 3D effects become available for Switzerland, we will increasingly be able to incorporate local site effects in our hazard map (Field, 2000).

In conclusion, the new '*Seismic Hazard of Switzerland, 2004*,' sets the basis for a modern policy of earthquake risk mitigation and at the same time allows to plan the future generation of hazard assessment for Switzerland.

## 7 References

- Abrahamson, N. (2000). State of the practice of Seismic Hazard Evaluation, Proc. GeoENG., 19-24 Nov. 2000.
- Agnew, D.C. & L.M. Jones (1991). Prediction probabilities from foreshocks, *J. Geophys. Res.*, v. 96, p. 11 959-11 971.
- Akaike, H. (1974). New Look at Statistical-Model Identification, *IEEE Transactions on Automatic Control*, AC19 (6), 716-723, 1974.
- Aki, K. (1965). Maximum likelihood estimate of  $b$  in the formula  $\log N = a - b M$  and its confidence limits, *Bull. Earthq. Res. Inst.*, v. 43, p. 237-239.
- Ambraseys, N. N., K. A. Simpson & J. J. Bommer (1996). Prediction of horizontal response spectra in Europe, *Earthquake Engineering and Structural Dynamic*, 25, 371-400.
- Arabasz, W.J. & S.J. Hill (1996). Applying Reasenberg's cluster-analysis algorithm to regional earthquake catalogs outside California, *Seism. Res. Lett.*, v. 67, p. 30.
- Arthaud F. & P. Matte (1975). Les décrochements tardi-hercyniens du Sud-Ouest de l'Europe, *Géométrie et essai de reconstitution des conditions de la déformation*, *Tectonophysics* 25, 139-171.
- Baer, M., N. Deichmann, J. Braunmiller, F. Bernardi, C. Cornou, D. Fäh, D. Giardini, S. Huber, P. Kastli, F. Kind, U. Kradolfer, M. Mai, S. Maraini, I. Oprsal, T. Schler, D. Schorlemmer, S. Sellami, S. Steimen, S. Wiemer, J. Wossner, J. & A. Wyss (2003). Earthquakes in Switzerland and surrounding regions during 2002, *Eclogae Geol. Helv.*, v. 96, p. 313-324.
- Bakun, W.H. & C.M. Wentworth (1999). Estimating earthquake location and magnitude from seismic intensity data (vol 87, pg 1502, 1997), *Bull. Seismol. Soc. Am.*, v. 89, p. 557-557.
- Bay, F. (2002). Ground-motion scaling in Switzerland: Implications for hazard assessment, PhD Thesis Nr. 14567, Swiss Federal Institute of Technology, Zurich.
- Bay, F., D. Fäh, L. Malagnini & D. Giardini (2003). Spectral shear wave ground-motion scaling in Switzerland, *Bull. Seism. Soc. Am.*, 93, 414-429.
- Bay, F., S. Wiemer, D. Fäh & D. Giardini (2004). Predictive ground-motions relationships for Switzerland: Best estimates and uncertainties, *J. Seismology*, in press.
- Becker, A. & C.A. Davenport (2003). Rockfalls triggered by the AD 1356 Basle Earthquake, *Terr. Nova*, v. 15, p. 258-264.
- Becker, A., C.A. Davenport & D. Giardini (2002). Paleoseismicity studies on end-Pleistocene and Holocene lake deposits around Basle, Switzerland, *Geophys. J. Int.*, 149, 659-678.
- Bender, B. (1983). Maximum likelihood estimation of  $b$ -values for magnitude grouped data, *Bull. Seism. Soc. Am.*, 73, 831-851.
- Bender, B. & D.M. Perkins (1987). SEISRISK III: A computer program for seismic hazard estimation, *U.S. Geological Survey Bulletin*, v. 1772, 20 pages.
- Bommer, J.J., N.A. Abrahamson, F.O. Strasser, A. Pecker, P.Y. Bard, H. Bungum, F. Cotton, D. Fäh, F. Sabetta, F. Scherbaum & J. Studer (2004). The challenge of defining upper bounds on earthquake ground-motions, *Seism. Res. Lett.*, v. 75, p. 82-95.
- Boore, D.M. (1983). Stochastic simulation of high-frequency ground-motion based on seismological models of the radiated spectra, *Bull. Seism. Soc. Am.* 73, 1865-1894.
- Boore, D.M. (2001). Fortran programs for simulating ground-motions from earthquakes: Version 2.0 – A revision of Open-File Report 96-80-A, Open-File Report 00-509, U.S. Geological Survey.
- Boore, D.M. (2003). Prediction of ground-motion using the stochastic method, *Pure and Applied Geophys.*, 160, 635-676.
- Braunmiller, J., N. Deichmann, D. Giardini & S. Wiemer (2004). Homogeneous moment magnitude calibration in Switzerland, *Bull. Seismol. Soc. Am.*, in press.
- Brune, J.N. (1970). Tectonic stress and the spectra of seismic shear waves from earthquakes, *J. Geophys. Res.* 75, 4997-5009.
- Burg J.-P., J. Van Den Driessche & J.-P. Brun (1994). Syn- to post-thickening extension in the Variscan Belt of Western Europe: Mode and structural consequences, *Géologie de la France* 3, 33-51.
- Burkhard M. (1990). Aspects of the large-scale Miocene deformation in the most external part of the Swiss Alps (Subalpine Molasse to Jura fold belt), *Eclogae Geologicae Helveticae*, 83(3), 559-583.
- Camelbeeck, T., P. Alexandre, K. Vanneste & M. Meghraoui (2000). Long-term seismicity in regions of present day low seismic activity: the example of western Europe, *Soil Dynamics Earthquake*

Engineering 20, 405-414.

- Choy, G.L. & J. Boatwright (1995). Global patterns of radiated seismic energy and apparent stress, *J. Geophys. Res.* 100, 18205-18226.
- Cocco, M. & A. Rovelli (1989). Evidence for the variation of stress drop between normal and thrust faulting earthquakes in Italy, *J. Geophys. Res.* 94, 9399-9416.
- Coppersmith, K. J. (1994). Conclusions regarding maximum earthquake assessment, The earthquakes of stable continental regions, 1: Assessment of large earthquake potential, Electric Power Research Institute, Report TR-102261-V1, 1: a, 6-1 - 6-24.
- Cornell, C.A. (1968). Engineering seismic risk analysis, *Bull. Seismol. Soc. Am.*, v. 58, p. 1583-1606.
- Deichmann, N. (1992). Structural and rheological implications of lower-crustal earthquakes below northern Switzerland, *Phys. Earth Planet. Int.* 69, 270- 280.
- Deichmann, N., M. Baer, J. Braunmiller, D. Ballarin Dolfin, F. Bay, F. Bernardi, B. Delouis, D. Fäh, M. Gerstenberger, D. Giardini, S. Huber, U. Kradofer, S. Maraini, I. Oprsal, R. Schibler, T. Schler, S. Sellami, S. Steimen, S. Wiemer, J. Wössner & A. Wyss (2002). Earthquakes in Switzerland and surrounding regions during 2001, *Eclogae Geol. Helv.*, 95/2, 249-261.
- Deichmann, M. Baer, J. Braunmiller, D. Ballarin Dolfin, F. Bay, B. Delouis, D. Fäh, D. Giardini, U. Kastrup, F. Kind, U. Kradofer, W. Kuenzle, S. Roethlisberger, T. Schler, J. Salichon, S. Sellami, E. Spuehler & S. Wiemer (2000). Earthquakes in Switzerland and surrounding regions during 1999, *Eclogae Geol. Helv.*, 93.
- Deichmann, N. (1992). Structural and rheological implications of lower crustal earthquakes below northern Switzerland, *Phys. Earth. Plant. Inter.*, 69, 270-280.
- DeMets, C., R.G. Gordon, D.F. Argus & S. Stein (1990). Current plate motions, *Geophys. J. Int.*, 101, 425-478.
- Eckardt, P., H.P. Funk & T. Labhart (1983). Postglaziale Krustenbewegungen an der Rhein-Rhone-Linie, *Vermessung, Photogrammetrie, Kulturtechnik*, 2, 43-56.
- ECOS (2002) ECOS: Earthquake Catalogue of Switzerland. PEGASOS technical report EXT-TB-0032. SED.
- Electric Power Research Institute (EPRI) (1993). Guidelines for Determining Design Basis Ground-motions, Vol. I: Early Site Permit Demonstration Program, Palo Alto, CA, November.
- Fäh, D. (1985). Seismische Mikrozonierung der Schweiz, Diplomarbeit am Institut für Geophysik, ETH Zürich.
- Fäh, D., H. Bachmann, F. Bay, A. Becker, D. Giardini, P. Huggenberger, F. Kind, K. Lang, D. Mayer-Rosa, T. Noack, S. Sellami & T. Wenk. (2000). Earthquake scenarios for Switzerland, Proc. XII World Conference on Earthquake Engineering, New Zealand, Feb. 2000, Paper number 205.
- Fäh, D. & K. Koch, (2002). Discrimination between earthquakes and, chemical explosions by multivariate statistical analysis: A case study for Switzerland, *Bull. Seismol. Soc. Am.*, v. 92, p. 1795-1805.
- Fäh, D., D. Giardini, F. Bay, F. Bernardi, J. Braunmiller, N. Deichmann, M. Furrer, L. Gantner, M. Gisler, D. Isenegger, M.J. Jimenez, P. Kastli, R. Koglin, V. Masciadri, M. Rutz, C. Scheidegger, R. Schibler, D. Schorlemmer, G. Schwarz-Zanetti, S. Steimen, S. Sellami, S. Wiemer & J. Wossner (2003). Earthquake Catalogue Of Switzerland (ECOS) and the related macroseismic database, *Eclogae Geologicae Helvetiae*, v. 96, p. 219-236.
- Fäh, D., F. Kind & D. Giardini (2001). A theoretical investigation of average H/V ratios, *Geophys. J. Int.*, 145, 535-549.
- Fäh, D., F. Kind & D. Giardini (2003). Inversion of local S-wave velocity structures from average H/V ratios, and their use for the estimation of site-effects, *J Seismology*, 7, 449-467.
- Fäh, D., F. Kind, K. Lang & D. Giardini (2001). Earthquake scenarios for the city of Basel, *Soil Dyn. Earthq. Eng.*, v. 21, p. 405-413.
- Fäh, D., E. Rüttener, T. Noack & P. Kruspan (1997). Microzonation of the city of Basel, *J Seismology*, 1, 87-102.
- Field, E.H. & the SCEC Phase III Working Group (2000). Accounting for site effects in probabilistic seismic hazard analyses of Southern California: Overview of the SCEC Phase III Report, *Bull. Seism. Soc. Am.* 90, 1-31.
- Frankel, A. (1995). Mapping seismic hazard in the central and eastern United States, *Seism. Res. Lett.*, v. 66, p. 8-21.
- Frankel, A., C. Mueller, T. Barnhard, D. Perkins, E.V. Leyendecker, N. Dickman, S. Hanson & M. Hopper (1997). Seismic hazard maps for California, Nevada and western Arizona/Utah, United States

- Geological Survey Open-File Report, 97-130.
- Frankel, A., C. Mueller, T. Barnhard, D. Perkins, E.V. Leyendecker, N. Dickman, S. Hanson & M. Hopper (1996). National Seismic Hazard Maps: Documentation June 1996, U.S. Geological Survey Open-File Report 96-532, 44 p.
- Frankel, A., C. Mueller, T. Barnhard, D. Perkins, E.V. Leyendecker, N. Dickman, S. Hanson & M. Hopper, M. (1997b). Seismic hazard maps for California, Nevada and western Arizona/Utah, United States Geological Survey Open-File Report, p. 97-130.
- Frischknecht, C. (2000). Seismic soil amplification in Alpine valleys. A case study: the Rhone Valley, Valais, Switzerland, PhD thesis, Universite de Geneve, 144 p.
- Gardner, J.K. & L. Knopoff (1974). Is the sequence of earthquakes in Southern California, with aftershocks removed, Poissonian?, *Bull. Seismol. Soc. Am.*, v. 64, p. 1363-1367.
- Gerstenberger, M. (2003). Earthquake clustering and time-dependent probabilistic hazard analysis for California (Ph.D. thesis), ETH Zurich, Switzerland.
- Giardini, G. Grünthal, K.M. Shedlock, & P.Z. Zhang (1999). The GSHAP Global Seismic Hazard Map, *Annal. Geofis.*, v. 42, p. 1225-1230.
- Giardini, D. (1999). The Global Seismic Hazard Assessment Program (GSHAP) - 1992/1999, *Annali de Geofisica*, 42, 957-974.
- Gisler, M., S. Fäh & R. Schibler, R. (2003). Two serious earthquakes in the Rhine Valley at the end of the 18<sup>th</sup> century, The events of December 6, 1795 and April 20, 1796, *Eclogae geol. Helv.*, 96, 357-366.
- Grünthal, G. (Ed.) (1998). European macroseismic scale 1998, *Cahiers du Centre Européen de Géodynamique et de Séismologie 1998*, Vol. 15, 100pp.
- Grünthal, G., C. Bosse, S. Sellami, D. Mayer-Rosa & D. Giardini (1999). Compilation of the GSHAP regional seismic hazard for Europe, Africa and the Middle East, *Annal. Geofis.*, v. 42, p. 1215.
- Grünthal, G., D. Mayer-Rosa & W. A. Lenhardt (1998). Abschätzung der Erdbebengefährdung für die D-A-CH-Staaten - Deutschland, Österreich, Schweiz, *Bautechnik*, 10, 753-767.
- Gutenberg, R. & C.F. Richter (1944). Frequency of earthquakes in California, *Bull. Seismol. Soc. Am.*, 34, 185-188.
- Hanks, T. & R.K. Mc Guire (1981). The character of high-frequency strong ground-motion, *Bull. Seism. Soc. Am.* 71, 2071-2095.
- Hough, S.E. & L.M. Jones (1997). Aftershocks: Are the earthquakes or afterthoughts?, *Eos, Trans. AGU*, v. 78, p. 505.
- Hsü, K.J. (1995). *The geology of Switzerland*, Princeton University Press, cop., Princeton, New Jersey, USA.
- Husen, S., E. Kissling, N. Deichmann, S. Wiemer, D. Giardini & M. Baer (2003). Probabilistic earthquake location in complex three-dimensional velocity models: Application to Switzerland, *J. Geophys. Res.*, v. 108 (B2).
- Ide S. & G.C. Beroza (2001). Does apparent stress vary with earthquake size?, *Geophys. Res. Letts.* 28, 3349-3352.
- Ide S., G.C. Beroza, S.G. Prejean & W.L. Ellsworth (2003). Apparent break in earthquake scaling due to path and site effects on deep borehole recordings, *J. Geophys. Res.*, 108 (B5), art. no. 2271.
- Imoto, M. (1991). Changes in the Magnitude Frequency B-Value Prior to Large (M- Greater-Than-or-Equal-to-6.0) Earthquakes in Japan, *Tectonophysics*, 193 (4), 311-325.
- Ishimoto, M. & K. Iida (1939). Observations of earthquakes registered with the microseismograph constructed recently, *Bull. Earthq. Res. Inst.*, v. 17, p. 443-478.
- Jaboyedoff, M. & S. Pastorelli (2003). Perturbation of the heat flow by water circulation in a mountainous framework: Examples from the Swiss Alps, *Eclogae geologicae Helvetiae*, 96, 37-47.
- Jiménez, M.-J., D. Giardini & G. Grünthal (2003). The ESC-SESAME Unified Hazard Model for the European-Mediterranean Region, *EMSC/CSEM Newsletter*, v. 19, p. 2-4.
- Johnston, A.C., K.J. Coppersmith, L.R. Kanter & C.A. Cornell (1994). *The Earthquakes of Stable Continental Regions: Vol. 1: Assessment of Large Earthquake Potential*, Electric Power Research Institute (EPRI TR-102261-V1).
- Jones, L.M. (1984). Foreshocks (1966-1980) in the San Andreas system, California, *Bull. Seismol. Soc. Am.*, v. 74, p. 1361-1380.
- Joyner W.B. & D.M. Boore (1981). Peak horizontal acceleration and velocity from strong motion records including records from the 1979 Imperial Valley, California, earthquake, *Bull. Seism. Soc. Am.* 71, 2011-2083.

- Kagan, Y. & D. Jackson (2000). Probabilistic forecasting of earthquakes, *Geophys. J. Int.*, 143, 438-453.
- Kagan, Y. (1999). Universality of the seismic moment-frequency relation, *Pure and Applied Geophysics.*, 155, 537-574.
- Kanamori, H. & D.L. Anderson, D.L. (1975). Theoretical basis of some empirical relations in seismology, *Bull. Seismol. Soc. Am.*, v. 65, p. 1073-1095.
- Kastrup, U. (2002). Seismotectonics and stress field variations in Switzerland, PhD. Thesis Nr. 14527, ETH Zurich, pp153.
- Kastrup, U., M.L. Zoback, N. Deichmann, K. Evans, A.J. Michael & D. Giardini (2004). Stress field variations in the Swiss Alps and the northern Alpine Foreland derived from inversion of fault plane solutions, *J. Geophys. Res.*, 109, art. no.-B01402.
- Kenneth, P., K. P. Burnham & D. R. Anderson (2002). Model selection and multimodel inference: A practical information - Theoretic Approach, Springer, New York.
- Keefer, D.K. (1984). Landslides caused by earthquakes, *Bull. Geol. Soc. Am.* 95, 406-421.
- Kijko, A. & G. Graham (1998). Parametric-historic procedure for probabilistic seismic hazard analysis - Part I: Estimation of maximum regional magnitude  $M(\max)$ , *Pure and Applied Geophysics*, 152 (3), 413-442.
- Kijko, A. G. Graham, G. (1999). "Parametric-historic" procedure for probabilistic seismic hazard analysis - Part II: Assessment of seismic hazard at specified site, *Pageoph*, v. 154, p. 1-22.
- Kijko, A., S. Lasocki & G. Graham (2001). Non-parametric Seismic Hazard in Mines, *PAGEOPH*, 158 (9-10), 1655-1675.
- Kind, F. (2002). Development of Microzonation Methods: Application to Basle, Switzerland, PhD Thesis Nr. 14548, ETH Zurich.
- Kind, F., D. Fäh & D. Giardini (2004). Array measurements of S-wave velocities from ambient vibrations. *Geophys. J. Int.*, in press.
- Kind, F., D. Fäh, E. Zechner, P. Huggenberger & D. Giardini (2003). Seismic zonation from a 3D seismic velocity reference model of the area of Basle, Switzerland, *Bull. Seism. Soc. Am.*, submitted.
- Kissling, E. (1993). Deep-Structure of the Alps - What Do We Really Know, *Physics of the Earth and Planetary Interiors*, 79 (1-2), 87-112.
- Kisslinger, C. & L.M. Jones (1991). Properties of aftershocks in southern California, *J. Geophys. Res.*, v. 96, p. 11,947-11,958.
- Knopoff, L. (1964). Statistics of earthquakes in California, *Bull. Seism. Soc. Am.*, 54, 1871-1873.
- Koch, K. & D. Fäh (2002). Identification of earthquakes and explosions using amplitude ratios: The Vogtland Area revisited, *Pageoph*, v. 159, p. 735-757.
- Kostrov, B.V. (1974). Seismic moment and energy of earthquakes and seismic flow of rock, *Izv. Acad. Sci. USSR Phys. Solid Earth*, v. 1, p. 23-44.
- Lomax, A., A. Zollo, P. Capuano & J. Virieux (2001). Precise, absolute earthquake location under Somma-Vesuvius volcano using a new three-dimensional velocity model, *Geophys. J. Int.*, v. 146, p. 313-331.
- Maeda, K., (1996). The use of foreshocks in probabilistic prediction along the Japan and Kuril Trenches, *Bull. Seismol. Soc. Am.*, v. 86, p. 242-254.
- Malagnini, L. & R.B. Herrmann (2000). Ground-motion scaling in the region of the 1997 Umbria-Marche earthquakes (Italy), *Bull. Seism. Soc. Am.* 90, 1041-1051.
- Malagnini, L., R.B. Herrmann & K. Koch (2000b). Regional ground-motion scaling in central Europe, *Bull. Seism. Soc. Am.* 90, 1052-1061.
- Malagnini, L., R.B. Herrmann & M. Di Bona (2000a). Ground-Motion Scaling in the Apennines (Italy), *Bull. Seism. Soc. Am.* 90, 1062-1081.
- Mancktelow N. (1985). The Simplon Line: a major displacement zone in the Western Lepontine Alps, *Eclogae Geol. Helv.* 78, 73-96.
- Mayeda, K. & W.R. Walter (1996). Moment, energy, stress drop, and source spectra of western United States earthquakes from regional coda envelopes, *J. Geophys. Res.* 101, 11195-11208.
- Mayer-Rosa, D. & M.-J. Jimenez (2000). Seismic zoning. State-of-the-art and recommendations for Switzerland. *Landeshydrologie und -geologie, Geologischer Bericht Nr.26.*
- Mayer-Rosa, D., E. Rüttener, D. Fäh, C. Schindler, C. Beer, J.-J. Wagner & C. Frischknecht (1997). Erdbebengefährdung und Mikrozonierung in der Schweiz, Beitrag zur Erforschung des Erdbebenrisikos in Abhängigkeit vom geologischen Untergrund. VdF Hochschulverlag AG, ETH Zürich, pp 90.
- McGuire, R.K. & T.C. Hanks (1980). RMS acceleration and spectral amplitudes of strong ground-motion

- during the San Fernando, California, earthquake, *Bull. Seism. Soc. Am.* 70, 1907-1919.
- Meghraoui, M., B. Delouis, M. Ferry, D. Giardini, P. Huggenberger, I. Spottke & M. Granet (2001), Active normal faulting in the upper Rhine graben and paleoseismic identification of the 1356 Basel earthquake, *Science*, v. 293, p. 2070-2073.
- Musson, R.M.W. (2000). The use of Monte Carlo simulations for seismic hazard assessment in the UK, *Annal. Geofis.*, v. 43, p. 1-9.
- Noack, T., T. Kruspan, D. Fäh, E. Rüttener, (1997). Seismic microzonation of the city of Basel (Switzerland) based on geological and geotechnical data and numerical simulations, *Ecloga Geol. Helv.*, 90, 433-448.
- Noack, T., D. Fäh & P. Kruspan (1999). Erdbebenmikrozonierung für den Kanton Basel-Stadt. *Landeshydrologie und -geologie, Geologische Bericht Nr.24*, pp83.
- Ogata, Y. (1999). Seismicity analysis through point-process modeling: A review, *Pure and Applied Geophysics*, 155 (2-4), 471-507.
- Ogata, Y. (1983). Estimation of the Parameters in the Modified Omori Formula for Aftershock Frequencies by the Maximum-Likelihood Procedure, *Journal of Physics of the Earth*, 31 (2), 115-124.
- Omori, F. (1894). On aftershocks, Report of Imperial Earthquake Investigation Committee, v. 2, p. 103-109.
- Oprsal I., D. Fäh, M. Mai & D. Giardini (2004). Deterministic earthquake scenario for the Basel area – Simulating strong motion and site effects for Basel, Switzerland, *J. Geophys. Res.*, in press.
- Pavoni, N., H. Maurer, P. Roth & N. Deichmann (1997). Seismicity and seismotectonics of the Swiss Alps, Deep structures of the Swiss Alps, results of NRP 20, Birkhäuser, Basel, Switzerland, 241-250.
- Raoof, M., R.B. Herrmann & L. Malagnini (1999). Attenuation and excitation of three-component ground-motion in Southern California, *Bull. Seism. Soc. Am.* 89, 888-902.
- Reasenber, P. (1985). Second-order moment of Central Californian seismicity, 1969-1982, *J. Geophys. Res.*, 90, 5479-5495.
- Reasenber, P. (1999). Foreshock occurrence rate before large earthquakes worldwide, *Pageoph*, v. 155, p. 355-379.
- Reasenber, P.A. & L.M. Jones (1989). Earthquake hazard after a mainshock in California, *Science*, v. 243, p. 1173-1176.
- Regenauer-Lieb, K. & J.P. Petit (1997). Cutting of the European continental lithosphere: Plasticity theory applied to the present Alpine collision, *J. Geophys. Res.*, 102 (B4), 7731-7746.
- Résonance Ing.-conseils SA, Geologiebüro Rovina&Partner AG, Tissières bureau d'ing. (2000). Praxisbezogene seismische Mikrozonierung der Region Brig-Visp (Wallis), Unveröffentlicher Bericht für Staat Wallis, 65 Seite.
- Ricou L.-E. (1994). Tethys reconstructed: plates, continental fragments and their boundaries since 260 Ma from Central America to South-eastern Asia, *Geodynamica Acta* 7(4), 169-218.
- Rodriguez-Pascua, M.A., J.P. Calvo, G. De Vicente, D. Gomez-Gras (2000). Soft-sediment deformation structures interpreted as seismites in lacustrine sediments of the Prebetic Zone, SE Spain, and their potential use as indicators of earthquake magnitudes during the late Miocene, *Sed. Geol.* 135, 117-135.
- Roten, D., D. Fäh, C. Cornou, & D. Giardini (2004). 2D resonances in alpine valleys identified from ambient vibration wavefields. *Bull. Seism. Soc. Am.*, submitted.
- Ruettener, E. (1995). Earthquake hazard evaluation for Switzerland, *Matériaux pour la Géologie de la Suisse, Géophysique No 29* publié par la Commission Suisse de Géophysique. Schweizerischer Erdbebendienst, Zürich, pp. 106.
- Ruettener, E., J.J. Egozcue D. MayerRosa & S. Mueller (1996). Bayesian estimation of seismic hazard for two sites in Switzerland, *Nat. Hazards*, v. 14, p. 165-178.
- Rydelek, P.A. & I.S. Sacks (1989). Testing the completeness of earthquake catalogs and the hypothesis of self-similarity, *Nature*, 337, 251-253, 1989.
- Rydelek, P.A., and Sacks, I.S. (2003). Comment on "Minimum magnitude of completeness in earthquake catalogs: Examples from Alaska, the western United States, and Japan," by Stefan Wiemer and Max Wyss, *Bull. Seismol. Soc. Am.*, v. 93, p. 1862-1867.
- Sabetta, F. & A. Pugliese (1987). Attenuation of peak horizontal acceleration and velocity from Italian strong-motion records, *Bull. Seism. Soc. Am.* 77, 1491-1513.
- Sägesser, R. & D. Mayer-Rosa (1978). Erdbebengefährdung in der Schweiz, *Schweizerische Bauzeitung SIA*, 3-18.

- Schindler, C., C. Beer, D. Mayer-Rosa, E. Rüttener, J.-J. Wagner, J.-M. Jaquet & C. Frischknecht (1993). Earthquake Hazard Assessment in the Canton Obwalden using Geographic Information System (GIS), In: Floods and Geological Hazards, Swiss National Committee of the UN-IDNDR, Report 1991-1993.
- Schmid, S. & E. Kissling (2000). The arc of the western Alps in the light of geophysical data on deep crustal structure, *Tectonics*, vol. 19, no 1, p. 62-85.
- Schmid, S.M., N. Froitzheim, O.A. Pfiffner, G. Schonborn & E. Kissling (1997). Geophysical-geological transect and tectonic evolution of the Swiss-Italian Alps (vol 15, pg 1036, 1996), *Tectonics*, 16 (1), 186-188.
- Schnellmann, M., F.S. Anselmetti, D. Giardini, D., J.A. McKenzie & S.N. Ward (2002). Prehistoric earthquake history revealed by lacustrine slump deposits, *Geology*, v. 30, p. 1131-1134.
- Schnellmann, F.S. Anselmetti, D. Giardini & J.A. McKenzie (2004). Propagating fold-and-thrust-belt structures induced by lacustrine sediment slides, *Sedimentology*, submit.
- Schorlemmer, D., S. Wiemer & M. Wyss (2004a). Earthquake Statistics at Parkfield: 1. Stationarity of  $b$ -values, *J. Geophys. Res.*, v. in press.
- Schorlemmer, D., S. Wiemer, M. Wyss & D. Jackson (2004b). Earthquake Statistics at Parkfield: 2 Probabilistic Forecasting and Testing, *J. Geophys. Res.*, v. in press.
- Schumacher, M.E. (2002). Upper Rhine Graben: Role of preexisting structures during rift evolution, *Tectonics*, 21, 10.1029/2001TC900022.
- Schwarz-Zanetti, G., N. Deichmann, D. Fäh, D. Giardini, M.J. Jimenez, V. Masciadri, R. Schibler & M. Schnellman (2003). The earthquake in Unterwalden on September 18, 1601: A historico-critical macroseismic evaluation, *Eclogae Geol. Helv.*, v. 96, p. 441-450.
- Shi, Y. & B.A. Bolt (1982). The standard error of the magnitude-frequency  $b$  value, *Bull. Seismol. Soc. Am.*, v. 72, p. 1677-1687.
- SIA (2003). Norm SIA261- Einwirkungen auf Tragwerke, Schweizerischer Ingenieur und Architekten Verein.
- Sissingh, W. (1998). Comparative Tertiary stratigraphy of the Rhine Graben, Bresse Graben and Molasse Basin: correlation of Alpine foreland events, *Tectonophysics*, 300 (1-4), 249-284.
- Slejko, D., L. Peruzza & A. Rebez (1998). Seismic hazard maps of Italy, *Annali di Geofisica*, 41/2, 183-214.
- Smit, P. (1996). Datenerfassung und Bestimmung der Abminderung der Bodenbewegung bei Erdbeben in der Schweiz, PhD.-thesis, ETH-Zurich.
- Sommaruga A. (1999). Décollement tectonics in the Jura foreland fold-and-thrust belt, *Marine and Petroleum Geology* 16, 111-134.
- Steimen S., D. Fäh, F. Kind, C. Schmid & D. Giardini (2003). Identifying 2D Resonance in Microtremor Wave Fields, *Bull. Seism. Soc. Am.* 93, 583 – 599.
- Stepp, J.C. (1972). Analysis of completeness of the earthquake sample in the Puget Sound area and its effect on statistical estimates of earthquake hazard, *International Conference on Microzonation, Proceedings* 2, 897-910.
- Taubenheim, J. (1969). Statistische Auswertung geophysikalischer und meteorologischer Daten, *Geophysikalische Monographien*, akademische Verlagsgesellschaft Geest & Portig K.-G., Leipzig.
- Thouvenot, F., J. Fréchet, P. Tapponnier, J.-Ch. Thomas, B. Le Brun, G. Ménard, R. Lacassin, L. Jenatton, J.-R. Grasso, O. Coutant, A. Paul & D. Hatzfeld (1998). The ML 5.3 Épagny (French Alps) earthquake of 1996 July 15: a long-awaited event on the Vuache fault, *Geophys. J. Int.* 135, 876-892.
- Toro, G.R., N.A. Abrahamson & J.F. Schneider (1997). Model of strong ground-motions from earthquakes in central and eastern North America: Best estimates and uncertainties, *Seism. Res. Letts.* 6, 41-57.
- Truffert C., J.-P. Burg, M. Cazes, R. Bayer, B. Damotte B. & D. Rey (1990). Structures crustales sous le Jura et la Bresse: contraintes sismiques et gravimétriques le long des profils ECORS Bresse-Jura et Alpes II, *Mémoires de la Société Géologique de France*, 156, 157-164.
- Trümpy, R. (1985). Die Plattentektonik und Entstehung der Alpen, Orell Füssli, Zurich, Switzerland.
- Uhrhammer, R. (1986). Characteristics of northern and southern California seismicity: *Earthquake Notes*, v. 57, p. 21.
- Utsu, T. (1999). Representation and analysis of the earthquake size distribution: a historical review and some new approaches, *Pure and Applied Geophysics*, 155 (2-4), 509-535.
- Utsu, T., Ogata, Y., and Matsu'ura, R.S., (1995). The centenary of the Omori formula for a decay law of

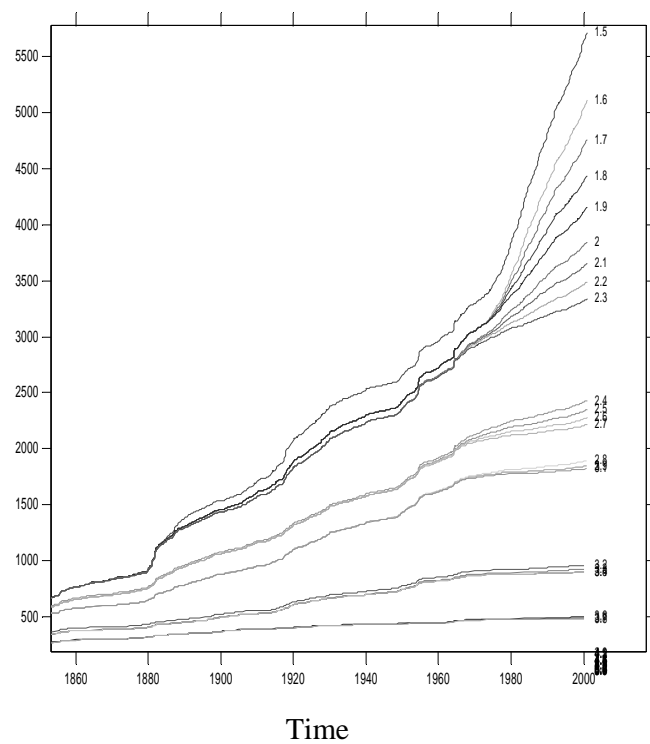
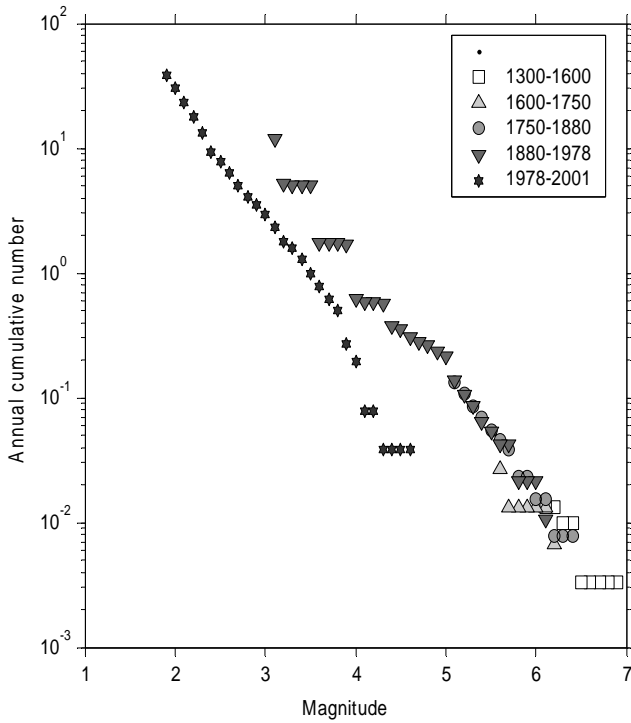
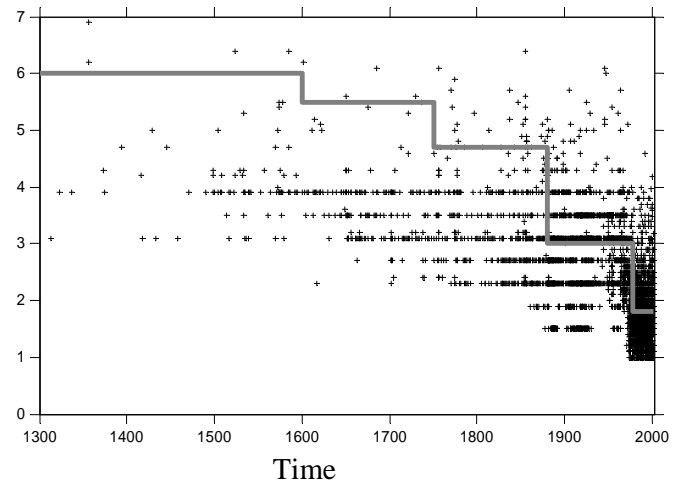
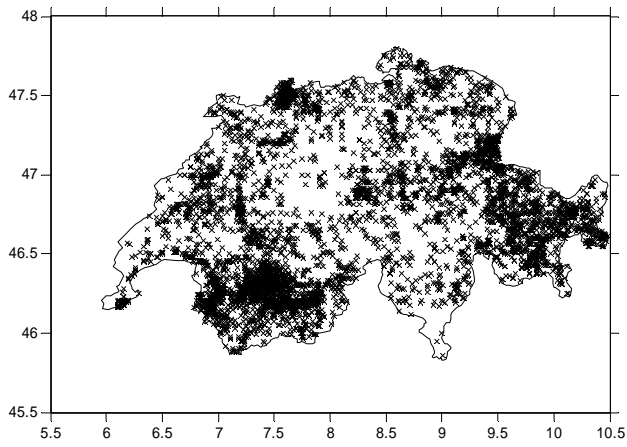
- aftershock activity, *Journal of the Physics of the Earth*, v. 43, p. 1-33.
- Villemin, T., F. Alvarez & J. Angelier (1986). The Rhinegraben - Extension, Subsidence and Shoulder Uplift, *Tectonophysics*, 128 (1-2), 47-59.
- Wagner J.-J., C. Frischknecht, P. Rosset, M. Sartori, C. Schindler, C. Beer, D. Mayer-Rosa, E. Rüttener & P. Smit (2000). Contribution au zonage sismique dans la vallée du Rhône, entre Sion et Brigue (Valais), Office fédéral de l'environnement, des forêts et du paysage, Service hydrologique et géologique national; Rapport géologiques No 25, 123 p.
- Waldhauser, F., E. Kissling, J. Ansorge & S. Mueller (1998). Three-dimensional interface modelling with two-dimensional seismic data: the Alpine crust-mantle boundary, *Geophys. J. Int.*, v. 135, p. 264-278.
- Wells, D.L. & K.J. Coppersmith (1994). New empirical relationships among magnitude, rupture length, rupture width, rupture area and surface displacement, *Bull. Seism. Soc. Am.*, 84, p. 974-1002.
- Wesson, R.L., W.H. Bakun & D.M. Perkins, (2003). Association of earthquakes and faults in the San Francisco Bay area using Bayesian inference, *Bull. Seismol. Soc. Am.*, v. 93, p. 1306-1332.
- Wiemer, S. & M. Baer (2000). Mapping and removing quarry blast events from seismicity catalogs, *Bull. Seismol. Soc. Am.*, v. 90, p. 525-530.
- Wiemer, S. & M. Wyss (1997). Mapping the frequency-magnitude distribution in asperities: An improved technique to calculate recurrence times?, *J. Geophys. Res.*, 102, 15115-15128.
- Wiemer, S. & M. Wyss (2000). Minimum magnitude of complete reporting in earthquake catalogs: examples from Alaska, the Western United States and Japan, *Bull. Seismol. Soc. Am.*, 90, 859-869.
- Wiemer, S. & M. Wyss (2002). Mapping spatial variability of the frequency-magnitude distribution of earthquakes, *Advances in Geophysics*, v. 45, p. 259-302.
- Wiemer, S. & M. Wyss, M. (1997). Mapping the frequency-magnitude distribution in asperities: An improved technique to calculate recurrence times?., *J. Geophys. Res.*, v. 102, p. 15115-15128.
- Wiemer, S. & M. Wyss, (2003). Reply to "Comment on 'Minimum magnitude of completeness in earthquake catalogs: Examples from Alaska, the western United States, and Japan,' by Stefan Wiemer and Max Wyss," by Paul A. Rydelek and I.S. Sacks, *Bull. Seismol. Soc. Am.*, v. 93, p. 1868-1871.
- Wuster, J. (1993). Discrimination of chemical explosions and earthquakes in central Europe - A case study, *Bull. Seismo. Soc. Am.*, v. 83, p. 1184-1212.
- Wyss, M. & Y. Toya (2000). Is background seismicity produced at a stationary poissonian rate?, *Bull. Seismol. Soc. Am.*, 90 (5), 1174-1187.
- Wyss, M., K. Shimazaki & T. Urabe (1996). Quantitative mapping of a precursory quiescence to the Izu-Oshima 1990 (M6.5) earthquake, Japan, *Geophys. J. Int.*, v. 127, p. 735-743.
- Yazd, M.R.S. (1993). Ground-motion studies in the southern Great Basin of Nevada and California, PhD. - thesis, St.Louis University, USA.
- Ye, S., J. Ansorge, E. Kissling & S. Mueller (1995). Crustal Structure beneath the Eastern Swiss Alps Derived from Seismic-Refraction Data, *Tectonophysics*, 242 (3-4), 199-221.
- Youngs, R.-R., F.-H. Swan, M.-S. Power, D.-P. Schwartz & R.-K. Green (1987). Probabilistic analysis of earthquake ground shaking hazard along the Wasatch Front, Utah, in Glori, P.-L., and Hays, W.-W., eds., *Assessment of regional earthquake hazard and risk along the Wasatch Front, Utah*, p. M110.



# Appendix 1: Completeness Estimation by Country

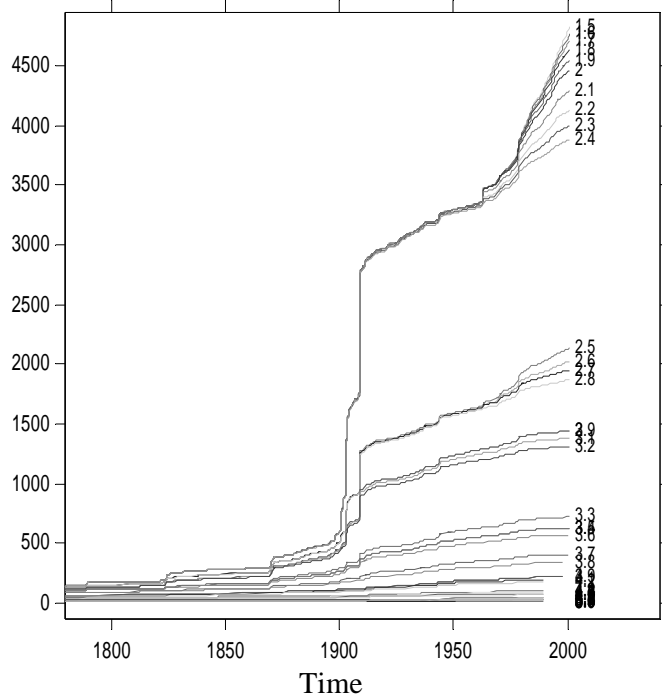
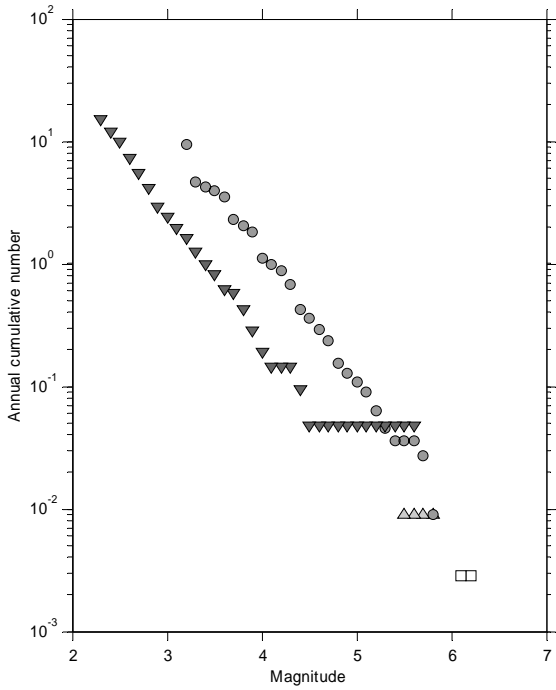
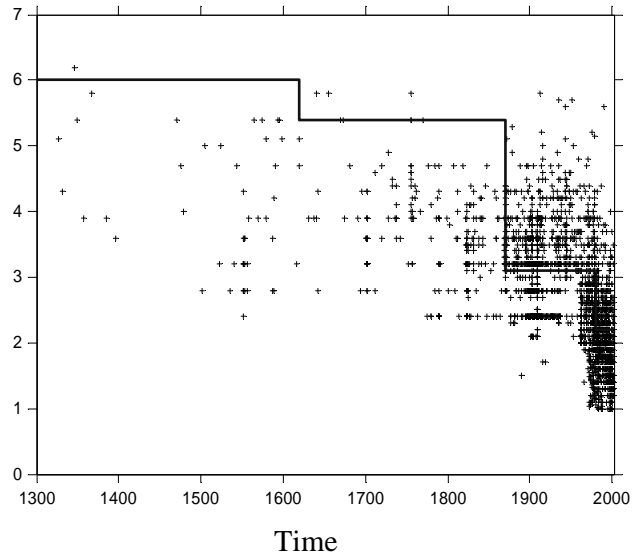
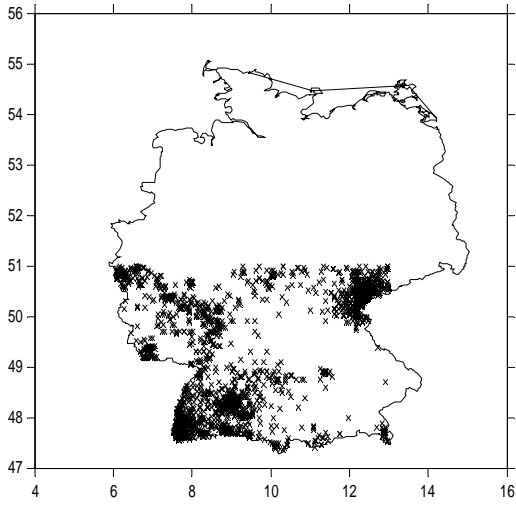
## Switzerland

Period	Mc - Model 1 (Mw)	Mc - Model 2 (Mw)
1300 - 1600	6.0	6.0
1600 - 1750	5.5	5.7
1750 - 1880	4.7	5.0
1880 - 1977	3.0	4.2
1977 - 2001	1.8	1.9



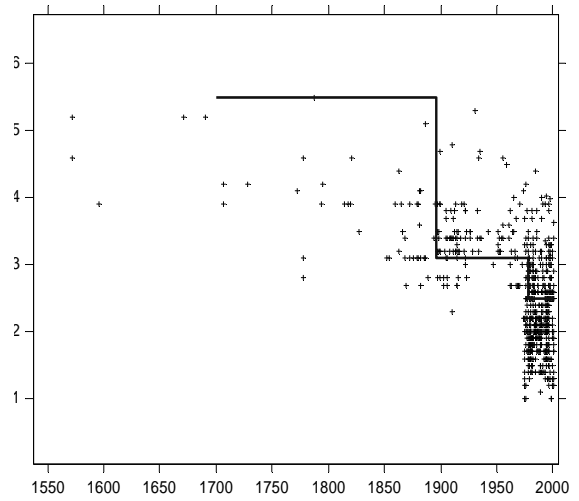
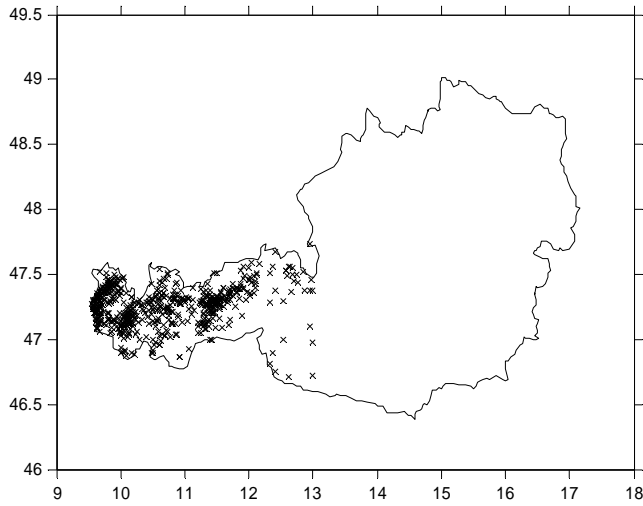
# Germany

Period	Mc – Model 1 (Mw)	Mc – Model 2 (Mw)
1300 - 1620	6.0	6.5
1620 - 1870	5.4	5.6
1870 - 1980	3.1	3.5
1980 - 2001	3.0	3.1

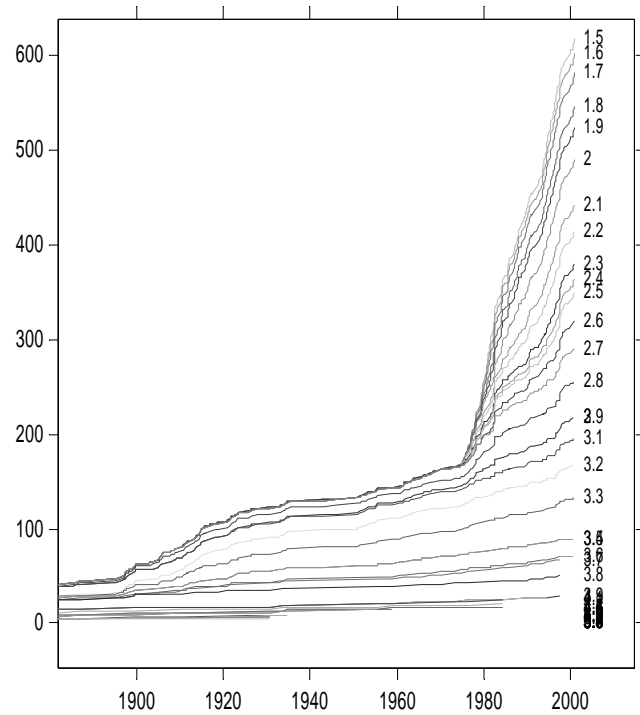
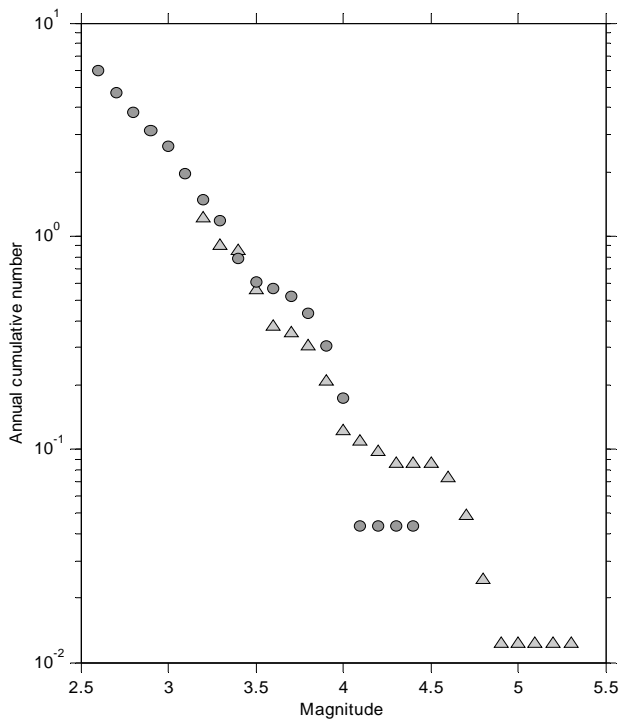


# Austria

Period	Mc – Model 1 (Mw)	Mc – Model 2 (Mw)
1700 - 1896	5.5	6
1896 - 1978	3.1	3.3
1978 - 2001	2.5	2.5



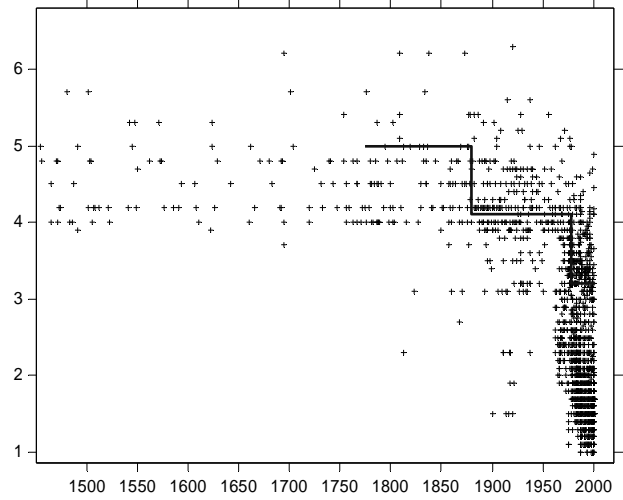
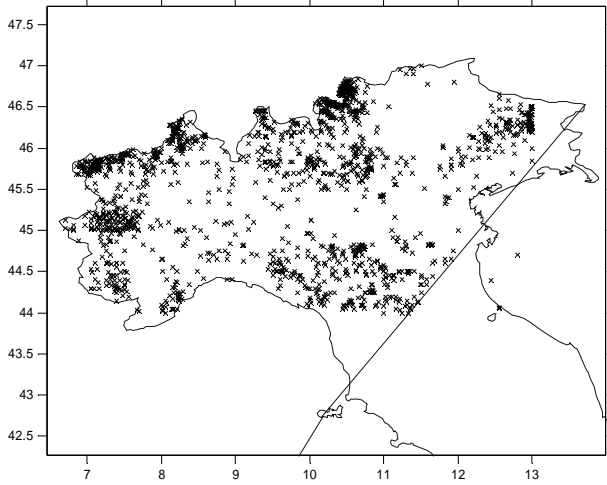
Time



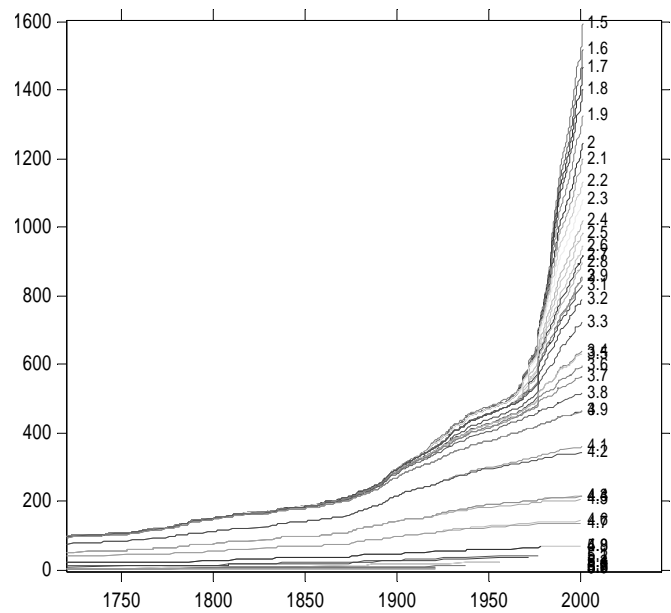
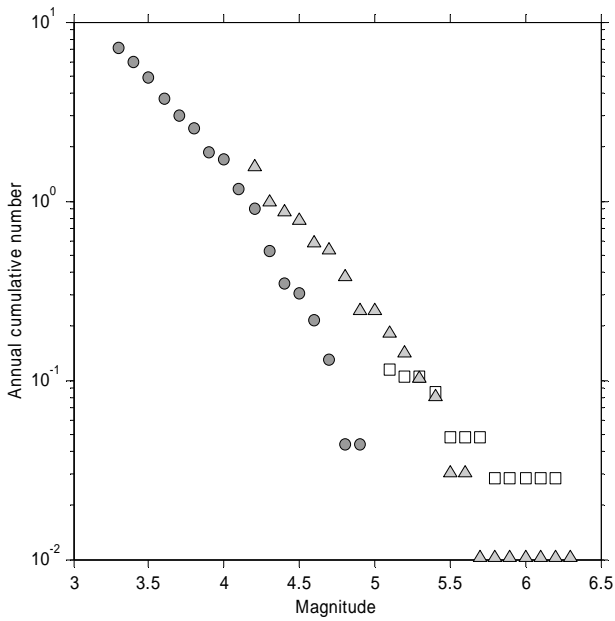
Time

# Italy

Period	Mc – Model 1 (Mw)	Mc – Model 2 (Mw)
1775 - 1880	5.5	5.7
1880- 1979	4.1	4.3
1979 - 2001	3.2	3.2



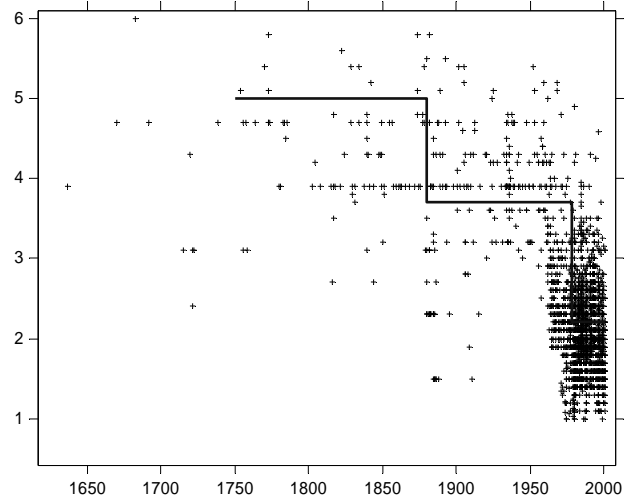
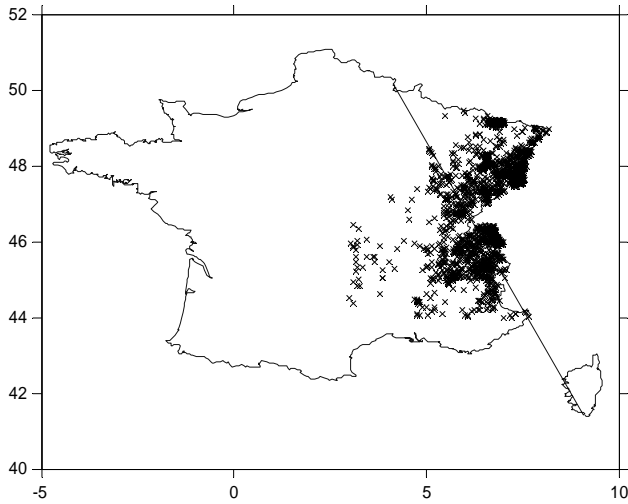
Time



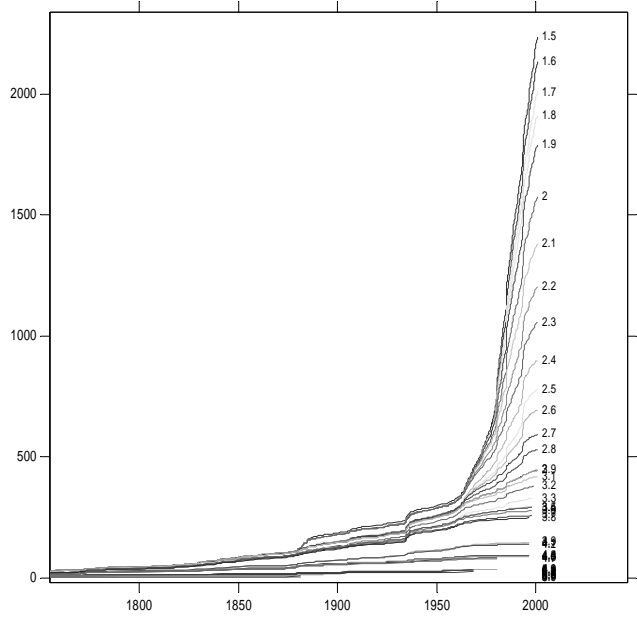
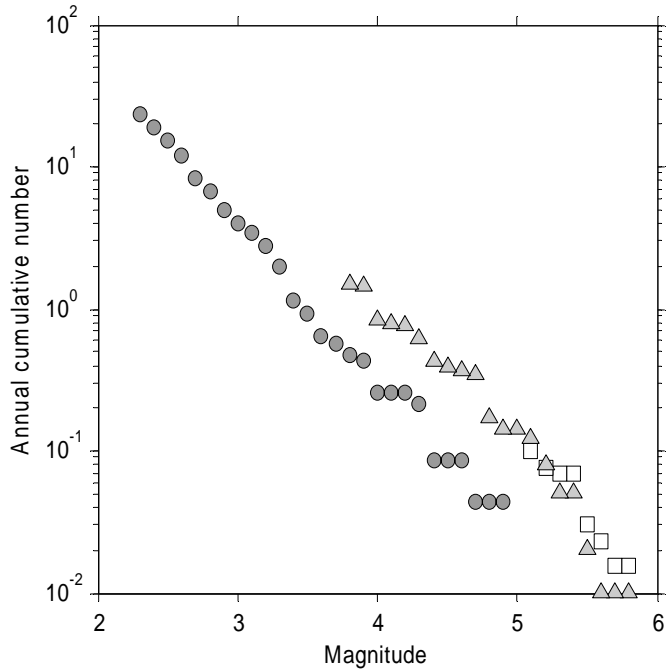
Time

# France

Period	Mc – Model1 (Mw)	Completeness (Mw)
1700 - 1880	5.3	5.3
1880- 1978	3.7	4.0
1978 - 2001	2.2	2.2



Time



Time



## Appendix 2: Tables

**Table A1:** Percent of earthquakes as a function of depth north and south of the Helvetic Front (HF).

Depth Range [km]	North of HF percent]	South of HF [percent]
0-4.99	12.50	44.48
5-9.99	23.91	47.00
10-14.99	27.17	8.02
15-19.99	14.67	0.38
20-24.99	13.58	0.1
25-29.99	5.43	0
30-34.99	1.08	0
35-39.99	1.08	0
40-44.99	0.54	0
45-49.99	0	0



**Table A3:** Completeness ( $M_{c0}$ ,  $M_{c1}$ ), recurrence parameters (a, and b-values) and relative model weight for each source of Model SEIS. See Figure 16 for location of zones.

Zone number and name	$M_0$	$M_1$	a-value	b-value	AICc weight
1 Piemonte_W	3.3	4.2	2.76	-0.90	0.58
			2.80	-0.90	0.22
			2.54	-0.84	0.20
	3.2	4.1	2.69	-0.90	0.57
			2.72	-0.90	0.21
			2.30	-0.79	0.22
2 Graubuenden_N	2.0	4.2	2.01	-0.90	0.60
			2.12	-0.90	0.20
			2.15	-0.97	0.20
	1.8	3.0	2.40	-0.90	0.99
			1.84	-0.72	0.01
3 Graubuenden_S	2.0	4.2	2.43	-0.90	0.56
			2.46	-0.90	0.22
			2.45	-0.91	0.22
	2.0	3.0	2.54	-0.90	0.04
			2.63	-0.90	0.92
			2.31	-0.80	0.04
4 Helvetic_E	2.0	4.1	2.46	-0.90	0.54
			2.57	-0.90	0.25
			2.37	-0.86	0.21
	2.0	3.0	2.54	-0.90	0.08
			2.62	-0.90	0.71
			2.24	-0.77	0.21
5 Hohenzollern	3.1	3.5	2.72	-0.90	0.09
			2.70	-0.90	0.78
			1.87	-0.65	0.13
	3.0	3.1	2.56	-0.90	0.49
			2.53	-0.90	0.51
6 Innsbruck	3.1	3.5	2.65	-0.90	0.55
			2.63	-0.90	0.22
			2.19	-0.76	0.23
	3.0	3.1	2.59	-0.90	0.43
			2.59	-0.90	0.27
				2.00	-0.70
7 Trentino	3.2	4.3	2.43	-0.90	0.62
8 Bergamo	3.2	4.3	2.59	-0.90	0.38
			2.46	-0.90	0.76
	3.2	4.1	2.60	-0.90	0.24
			2.47	-0.90	0.72
9 Rhein-Graben	2.5	4.1	2.54	-0.90	0.28
			2.53	-0.90	0.17
			2.80	-0.90	0.69
	2.5	3.5	2.05	-0.72	0.14
			2.54	-0.90	0.27
			2.64	-0.90	0.42
10 Bayern	2.5	3.5	2.00	-0.71	0.31
			2.32	-0.90	0.52
			2.39	-0.90	0.28
	2.0	3.0	2.09	-0.82	0.20
			2.33	-0.90	0.54
11 Alto-Adige	2.5	4.0	2.29	-0.90	0.23
			2.44	-0.95	0.23
			2.15	-0.90	0.62
	2.0	3.5	2.00	-0.90	0.17
			2.87	-1.19	0.21
			2.14	-0.90	0.57
12 Zurich-Bodensee	2.5	4.1	2.06	-0.90	0.21
			2.28	-0.96	0.22
			2.34	-0.90	0.58
	2.5	3.0	2.42	-0.90	0.19
			1.98	-0.76	0.23
13 Haute-Saone	2.5	4.1	2.50	-0.90	0.21
			2.52	-0.90	0.43
			1.84	-0.66	0.36
	2.0	3.5	1.91	-0.90	0.62
			2.15	-0.90	0.18
				1.35	-0.68
			2.02	-0.90	0.59
			2.01	-0.90	0.21
			2.05	-0.91	0.20

14 Berner-Oberland	2.0	3.0	1.39	-0.90	0.73
			1.36	-0.90	0.13
			1.15	-0.79	0.14
	2.0	2.8	1.30	-0.90	0.71
			1.18	-0.90	0.16
1.26			-0.89	0.13	
15 Basel	2.5	4.1	2.31	-0.90	0.46
			2.46	-0.90	0.19
			1.78	-0.70	0.35
	2.4	3.8	2.20	-0.90	0.37
			2.31	-0.90	0.15
1.57	-0.66	0.48			
16 Savoie	3.0	4.0	2.66	-0.90	0.39
			2.75	-0.90	0.26
			1.78	-0.64	0.35
	2.2	3.7	2.54	-0.90	0.33
			2.67	-0.90	0.33
2.22	-0.77	0.34			
17 Piemonte-Aosta	2.5	4.0	1.83	-0.90	0.57
			2.19	-0.90	0.43
	2.2	3.7	1.93	-0.90	0.57
			2.09	-0.90	0.23
			1.63	-0.77	0.20
18 Chiasso-Domodossola	2.0	3.5	1.85	-0.90	0.61
			1.81	-0.90	0.18
			2.11	-1.03	0.21
	2.0	3.3	1.83	-0.90	0.58
			1.72	-0.90	0.20
2.19	-1.07	0.22			
19 Ticino	2.0	3.0	2.15	-0.90	0.07
			2.28	-0.90	0.85
			1.66	-0.68	0.08
20 Valais_S	1.9	4.2	1.95	-0.80	0.21
			2.21	-0.80	0.27
			1.60	-0.63	0.52
	1.8	3.0	2.06	-0.80	0.02
			2.18	-0.80	0.72
1.68	-0.63	0.26			

21 Valais_N	2.0	4.1	2.18	-0.80	0.54
			2.09	-0.80	0.21
			2.34	-0.87	0.25
	2.0	3.5	2.25	-0.80	0.28
			2.37	-0.80	0.61
2.16			-0.76	0.11	
22 Zentral-Molasse_E	2.5	4.1	1.95	-0.90	0.69
			1.95	-0.90	0.15
			1.65	-0.78	0.16
	2.0	3.0	2.02	-0.90	0.45
			2.10	-0.90	0.31
1.71	-0.77	0.24			
23 Zentral-Molasse_W	2.0	4.1	2.30	-0.90	0.22
			2.62	-0.90	0.52
			1.97	-0.74	0.26
	2.0	3.0	2.42	-0.90	0.01
			2.54	-0.90	0.80
1.89	-0.67	0.19			
24 Helvetic_W	2.0	4.1	2.44	-0.90	0.29
			2.68	-0.90	0.37
			2.16	-0.77	0.34
	2.0	3.0	2.47	-0.90	0.23
			2.53	-0.90	0.24
2.15	-0.76	0.53			
25 Jura	2.4	3.6	2.17	-0.90	0.57
			2.08	-0.90	0.19
			2.71	-1.12	0.24
	2.0	3.0	1.76	-0.90	0.68
			3.22	-1.39	0.32
26 Geneve	2.0	3.9	2.19	-0.90	0.21
			2.50	-0.90	0.60
			1.87	-0.75	0.19
	2.0	3.0	2.10	-0.90	0.54
			2.06	-0.90	0.24
2.01	-0.86	0.22			

**Table A4:** Completeness ( $M_{c0}$ ,  $M_{c1}$ ), recurrence parameters (a, and b-values) and relative model weight for each source of Model TECTO. See Figure 16 for the location of zone.

Zone number and name	$M_{c0}$	$M_{c1}$	a-value	b-value	weight
1 Piemonte Savoie	2.0	4.1	2.80	-0.90	0.09
			3.02	-0.90	0.53
			2.55	-0.78	0.38
	3.2	4.1	3.01	-0.90	0.44
			3.06	-0.90	0.31
			2.66	-0.80	0.25
2 Ticino	2.0	3.3	2.10	-0.90	0.39
			2.26	-0.90	0.39
			1.77	-0.75	0.22
	2.0	3.0	2.22	-0.90	0.04
			2.35	-0.90	0.88
			1.65	-0.64	0.08
3 Graubunden- Innsbruck	2.0	4.1	2.76	-0.90	0.48
			2.83	-0.90	0.22
			2.63	-0.84	0.30
	2.0	3.0	2.96	-0.90	0.97
			2.51	-0.75	0.03
4 Helvetic	2.0	4.1	2.91	-0.90	0.36
			3.05	-0.90	0.40
			2.80	-0.85	0.24
	2.0	3.0	2.97	-0.90	0.01
			3.04	-0.90	0.83
5 Rhein-Graben_N	2.0	3.7	2.73	-0.80	0.16
			2.22	-0.90	0.48
			2.23	-0.90	0.17
	2.5	3.5	1.90	-0.75	0.35
			2.35	-0.90	0.59
			2.33	-0.90	0.20
6 Rhein-Graben_S	2.5	4.1	2.12	-0.82	0.21
			2.56	-0.90	0.13
			2.83	-0.90	0.63
	2.5	3.7	1.93	-0.66	0.24
			2.59	-0.90	0.11
2.74	-0.90	0.55			
7 Bresse	2.2	4.1	1.91	-0.65	0.34
			2.49	-0.90	0.49
			2.64	-0.90	0.31
	2.2	3.7	2.47	-0.89	0.20
			2.49	-0.90	0.52
			2.57	-0.90	0.27
8 Valais_S	2.0	4.1	2.45	-0.88	0.21
			2.00	-0.80	0.29
			2.20	-0.80	0.28
	2.0	3.4	1.68	-0.65	0.43
			2.11	-0.80	0.01
9 Bayern	2.5	3.5	2.28	-0.80	0.85
			1.67	-0.62	0.14
			2.84	-0.90	0.96
	2.0	3.0	1.94	-0.64	0.04
			2.68	-0.90	0.10
10 Molasse-Jura	2.0	4.0	2.08	-0.69	0.90
			2.88	-0.90	0.39
			3.00	-0.90	0.41
	2.0	3.0	2.81	-0.87	0.20
			2.93	-0.90	0.03
11 Basel	2.5	4.1	2.99	-0.90	0.79
			2.70	-0.80	0.18
			2.31	-0.90	0.52
	2.0	3.0	2.46	-0.90	0.22
			1.92	-0.76	0.26
12 Alto-Adige	2.5	4.1	2.11	-0.90	0.40
			2.10	-0.90	0.15
			1.73	-0.74	0.45
	2.5	3.5	2.66	-0.90	0.18
			2.87	-0.90	0.33
2.06	-0.68	0.49			
2.64	-0.90	0.24			
2.69	-0.90	0.14			
2.04	-0.69	0.62			

